



HAL
open science

Détection des interactions photon-photon dans un circuit supraconducteur

Lijing Jin

► **To cite this version:**

Lijing Jin. Détection des interactions photon-photon dans un circuit supraconducteur. Supraconductivité [cond-mat.supr-con]. Université Grenoble Alpes, 2016. Français. NNT : 2016GREAY002 . tel-01499904

HAL Id: tel-01499904

<https://theses.hal.science/tel-01499904>

Submitted on 1 Apr 2017

HAL is a multi-disciplinary open access archive for the deposit and dissemination of scientific research documents, whether they are published or not. The documents may come from teaching and research institutions in France or abroad, or from public or private research centers.

L'archive ouverte pluridisciplinaire **HAL**, est destinée au dépôt et à la diffusion de documents scientifiques de niveau recherche, publiés ou non, émanant des établissements d'enseignement et de recherche français ou étrangers, des laboratoires publics ou privés.

THÈSE

Pour obtenir le grade de

DOCTEUR DE L'UNIVERSITÉ GRENOBLE ALPES

Spécialité : **PHYSIQUE THEORIQUE**

Arrêté ministériel : 7 août 2006

Présentée par

LIJING JIN

Thèse dirigée par **Manuel HOUZET** et
codirigée par **Julia S. MEYER** et **Frank W.J. HEKKING**

préparée au sein du **Laboratoire de Physique et Modélisation
des Milieux Condensés**
dans l'**École Doctorale de physique de Grenoble**

Détection des interactions photon-photon dans un circuit supraconducteur

Thèse soutenue publiquement le **10 Février 2016**,
devant le jury composé de :

M. Fabien PORTIER

Chercheur, Service de Physique de l'Etat Condensé, CEA Saclay,
Rapporteur

Mme. Inès SAFI

Chargée de recherche, Laboratoire de Physique des Solides, Université
Paris-Sud 11, Rapporteur

Mme. Wiebke GUICHARD

Professeur des universités, Université Joseph Fourier, Président

M. Fabio PISTOLESI

Directeur de Recherche, Laboratoire Ondes et Matière d'Aquitaine,
Université de Bordeaux and CNRS, Examineur

Mme. Julia S. MEYER

Professeur des universités, Université Joseph Fourier, Co-Directeur de
thèse

M. Manuel HOUZET

Researcher, Service de Physique Statistique, Magnétisme et
Supraconductivité, CEA Grenoble, Directeur de thèse



To my parents JIN You-tai and LI Xian-zhi

Table of Contents

Abstract (English version)	iii
Abstract (French version)	v
1 Introduction	1
1.1 Background and Motivation	1
1.2 Structure of the thesis	5
2 Key elements of the studied circuit	11
2.1 Josephson junction	11
2.1.1 Current-voltage characteristic	13
2.1.2 Summary	14
2.2 Cooper pair box	14
2.2.1 Weakly anharmonic oscillator	16
2.2.2 Charge qubit	17
2.2.3 Summary	22
2.3 <i>LC</i> transmission line	23
2.3.1 Josephson junction chain	25
2.3.2 Transmission line	27
2.3.3 Summary	33
3 Dynamical Coulomb blockade theory in Josephson junctions	35
3.1 Introduction	35
3.2 Cooper pair tunnelling rates	37
3.3 Phase-phase correlator: linear regime	42
3.3.1 Electromagnetic environment: the transmission line	43
3.3.2 Summary	49
3.4 Phase-phase correlator: nonlinear regime	49
3.4.1 Green's function perturbation theory	49
3.4.2 Path integral method	59
3.4.3 Summary	63

4	Detecting photon-photon interactions in a transmission line side-coupled with a weakly anharmonic oscillator	65
4.1	The studied circuit	65
4.2	The linear regime	68
4.2.1	Two-point Green's function	69
4.2.2	Phase-phase correlator	72
4.2.3	Current-voltage characteristic	72
4.3	The weakly nonlinear regime	75
4.3.1	Two-point Green's function	76
4.3.2	Four-point Green's function	77
4.3.3	Phase-phase correlator	79
4.3.4	Current-voltage characteristic	79
4.4	Summary	82
5	Detecting photon-photon interactions in a transmission line side-coupled with a charge qubit	83
5.1	Hamiltonian of the system	83
5.2	Phase-phase correlator	85
5.2.1	Single photon processes	85
5.2.2	Two photon processes	90
5.2.3	Multiple photon processes	94
5.3	Spin-spin Green's function	98
5.4	Current-voltage characteristic	101
5.5	Summary	102
6	Conclusion and perspectives	105
A	The Hamiltonian of the studied circuit	107
B	Quantum theory of the transmission line	111
C	Photon-photon interactions: weakly nonlinear regime	113
D	Time-ordered Green's function: strongly nonlinear regime	115
E	Two-point Green's functions in k-space	119
	Bibliography	119
	Acknowledgement	135

Abstract (*English version*)

Creating strong photon-photon interactions in circuit quantum electrodynamics attracts increasing attention due to both fundamental reasons and its potential application in quantum communication science. In this thesis, we focus on detecting photon-photon interactions in a superconducting circuit. In particular, a local interaction between photons can be engineered by coupling a nonlinear system to a transmission line. The required transmission line can be conveniently formed from a chain of Josephson junctions. The nonlinearity is generated by side-coupling this chain to a Cooper pair box. We propose to probe the resulting photon-photon interactions via a voltage-biased Josephson junction (the probe junction) connected to the line. When a finite voltage V (smaller than the superconducting gap voltage) is applied, a Cooper pair tunnels inelastically through the probe junction, simultaneously releasing the energy $2eV$ (e is elementary charge) to the environment via emitting one or several photons. The emission depends on the properties of the environment. In our case, individual photons freely propagate down the transmission line and are scattered by the side-coupled Cooper pair box. In contrast, when multiple photons are emitted, these photons may interact with each other. The elastic and inelastic scattering properties of photons will in turn influence the current through the probe junction. Therefore, the dc current-voltage characteristic of the Josephson junction provides a probe to study photon-photon interactions in a nonlinear environment.

We first investigate the weakly nonlinear regime where the Cooper pair box can be described as a weakly anharmonic oscillator with resonant frequency ω_s . Using Green's function theory, we find that the non-linearity renormalizes the resonance frequency to ω'_s for single photon processes. As a result, the $I - V$ characteristic shows a resonance feature around $2eV = \omega'_s$. By contrast, the interactions due to the non-linearity yield an additional resonance features at $2eV = 2\omega'_s$ due to two-photon processes. Such a feature is thus a clear indication of photon-photon interactions. Using realistic parameters, we estimate that the current signal of the two-photon interaction feature can reach up to 1 pA which is well within reach of current measurement technology.

We then switch to the strongly nonlinear regime. In this regime, the Cooper pair box is reduced to a charge qubit under certain conditions. The environment

seen by the probe junction can be described by a spin-boson model, which consists of a charge qubit (the spin) bilinearly coupled to the photons in the transmission line (the bosons). Using Green's function theory and the path integral method, we compute the environmental phase-phase correlators that are directly related to the current through the probe junction. Our results indicate that scattering of individual photons by the side-coupled qubit results in a resonance feature in the $I-V$ characteristic of the probe junction at $2eV = \omega_q b$, where $\omega_q b$ is the resonance frequency of the qubit. We further propose to use Bloch equations to obtain the contribution from the photon-photon interaction in this regime.

Abstract (*French version*)

La génération d'une forte interaction photon-photon en électrodynamique quantique des circuits attire une attention croissante, tant pour des raisons fondamentales que pour son application potentielle en communication quantique. Dans cette thèse, je m'intéresse plus particulièrement la détection de l'interaction photon-photon dans un circuit supraconducteur. Une interaction locale entre les photons peut être conue en couplant un système non linéaire avec une ligne de transmission. Cette dernière peut être réalisée grâce à une chaîne de jonctions Josephson. La non-linéarité, quant à elle, est générée en couplant une jonction de la chaîne à une boîte à paires de Cooper. Nous proposons de sonder les interactions photon-photon résultantes via une jonction Josephson (nommée "jonction-sonde") connectée à la ligne et polarisée en tension. La théorie du blocage de Coulomb dynamique prédit que les paires de Cooper traversent la jonction de la sonde par effet tunnel inélastique, libérant une énergie égale à $2eV$ (où e est la charge fondamentale et V la tension de polarisation) dans l'environnement par l'émission d'un ou plusieurs photons. Les photons individuels se propagent librement le long de la ligne et sont diffusés par la boîte à paires de Cooper couplée à la chaîne. Par ailleurs, deux (ou plusieurs) photons peuvent interagir. Les propriétés de diffusion élastique et inélastique des photons vont à leur tour influencer le courant é travers la jonction-sonde. Par conséquent, la caractéristique courant-tension de la jonction Josephson fournit une sonde pour étudier l'interaction photon-photon dans un milieu non linéaire.

Nous étudions d'abord un régime faiblement non linéaire où la boîte à paires de Cooper est assimilée à un oscillateur faiblement anharmonique avec une fréquence de résonance ω_s . En utilisant la théorie des fonctions de Green, nous trouvons que la non-linéarité renormalise la fréquence de résonance à ω'_s pour les processus à photon unique. En conséquence, la caractéristique $I(V)$ présente une résonance autour de $2eV = \omega'_s$. Lorsque plusieurs canaux de photons sont impliqués, la non-linéarité excite l'interaction photon-photon, conduisant à une structure résonante dans courant continu à travers la jonction-sonde autour de $2eV = n\omega'_s (n \geq 2)$. Cette structure peut être considérée comme une signature directe des interactions photon-photon. En utilisant des paramètres réalistes, nous estimons que le signal de courant peut atteindre 1 pA, ce qui est à la portée des technologies actuelles de

mesure de courant.

Nous considérons enfin le régime fortement non linéaire. Dans ce cas, la boîte à paires de Cooper est peut être équivalente à un qubit de charge. L'environnement vu par la jonction-sonde peut être décrit par un Hamiltonien de type spin-boson. En combinant la théorie des fonctions de Green et l'intégrale de chemin, nous calculons les corrélateurs phase-phase dans la ligne de transmission, qui interviennent dans le calcul du courant à travers la jonction-sonde. Nos résultats indiquent que la diffusion de photons individuels par le qubit couplé latéralement donne lieu à une résonance dans la caractéristique courant-tension de la jonction de la sonde à $2eV = \omega_q b$, où $\omega_q b$ est la fréquence de résonance du qubit. Partant de ce résultat, il sera intéressant de voir comment l'interaction photon-photon modifie les caractéristiques de la résonance dans ce régime.

Introduction

1.1 Background and Motivation

Photons, the elementary particles which describe light, do not interact with each other in vacuum. They just pass through each other without having an effect on each other. This is apparent from classical electrodynamic: Maxwell's equations are linear and therefore do not describe any interactions. However, this is not the case in a medium. Non-linear optical media have previously been used to indirectly alter one beam of light using another one. This process involves electromagnetic energy striking the medium, which then alters the second beam. Normally, this technique involves the use of vast quantities of light particles. Very recently, such interactions were also realized at the level of individual photons [1]. The two simultaneous photons that interact show a completely different behaviour than single photons.

Creating strong photon-photon interactions [2–14] attracts increasing attention due to both fundamental reasons [15–18] and its potential application [15, 19–22]. Studying individual quantum systems provides us with the means of directly testing the foundation the quantum theory. Besides, photons are excellent carriers of quantum information owing to their long lifetime and ease of distribution. Thus, entangled photons are able to carry out quantum information processing [23–28]. Moreover, for many other applications in quantum technology, the interactions among photons are a crucial prerequisite as well, e.g., 1) for building single-photon transistors¹ [29]. They are devices for quantum computing which deals with the question how and whether one can build a quantum computer; 2) for quantum teleportation [30–32]: it is a process by which quantum information (e.g., the exact state of a photon) can be transmitted from one location to another. This can be realized with the help of classical communication and previously shared quantum entanglement between the sending and receiving location; 3) for metrology beyond the standard quantum limit [33].

¹It is a device in which a gate light pulse switches the transmission of a target light pulse with a gain above unity.

On the way to explore photon-photon interactions, impressive results have already been achieved in various systems, for instance: 1) in a system exhibiting electromagnetically induced transparency [34–37] which is a coherent optical nonlinearity which renders a medium transparent over a narrow spectral range within an absorption line; 2) in an ultra-thin glass fibre, a team [1] from University of Vienna created a strong interaction between two photons; 3) in nanoscale surface plasmons [23], which enables strong, coherent coupling between individual photons in conducting nano-structures, via excitation of guided plasmons localized to nanoscale dimensions; 4) in cavity quantum electrodynamic (cavity QED), where a single confined electromagnetic mode is coupled to an atomic system (e.g. a Rydberg atom, or a quantum dot) [38–42].

The achievements we mentioned above are mainly in optical frequencies. Recently, circuit quantum electrodynamic (circuit QED), which studied quantum interactions between light (the electromagnetic field) and atoms in the framework of electric circuits, are gradually becoming a routine tool for exploring the interactions between microwave photons [43–45]. In the world of electric circuits, photons can be understood as the quantized excitations of the electromagnetic field. As in cavity QED, a single photon within a single mode cavity coherently couples to a quantum object (atom). Interaction between the atom and a beam of light is very weak due to the unstable atom. As a result, it is hard to observe the effects which arise at the single-particle level. Normally, the solution is to confine the light in a cavity so that it bounces back and forth. In this way, a single photon can interact with an atom many times before it decays. In contrast, the photon in circuit QED is stored in a one-dimensional on-chip resonator and the quantum object is not a natural atom but an artificial one. The artificial atom is made of a small electronic circuit which can be positioned very precisely. It enable us to realize a strong coupling between the microwave field and the artificial atom. Beyond this, there are several other key advantages of circuit QED: 1) it gives us a huge amount of flexibility in how we design them – subject only to the engineering limitations of the fabrication techniques; 2) one can tune and tweak all the operating the desired parameters; 3) quantum effects in “*macroscopic*” systems are available to be explored. This opens up a new territory for quantum mechanics. Actually, circuit QED is worthwhile and interesting, not only because of the advantages mentioned above, but also for its potential applications. It is a prominent example for quantum information processing and a promising candidate for quantum computation.

As we argued above, the prototypical system for achieving strong photon-photon interactions in circuit QED consists of a quantum system coupled to a one-dimensional resonator. Such systems were first proposed theoretically [10, 24, 46–48], and soon afterwards achieved experimentally by means of a metallic

nanowire coupled to a quantum dot² [49, 50], and a transmission line coupled to one or several qubits³ [51–54].

The strength of the coupling between the local quantum system and the transmission line (or nanowire) has been studied theoretically in detail in the ohmic spin-boson model, which consists of a single two-level system (the spin) linearly coupled to the photons in the line (the bosons). It was shown [55, 56] that the coupling parameter is set by the ratio of the line impedance, Z , to the quantum of resistance, $R_Q = h/(2e)^2 \approx 6.45 \text{ k}\Omega$. The impedance of typical transmission lines (consisting of only geometric inductors and capacitors) is of order the vacuum impedance, $Z_{\text{vac}} \approx 377 \Omega$, thereby allowing only weak coupling.

Superconducting circuits are a promising platform for exploring strong coupling phenomena, and, indeed, the first experiments observing such phenomena have appeared [57, 58]. One benefit of using superconducting circuits is that a chain of Josephson-coupled superconducting islands acts as a transmission line with a large tunable impedance $Z \leq R_Q$, which is only limited by the superconductor/insulator transition [59]. Such transition originates from the competition between the charging energy and the Josephson energy of the Josephson junctions. More precisely, the Josephson junctions chain might be insulating at zero temperature even though each island is still superconducting. In the classical limit, i.e., the Josephson energy is much larger than the charging energy, the chain turns superconducting at low temperatures since the fluctuations of the phases are weak and the system is globally phase coherent. In the opposite limit (charging energy dominates over Josephson energy), the chain becomes a Mott insulator since the charges on each island are localized and an activation energy of the order of the charging energy is required to transport charges through the system (Coulomb blockade of Cooper pairs). Strong quantum fluctuations of the phases prevent the system from reaching long-range phase coherence in this regime. Recent experiments have studied the microwave properties of such Josephson junction chains [60–63]. Moreover, superconducting circuits allow the realization of a variety of quantum systems that behave like artificial atoms [15, 64]. In particular, these artificial atoms are usually realized using Josephson junction devices. As the only nonlinear dissipationless circuit element we know, Josephson junctions exhibit an atom-like energy spectrum. Last but not least, it is noticeable that quantum effects we studied are quite sensitive to the influence of the environment. Nevertheless, superconducting circuits provide a good platform. The superconducting state involves macroscopic degrees of freedom and thus exhibits better quantum coherence. By reducing the size of the superconductor, one can weaken the coupling between the superconducting state and the environment and thereby further

²Tiny particles or nanocrystals of a semiconducting material in the nanometer range.

³Two-state quantum systems that can be in a superposition of both states at the same time.

improve the quantum coherence. Owing to this, we have a non-dissipative system to study photon-photon interactions.

Using the superconducting circuit elements discussed above, we may construct a dual geometry (similar to cavity) in which a quantum system (realized by Josephson junction devices) is placed inside a transmission line (constituted by a chain of Josephson junctions). In fact, such experiments have already been reported [65, 66]. In the absence of coupling, photons propagate freely down the transmission line. A coupling between the quantum system and the line generates an effective photon-photon interaction that causes correlations among the photons. Thus, Josephson junction devices embedded in a chain of Josephson junctions (in the transmission line regime) constitute a good system to explore photon-photon interactions.

Other than the ones we have mentioned above, superconducting circuits are investigated widely in many aspects [67]. In particular, Josephson junction devices are supposed to be a two-level quantum system (qubit) at certain conditions [68]. More precisely, devices based on low-capacitance Josephson junctions exploit the coherence of the superconducting state, combined with the possibility to control individual charges by Coulomb blockade effects. Actually, various other physical systems were also suggested as possible realizations of qubits and gates, e.g., ions in electro-magnetic traps manipulated by laser irradiation [69], nuclear magnetic resonance on ensembles of molecules in liquids [70, 71], and cavity QED systems [72]. In comparison, the Josephson junction qubits are more easily embedded in electronic circuits and scaled up to large registers. This makes them appealing from the viewpoint of readout and gate implementation.

A long-term goal in quantum superconducting circuits is to build and couple several quantum bits in a controllable way for the ultimate design of practical quantum computers which may run exponentially faster than the classical ones. Impressive achievements such as the qubit control, entanglement [73–77], and demonstration of simple quantum algorithms [78] have already been obtained along the way. Specifically, the experiments show that two nearby qubits can be readily coupled with local interactions. However, realizing gates between an arbitrary pair of distant qubits is highly desirable for any quantum computer architecture. Very recently, Majer et al. [79] demonstrated a coherent, non-local coupling between two qubits [strongly coupled to a cavity (as a “qubit bus”)] in a circuit QED experiment. Theoretically, a possible qubit bus is proposed to be a one-dimensional waveguide [80]. By calculating the second-order correlation function $g_2(t)$, they indicated that a high degree of long-distance entanglement is generated between two qubit. In the system, quantum information carried by the “qubit bus” is transferred from one qubit to another one using microwave photons as the intermediary. As we argued before, the interactions among photons are essential for the information processing. Motivated by this, it will be interesting

to study photon-photon interactions in a system of one or several superconducting qubits embedded in a chain of Josephson junctions (in the transmission line regime). As a starting point, we study the case involving one qubit in this work.

Above, we discussed photon-photon interactions in a superconducting circuit. Then, a natural question is how to detect the interactions? To answer it, we first see the consequences of photon-photon interactions. It has led to, for instance, the prediction of Kondo physics [81], anti-bunching resulting from a photon-blockade effect [82, 83], inelastic photon scattering [82, 84, 85], and giant Kerr nonlinearities [86]. These effects in turn can be used to probe photon-photon interactions. In addition to these, a Josephson junction itself is actually a direct and simple probe to detect photon-photon interactions generated by the studied circuits. In particular, this can be done by measuring the dc current-voltage characteristic of an additional Josephson junction connected to the transmission line. According to dynamical Coulomb blockade theory [87, 88], Cooper pairs can tunnel inelastically through the probe junction provided that they can emit one or several photons into the environment, which in our case consists of the transmission line with the side-coupled circuit. Therefore, the dc current reflects both the elastic and inelastic scattering properties of photons.

The aim of this thesis is to describe the interaction between light and matter in circuit QED. In particular, we focus on probing the interactions of photons in a superconducting circuit. A long-term goal will be to understand how to generate and manipulate photons thanks to time-resolved electric control of the circuit.

1.2 Structure of the thesis

In this thesis we propose a method to realize and detect photon-photon interactions in a superconducting circuit. As shown in the dashed box of Fig. 1.1, the system we consider consists of a transmission line to which a nonlinear element is capacitatively side-coupled. The transmission line is realized by a chain of Josephson junctions with the Josephson energy dominating over the charging energy. In this regime, the phase fluctuations are largely suppressed and, thus, the chain behaves like a LC transmission line. In the absence of side-coupling, photon modes propagate freely down the line. The nonlinear element is realized by a Cooper pair box, which consists of a superconducting island coupled to a superconducting electron reservoir by a small Josephson junction. The coupling between the line and the Cooper pair box generates effective photon-photon interactions. We propose to detect this interaction using another voltage-biased Josephson junction (outside of the dashed box, named “*probe*”). Obviously, the current-voltage characteristic of the probe junction is influenced by the external environment in which photons interact with each other. Thus, we may use the

$I - V$ characteristic to probe the photon-photon interactions.

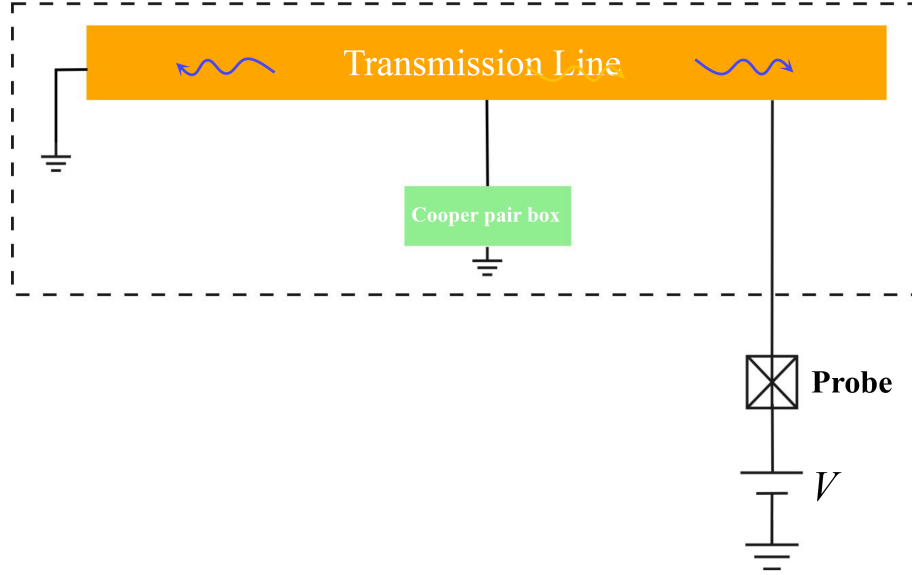


Figure 1.1: Schematic of the setup. The system consists of a transmission line and a side-coupled Cooper pair box, shown inside the dashed box. In absence of the side-coupling, photons propagate freely down the transmission line. The coupling between the line and the Cooper pair box generates photon-photon interactions. The resulting interactions are probed using another Josephson junction (outside the dashed box) whose current-voltage characteristic is sensitive to the properties of the photons.

We study the system in both the weakly and strongly nonlinear regimes. This can be achieved by modifying the two externally controllable electrodynamic parameters of the Cooper pair box: the gate voltage V_g , and the ratio of Josephson energy E_J to the charging energy E_c . In particular, varying the ratio E_J/E_c can be realized by replacing the Josephson junction of the Cooper pair box by two Josephson junctions in a loop configuration [i.e., the superconducting quantum interference device (SQUID)]. In this way, the effective Josephson coupling energy $E_J(\Phi) = E_J \cos(\pi\Phi/\Phi_0)$ is tunable, where Φ_0 denotes the quantum flux. By applying a flux Φ through the loop, we can get the desired ratio E_J/E_c . When $E_J/E_c \gg 1$ (weakly nonlinear regime), the Cooper pair box behaves as an weakly anharmonic oscillator; while for $E_J/E_c \ll 1$ (strongly nonlinear regime) the Cooper pair box effectively reduces to a two-level quantum system under certain conditions.

The thesis is organized in this way: we first introduce the elements of the studied circuit in chapter 2, as well as the needed theories and methods in chapter

3, respectively. After the two introductory chapters, we present our work in chapter 4 (weakly nonlinear regime) and chapter 5 (strongly nonlinear regime). We finally conclude in chapter 6.

In chapter 2, we introduce three elements of the studied circuit. Josephson junctions, being the basic elements in superconducting circuits, are presented at the beginning. The current-voltage characteristic of an ideal Josephson junction is also recalled. Then, the Cooper pair box is discussed. The relevant quantum degrees of freedom are excess Cooper pair charges on the small island. Under certain conditions, it allows us to realize different nonlinear elements. In the weakly nonlinear regime, when the Josephson energy dominates over the charging energy, the Cooper pair box behaves as a weakly anharmonic oscillator. In the strongly nonlinear regime, the Cooper pair box reduces to a quantum two-level system (qubit) with two states differing by one Cooper pair charge on the superconducting island. Next, we describe the properties of Josephson junction chains, including the superconductor/insulator transition [89]. In the regime where the Josephson energy dominates over charge energy, the chain behaves as a high-impedance (compared to the vacuum impedance) LC transmission line which contains the modes of propagating photons. Last but not least, Josephson junctions are a direct means to detect the influence of their environment. The photon properties in the environment affect the current-voltage characteristic of the Josephson junctions. Based on these elements, we can construct the studied circuit shown in Fig. 1.1.

In chapter 3, the adopted theories and methods are presented. First of all, we introduce dynamical Coulomb blockade theory [also called $P(E)$ -theory] [87], which describes how the current-voltage characteristic of a tunnel junction is influenced by its environment. In particular, we are interested in how the photon-photon interaction generated in the nonlinear electromagnetic system (dashed box of Fig. 1.1) affects the $I - V$ characteristic of the probe junction. $P(E)$ theory states that the current flowing through the probe junction is expressed in terms of the exponential phase-phase correlation function $\langle e^{i\phi}(t)e^{-i\phi}(0) \rangle_{H_{\text{env}}}$ of the nonlinear electromagnetic environment, ϕ being the phase of the probe node and H_{env} is the environmental Hamiltonian. Physically, we can interpret the correlation function in terms of photon processes. These processes can be decomposed into single photon processes (corresponding to two-point correlators), and n ($n \geq 2$)-photon processes (corresponding to $2n$ -point correlators). If H_{env} is linear, the multiple photons propagate freely. Otherwise photons may interact with each other. To compute the exponential phase-phase correlation function in nonlinear regime, we will adopt two different methods: Green's function perturbation theory and the path integral method. The former one will be applied to evaluate the two-point and four-point phase-phase correlators in both chapter 4 and chapter 5. The advantage of this method one is that it provides a clear physical picture which helps us to understand the scattering processes of photons, and particularly the interactions

between photons. By contrast, when the multiple photon processes do play a role, one must take care of the $2n$ ($n \geq 3$)-point correlators, and the calculations for the perturbation theory become cumbersome. Then we use the path integral method, which can be a convenient way to compute the entire exponential phase-phase correlation function. We will see an example in detail in chapter 5.

In chapter 4, we consider a weakly nonlinear system that consists of a transmission line to which a weakly anharmonic oscillator is side-coupled. As a starting point, we consider the linear regime, where photons do not interact with each other. The side-coupled element is a harmonic oscillator with resonance frequency ω_s . Green's functions are used to compute the phase-phase correlation functions, which are needed to calculate the current flowing through the probe junction. By numerically solving the integral equation defining the $P(E)$ function, we obtain a resonant feature around $2eV = \hbar\omega_s$ (\hbar is Plank constant) in the current-voltage characteristic of the probe junction. This resonance corresponds to single photon processes. The result can be understood: when a Cooper pair tunnels through the probe junction, it releases energy $2eV$ by emitting one or several photons to the environment. For single photon processes, the photon is exactly resonant on the side-coupled oscillator, thus no current flows as the photon is completely blocked. Whereas for the multiple photons processes, all the photons can not be on resonance with the side-coupled circuit at the same time, and therefore this results in a finite current.

We then add the effect of a weak nonlinearity. Green's function perturbation theory is applied to compute single photon processes and two photons processes, respectively. For the single photon processes, we find that the weak nonlinearity renormalizes the resonance frequency to ω'_s . For the two-photon processes, the interaction between two photons causes new contributions. This leads to an additional feature at $2eV = 2\hbar\omega'_s$ in the current-voltage characteristic. Cooper pairs tunnel through the probe junction, emitting photons with total energy $2\omega'_s$ to the environment. When each photon carries half of the emitted energy (namely ω'_s), both photons are resonant with the oscillator, and thus, they interact strongly. Comparing with the linear regime, we find that the resonant feature at $2eV = 2\hbar\omega'_s$ in the current-voltage characteristic of the probe is a direct signature of the photon-photon interaction in the system.

The amplitude of the resonant feature due to photon-photon interactions is estimated using realistic parameters [90–92]. It may reach amplitudes in the pA range which is well within current experimental measuring techniques.

In chapter 5, we study the strongly nonlinear regime. In contrast with chapter 4, the Cooper pair box reduces to a charge qubit which is described by a spin-1/2 representation. Furthermore, the diagonalized form of the transmission line can be written as a collection of photons (boson). Therefore, the system is described by a spin-boson Hamiltonian H_{sb} .

In order to evaluate the current through the probe junction, the exponential phase-phase correlator $\langle e^{i\phi_m(t)}e^{-i\phi_m(0)} \rangle_{H_{sb}}$ needs to be computed as before. We first use perturbation theory to evaluate the two-point and four-point phase-phase correlators, respectively. With this step, we find that computing phase-phase correlators is transformed to calculating spin-spin correlator at the “impurity” (the qubit). Then, the problem can be mapped to the well-studied problem that a two-state system coupled to a bosonic bath. In particular, the coupling term between the transmission line and the qubit is used as the perturbation. We sum up the interaction series to all orders. When the coupling between the transmission line and the charge qubit is weak, we may neglect higher orders contributions. However, when we are interested in strong coupling, the contributions of the $2n$ ($n \geq 3$)-point correlators must be considered. In this case, the calculations using perturbation theory become complicated. Therefore we prefer using the path integral method to compute the entire correlator. The resulting phase-phase correlator is expressed in terms of spin-spin Green’s functions. Next, we use Bloch equations (in the weak coupling regime) to evaluate the two-point spin-spin Green’s function.

Our results indicate that scattering of individual photons by the side-coupled qubit results in a resonant feature in the $I - V$ characteristic of the probe junction at $2eV = \hbar\omega_{qb}$, where ω_{qb} is the resonance frequency of the qubit. With this result as a starting point, it will be interesting to see how photon-photon interactions modify the resonant features in this regime.

In chapter 6, we list the main findings. Furthermore, future perspectives are elucidated with a description of the upcoming work.

Finally, we attach several **appendices**, in which we provide the details of some derivations/calculations.

Key elements of the studied circuit

This chapter aims to present the three key elements needed in our studied circuit. We start by reviewing the Josephson effect in Sec. 2.1, where the current-voltage characteristic of an ideal Josephson junction is discussed. Next, the Cooper pair box is described in Sec. 2.2. It enables us to realize two different elements: the anharmonic oscillator in the weakly nonlinear regime and the charge qubit in the strongly nonlinear regime. Finally, we introduce the LC transmission line in Sec. 2.3. Josephson junction chains are proposed to realize a high impedance (higher than the vacuum impedance) transmission line. The superconductor-insulator transition in the chain is discussed. In the superconducting regime, the chain behaves as an effective LC transmission line with freely propagating electromagnetic modes (photons).

2.1 Josephson junction

Superconductivity is a well-known macroscopic quantum phenomenon, with zero electrical resistance and expulsion of magnetic fields, occurring in certain materials when cooled below a critical temperature [93]. In a superconductor the electrons close to the Fermi energy μ bind together to form Cooper pairs which are bosons with charge $2e$. All the Cooper pairs in the boson condensate are in the same quantum state and can be characterized by a single wave function, also called the superconducting order parameter $\psi = \psi_0 e^{i\phi}$, with the amplitude ψ_0 and phase ϕ . Another essential property of superconductors is the existence of an energy gap 2Δ . In a superconductor, energy 2Δ is needed to break a Cooper pair. This is unlike the normal metal where the state of an electron can be changed by adding an arbitrarily small amount of energy.

A Josephson junction is formed when we separate two superconductors by a thin insulating layer, shown in Fig. 2.1. For simplification, we assume that the energy gaps of the two superconductors to be the same. The Cooper pair state in the left (right) superconductor of the junction is described by $\psi_{L(R)} e^{i\phi_{L(R)}}$. Because the barrier is quite thin, the wave functions of the two superconductors

can overlap, allowing the tunneling of Cooper pairs. This implies that the current could flow through the Josephson junction even without a voltage source. The amplitude of the current is proportional to the sine of the phase difference ($\Delta\phi = \phi_L - \phi_R$) across the junction, which was first predicted by Josephson [94]:

$$I = I_c \sin(\Delta\phi), \quad (2.1)$$

where the critical current I_c is the maximum supercurrent that the junction can support. At zero magnetic field and zero temperature, the critical current $I_c = \pi\Delta/(2eR_N)$ (R_N is the normal state resistance of the junction) which is called the Ambegaokar-Baratoff relation [95]. The relation (2.1) describes the well-known dc Josephson effect. As long as the current I is smaller than the critical current I_c , it can flow through the Josephson junction without any voltage drop.

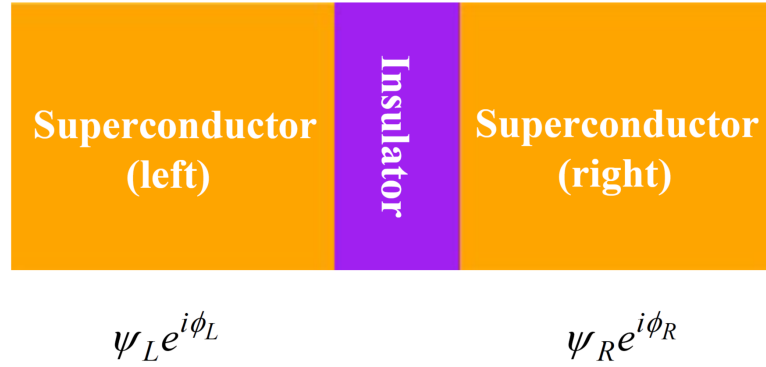


Figure 2.1: Diagram of a Josephson junction which consists of two superconductors separated by a thin insulator. The wave function $\psi_{L(R)} e^{i\phi_{L(R)}}$ is used to describe the Cooper pair state in the left (right) superconductor.

When a finite voltage V is applied, the phase across the junction evolves. The dynamics of this effect, known as the ac Josephson effect, is governed by the equation [94]:

$$\frac{d}{dt}(\Delta\phi) = \frac{2e}{\hbar}V, \quad (2.2)$$

Plugging Eq. (2.2) into Eq. (2.1), we obtain

$$I(V,t) = I_c \sin(2eVt/\hbar). \quad (2.3)$$

That is, the current oscillates with a frequency $\nu/V = 2e/h \approx 483.6$ GHz/mV ($h = 2\pi\hbar$). The quantum energy $h\nu$ equals the energy change of a Cooper pair transferred across the junction.

Using the Josephson relations (2.1) and (2.2), one can directly derive the energy stored in the junction

$$F \equiv \int dt V(t)I(t) = \frac{\hbar}{2e} I_c \int d(\Delta\phi) \sin \Delta\phi = -E_J \cos \Delta\phi + \text{const.}, \quad (2.4)$$

where the Josephson energy $E_J = \hbar I_c / 2e$ is the coupling energy.

2.1.1 Current-voltage characteristic

The current-voltage characteristic schematic of an ideal voltage-biased Josephson junction is shown in Fig. 2.2 (a). There is no current flow until $|V| = 2\Delta/e$. Beyond this point, the current is proportional to the applied voltage, i.e., the current-voltage characteristic is of the same form as an ohmic resistor, i.e., $I = V/R_N$.

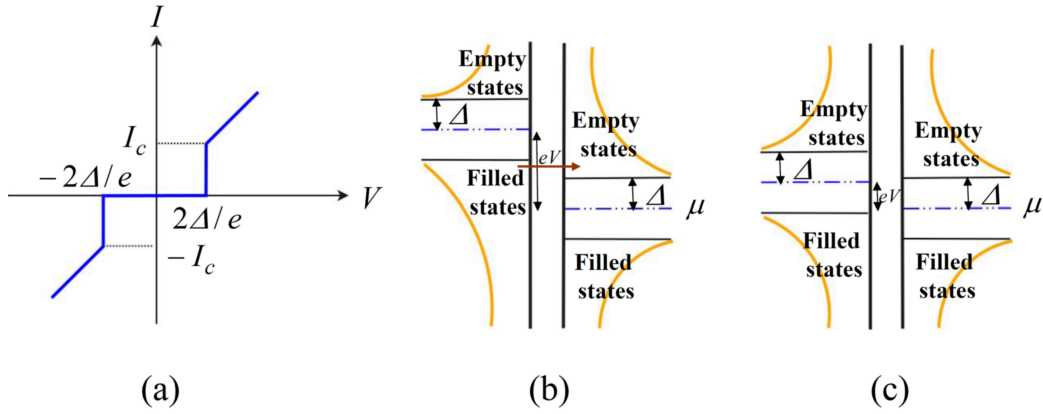


Figure 2.2: (a) The schematic of current-voltage characteristic of a voltage-biased Josephson junction. The density of states is plotted horizontally vs. energy vertically at zero temperature for two different voltage regimes: (b) $|V| > 2\Delta/e$ and (c) $|V| < 2\Delta/e$. The parts labelled as “Filled states” mean states occupied by quasiparticles. The horizontal arrow in (b) depicts quasiparticles tunnelling.

To understand this characteristic, we introduce the density of states in the superconducting leads on each side of the Josephson junction, shown in Fig. 2.2 (b) for $|V| > 2\Delta/e$ and (c) for $|V| < 2\Delta/e$, respectively. There are two kinds of charge carriers, namely Cooper pairs and quasiparticles. At zero temperature, all states up to the Fermi level μ are filled, and no quasiparticles is excited. At finite temperature T , the probability of the quasiparticles (with excitation energy $E_{\text{qp}} \geq \Delta$) which are excited in thermal equilibrium is given by the usual Fermi function $f(E_{\text{qp}}) = (1 + e^{E_{\text{qp}}/k_B T})^{-1}$. Considering the condition $\Delta \gg k_B T$, the probability of thermal excitation $f(E_{\text{qp}})$ goes to zero. Thus, it is a good approximation for

us to neglect the thermal fluctuations. Next, we discuss the two different voltage regimes, respectively.

In the regime $|V| > 2\Delta/e$, the potential difference supplies enough energy to break a Cooper pair, creating a hole on one side and a particle on the other. One can see from Fig. 2.2 (b) that the quasiparticles from the left “Filled states” band can tunnel into the “Empty states” on the right. Since the density of states of the quasiparticles is infinite at the gap edges, it turns out that there is a discontinuous jump in current at $|V| = 2\Delta/e$.

In the regime $|V| < 2\Delta/e$, the dc current vanishes. Indeed, the time average of the current [Eq. (2.3)] over a time period $h/2eV$, turns out to be zero. Actually, this can be understood from Fig. 2.2 (c). When a finite voltage V is applied, the Fermi level of the left superconductor moves up to $\mu + eV$. It is apparent that Cooper pair states can not tunnel through from left to right. In addition, the potential difference cannot provide enough energy to excite quasiparticles from the left “Filled states” to the “Empty states” on the right. Instead, Cooper pairs oscillate coherently between the leads.

However, what we discussed above is true only in the ideal case (dissipationless system). In real experiments, the current-voltage characteristic of the Josephson junction is definitely modified by the environment. Take the regime $|V| < 2\Delta/e$ as an example, Cooper pairs described in Fig. 2.2 (c) can tunnel inelastically by releasing energy $2eV$ to the dissipative environment. Detailed discussions will be deferred to chapter 3.

2.1.2 Summary

In this section, the dc and ac Josephson effects were recalled briefly. Moreover, we discussed the current-voltage characteristic of an ideal voltage-biased Josephson junction.

As fundamental elements in superconducting circuits, Josephson junctions are needed for the realization of other usable elements or devices. In our project, we will concentrate on two elements: a Cooper pair box, which is the simplest solid state device to realize a quantum bit; and a Josephson junction chain, which can be used to realize a high impedance (compared to vacuum impedance) transmission line.

2.2 Cooper pair box

In this section, we introduce a simple and controllable superconducting device: the Cooper pair box, which can be used to realize a weakly anharmonic

oscillator or a charge qubit under certain conditions.

The Cooper pair box was first proposed theoretically [96, 97] and afterwards realized in experiments [98]. As shown in Fig. 2.3, it consists of a superconducting island (green box) connected to a superconducting electron reservoir via a small Josephson junction. In classical regimes, a Josephson junction acts naturally like a capacitor with capacitance C . Therefore we often model the Josephson junction as a tunnel junction in parallel with a capacitor. Electrons tunnel from the reservoir to the island by means of a gate voltage V_g connected to the island via a gate capacitance C_g .

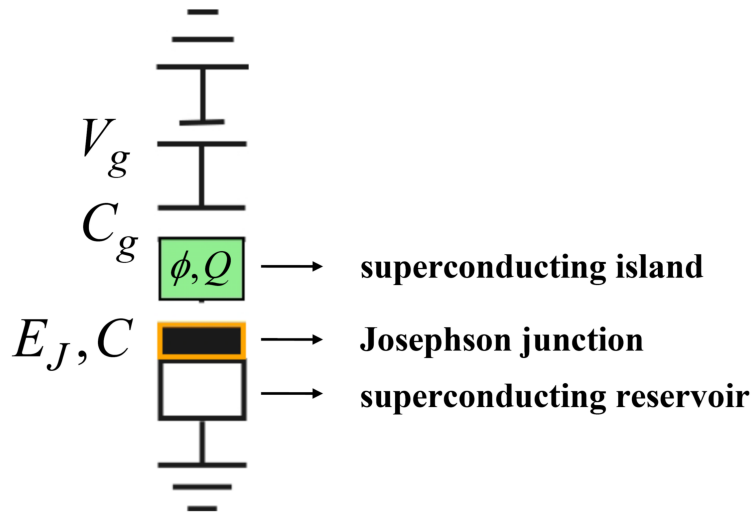


Figure 2.3: Schematic of a Cooper pair box. It is formed of a superconducting island (green box) coupled by a Josephson junction (with capacitance C) to a superconducting reservoir. Excess Cooper pairs tunnel into the island by applying a gate voltage V_g via a gate capacitor C_g . The system is described by the Hamiltonian (2.5).

Comparing with the Cooper pair tunnelling described in Sec. 2.1, there is one important difference. In addition to the Josephson energy E_J , a second energy scale: the Coulomb charging energy $E_c = e^2/C_\Sigma$ ($C_\Sigma = C + C_g$ is the total capacitance of the island), the energy needed to add an extra electron charge to the island, plays an important role when it exceeds the thermal energy $k_B T$ (k_B is the Boltzmann constant). This has become possible because low capacitances (by reducing the dimensions of the junction) are able to be fabricated with the development of microfabrication techniques. Taking an example, a Josephson junction with an area of $0.1 \times 0.1 \mu\text{m}^2$ and a typical oxide layer thickness of 1nm has a capacitance of about 1fF corresponding to a temperature close to 1K. Of course,

by decreasing capacitance, this restriction on temperature becomes more relaxed. Hence, the Hamiltonian of the Cooper pair box is written as

$$H_{\text{cpb}} = \frac{(Q + C_g V_g)^2}{2C_\Sigma} - E_J \cos \phi, \quad (2.5)$$

where $C_g V_g$ corresponds to the charge induced on the gate capacitance; Q is the charge operator of the excess Cooper pairs in the island, and ϕ is the operator of the phase difference across the Josephson junction. As charge is quantized (in units of $2e$), its conjugate variable is periodic. The competition between these two canonically conjugated variables is captured by the following Heisenberg relation,

$$[\phi, Q] = 2ie. \quad (2.6)$$

The interplay between charging effects and the Josephson effect causes interesting behaviours. In particular, taking different ratios of E_J/E_c , we realize two different kinds of nonlinear elements: a weakly anharmonic oscillator and a charge qubit.

2.2.1 Weakly anharmonic oscillator

If we consider the regime where the Josephson energy is much larger than the charging energy, the Josephson junction behaves as an inductor. Consequently, the Cooper pair box behaves like a quantum LC oscillator. At $E_J \gg E_c$, fluctuations of the phase are small. Thus, one may expand the cosine potential around one of its minima, e.g., $\phi = 0$. Phase slip events that connect two different minima of the cosine potential are exponentially suppressed in this regime and may therefore be neglected. Therefore, we expand the cosine up to second order (and drop the zeroth order term that is just a constant). Doing so, the Hamiltonian (2.5) reduces to

$$H_{\text{cpb}}^{(0)} = \frac{(Q + C_g V_g)^2}{2C_\Sigma} + \frac{E_J}{2} \phi^2. \quad (2.7)$$

The Hamiltonian (2.7) is diagonalized by using a mechanical analogue: the position coordinate corresponds to the phase ϕ , while the role of the conjugate momentum is played by the charge $Q + C_g V_g$. Rewriting the phase and charge operators in terms of creation and annihilation operators, i.e., $\phi = (2E_c/E_J)^{1/4}(a + a^\dagger)$ and $Q + C_g V_g = (e/i)(2E_c/E_J)^{1/4}(a - a^\dagger)$, and then substituting them into Eq. (2.7), we obtain the standard diagonalized form: $H^{(0)\text{diag}} = \hbar\omega_{\text{cpb}}(a^\dagger a + 1/2)$, where $\omega_{\text{cpb}} = \sqrt{8E_c E_J}/\hbar$ is the resonance frequency (known as the Josephson plasma frequency).

Actually, the Josephson junction is a nonlinear inductor. Beyond the harmonic case, we may expand the Josephson energy up to the quartic term in the phase, i.e.,

$-E_J \cos \phi \approx -E_J + \phi^2 E_J/2 - \phi^4 E_J/24$, which allows us to construct a weakly nonlinear element with the Hamiltonian

$$H_{\text{cpb}} = H_{\text{cpb}}^{(0)} - \frac{E_J}{24} \phi^4. \quad (2.8)$$

Using $\phi = (2E_c/E_J)^{1/4}(a + a^\dagger)$, we write the weakly anharmonic term in a simple form which is useful for first order perturbation theory,

$$-\frac{E_J}{24} \phi^4 = -\frac{1}{12} E_c (a^\dagger + a)^4 \approx -\frac{E_c}{2} (a^\dagger a^\dagger a a + 2a^\dagger a). \quad (2.9)$$

Here we dropped terms in which the number of creation and annihilation operators is not the same, because they do not contribute in perturbation theory.

Substituting $H_{\text{cpb}}^{(0)}$ and Eq. (2.9) into Eq. (2.8), the second term of Eq. (2.9) can be combined with $H^{(0)\text{diag}}$. Doing so, we find that the quartic term renormalizes the resonance frequency

$$H_{\text{cpb}} = \hbar \nu' (a^\dagger a + 1/2) - \frac{E_c}{2} a^\dagger a^\dagger a a \quad (2.10)$$

where the renormalized resonance frequency reads $\nu' = \nu - E_c/\hbar$. Using the definition of ω_{cpb} , we obtain the shifted frequency

$$\delta \nu = E_c/\hbar = \omega_{\text{cpb}}^2/(8E_J). \quad (2.11)$$

The second term of Eq. (2.10) introduces the anharmonicity. In particular, it describes two-particle processes. We will see that it plays an important role in chapter 4.

We studied the weakly nonlinear regime of the Cooper pair box. The advantage of this regime is that the charge noise is largely reduced, since the energy spectrum is approximately independent of gate charge.

2.2.2 Charge qubit

In contrast with the weakly nonlinear regime discussed above, we now switch to the opposite regime. In particular, we consider a low capacitance Josephson junction whose charging energy E_c dominates over the Josephson energy E_J . In this case, the superconducting energy gap Δ is assumed as the largest energy, i.e., larger than thermal energy $k_B T$ and the charging energy $e^2/(2C_\Sigma)$. Under these conditions, electrons on the island all are paired and condense into a single macroscopic ground state, separated by the superconducting gap from the excited states with quasiparticles. When the gate voltage V_g is switched on, Cooper pairs are

transferred from the reservoir to the island. Therefore the only degree of freedom of the island is the number of excess Cooper pairs n which is related to the total charge of the island by $Q = -2en$. Note that n can take any integer values. The island is electrically neutral for $n = 0$. Positive n represents Cooper pairs tunnelling onto the island, while negative n means Cooper pairs tunnelling out of the island. It is convenient to introduce number operator \hat{n} whose eigenstate $|n\rangle$ are the charge states of the island:

$$\hat{n}|n\rangle = n|n\rangle. \quad (2.12)$$

Using this basis, we rewrite the Hamiltonian (2.5) as

$$H_{\text{cpb}} = 4E_c \sum_n (\hat{n} - n_g)^2 |n\rangle\langle n| - \frac{E_J}{2} \sum_n \left(e^{i\phi} |n\rangle\langle n| + e^{-i\phi} |n\rangle\langle n| \right), \quad (2.13)$$

where we inserted an identity matrix $\sum_n |n\rangle\langle n| = I$, and $n_g = -C_g V_g / (2e)$ is the dimensionless gate charge and acts as a control parameter. The commutation relation (2.6) of the operators becomes $[\phi, \hat{n}] = i$. Additionally, two useful relations are

$$e^{i\phi} |n\rangle = |n+1\rangle, \quad e^{-i\phi} |n\rangle = |n-1\rangle, \quad (2.14)$$

which indicate that the operator $e^{i\phi}$ creates a Cooper pair on the island, while $e^{-i\phi}$ destroys a Cooper pair. Substituting Eq. (2.14) into Eq. (2.13), and rewriting it in a symmetric form, we get

$$H_{\text{cpb}} = 4E_c \sum_n (n - n_g)^2 |n\rangle\langle n| - \frac{E_J}{2} \sum_n (|n\rangle\langle n+1| + |n+1\rangle\langle n|). \quad (2.15)$$

As $E_J \ll E_c$, the charging energy dominates. In the limit $E_J = 0$, the eigenstates of the Hamiltonian are the Cooper pair number states $|n\rangle$ with electrostatic energy $E_n = 4E_c(n - n_g)$ as their eigenvalues. The energy spectrum (dashed parabolas) is plotted in Fig. 2.4. The electrostatic energy varies with n_g periodically¹. The adjacent states are degenerate when n_g is half-integer. As the voltage (namely n_g) is swept, the Cooper pairs enter the island one by one at the degeneracy point. Therefore the average value of the Cooper pair number n is quantized and exhibits a step-like function with a period of $n_g = 1$, as shown in Fig. 2.5.

When the Josephson energy E_J is finite, the energy spectrum is modified. For most values of n_g the energy levels are still dominated by the electrostatic energy. However, when n_g is approximately half-integer, i.e., the electrostatic energies of

¹In the weakly nonlinear regime, i.e., $E_J \gg E_c$, the case is different. We find that the energy scale [expressing as $\Delta\omega_{\text{cpb}}/\omega_{\text{cpb}} \sim (E_c/E_J)^{1/4} \exp(-\sqrt{E_J/E_c})$] related to oscillation is much smaller than the shifted frequency [see Eq.(2.11)]. As a result, the eigenstates and the eigenvalues are independent of the gate voltage. This consequence will be seen clearly in chapter 4.

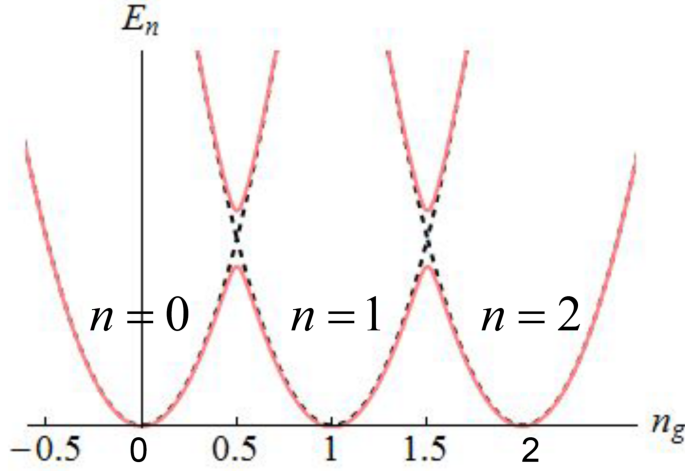


Figure 2.4: The energy spectrum of the Cooper pair box is shown as a function of the dimensionless gate charge n_g with different numbers of extra Cooper pairs n on the island (dashed parabolas). Near degeneracy points, the weaker Josephson coupling mixes the charge states and modifies the energy of the eigenstates (solid lines). In the vicinity of these points, the system effectively reduces to a two-level quantum system.

two adjacent states are close to each other, and the Josephson tunnelling mixes them strongly. As a result, the degeneracy points are lifted by the Josephson term. This can be seen clearly from the solid lines of Fig. 2.4, which are obtained by calculating numerically the eigenvalues of the Hamiltonian (2.15). Let us concentrate on the voltage range near a degeneracy point (e.g. $n_g = 0.5$) where only two charge states, say $|0\rangle$ and $|1\rangle$, play a role, while all other charge states, having much higher energies, can be ignored. In this case, the Cooper pair box reduces to a two-level quantum system (qubit) with the two states differing by one Cooper pair charge on the island.

Next, we can straightforwardly obtain the two-level Hamiltonian by taking $n = 0, 1$ only in Eq. (2.15). Transforming it to matrix form, we obtain

$$H_{\text{qb}} = \begin{pmatrix} 4E_c n_g^2 & -E_J/2 \\ -E_J/2 & 4E_c(1 - n_g)^2 \end{pmatrix} \quad (2.16)$$

We can identify this expression with the Hamiltonian of a spin-1/2 in a magnetic field \vec{B} by expressing H_{qb} using Pauli matrices $\sigma_x, \sigma_y, \sigma_z$. The Hamiltonian above is then rewritten as

$$H_{\text{qb}} = E_c [(1 - 2n_g)^2 + 1] \mathbf{I} - B_z \sigma_z - B_x \sigma_x = -\vec{B} \cdot \vec{\sigma} + \text{const.}, \quad (2.17)$$

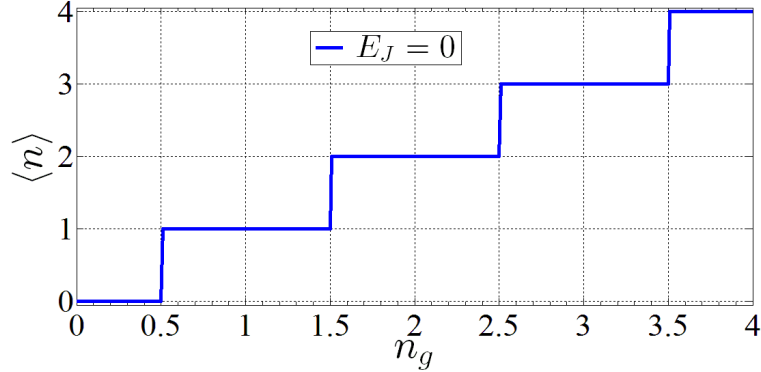


Figure 2.5: The average number of excess Cooper pairs on the island dependent of n_g in the absence of Josephson coupling energy ($E_J = 0$) at zero temperature.

where \mathbf{I} is the unit matrix, and the constant term can be dropped. $\vec{\sigma}$ is the spin operator with components $(\sigma_x, \sigma_y, \sigma_z)$. The magnetic field \vec{B} consists of components in the (x, y, z) space. The z -component of the magnetic field, $B_z = 2E_c(1 - 2n_g)$ (which is controlled by the gate voltage) corresponds to the charging energy splitting, while the Josephson energy provides the x -component of the magnetic field, $B_x = E_J/2$ (see Fig. 2.6).

For later convenience we rewrite the Hamiltonian (2.17) as

$$H_{\text{qb}} = -\frac{\Delta E}{2} (\cos \eta \sigma_z + \sin \eta \sigma_x), \quad (2.18)$$

where $\Delta E = \sqrt{[4E_c(1 - 2n_g)]^2 + E_J^2}$ is the energy difference between the ground state and the excited state, and $\eta = \tan^{-1} [E_J/4E_c(1 - 2n_g)]$ determines the direction of the magnetic field in the $x - z$ plane (see Fig. 2.6). At the degeneracy points, i.e., $\eta = \pi/2$, the splitting energy reduces to E_J and the system Hamiltonian becomes $H_{\text{qb}} = -(E_J/2)\sigma_x$.

We denote the ground (excited) state as $|g\rangle(|e\rangle)$. The eigenvalues $E_{g(e)}$ and eigenstates are solved from Eq. (2.18). Namely

$$\begin{aligned} E_g &= -\frac{\Delta E}{2}, & E_e &= \frac{\Delta E}{2}. \\ |g\rangle &= \cos \frac{\eta}{2} |0\rangle + \sin \frac{\eta}{2} |1\rangle, & |e\rangle &= -\sin \frac{\eta}{2} |0\rangle + \cos \frac{\eta}{2} |1\rangle, \end{aligned} \quad (2.19)$$

where $|0\rangle = (0, 1)^T$ and $|1\rangle = (1, 0)^T$, correspond to zero and one excess Cooper pair states, respectively. The ground state is a superposition of states $|0\rangle$ and $|1\rangle$.

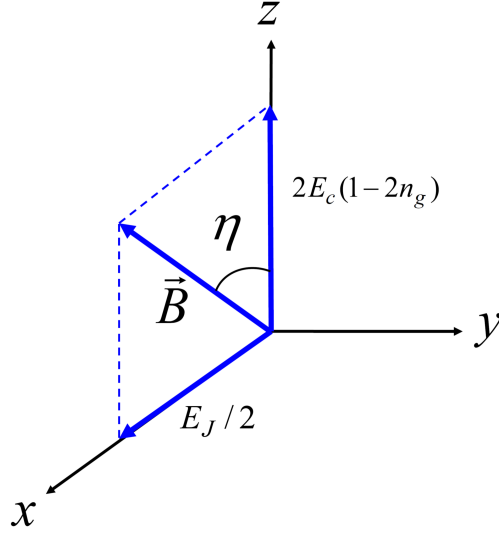


Figure 2.6: Spin representation for the charge qubit. The qubit Hamiltonian (2.18) is seen as a spin-1/2 interacting with an external magnetic field \vec{B} .

Then the average number of excess Cooper pairs is no longer quantized but varies continuously with the gate voltage n_g . We can compute the average number of Cooper pairs on the island by projecting \hat{n} on the ground state:

$$\langle n \rangle = \langle g | n | g \rangle = \sin^2 \frac{\eta}{2} = \frac{1}{2} (1 - \cos \eta). \quad (2.20)$$

Substituting the definition of η and defining the ratio $\Upsilon = E_J/4E_c$, we obtain

$$\langle n \rangle = \frac{1}{2} \left[1 - \frac{1 - 2n_g}{\sqrt{(1 - 2n_g)^2 + \Upsilon^2}} \right]. \quad (2.21)$$

According to Eq. (2.21), we plot the average number of the Cooper pairs on the island dependent of n_g with different ratio Υ , as shown in Fig. 2.7. By increasing the value of Υ , the fluctuations of the charge are stronger and stronger. Consequently the slope at the degeneracy point ($n_g = 0.5$), which is equal to $1/\Upsilon$, gradually flattens.

Taking advantage of the period of $n_g = 1$, we can extend the results to the whole n_g range, as shown in Fig. 2.8. Comparing to the case with zero coupling energy (see Fig. 2.5), the steps become round due to the existence of charge fluctuations. This feature was verified experimentally [98].

Finally, we transform the charge $Q + C_g V_g = 2e(\hat{n} - n_g)$ on the island to the spin-representation, which will be needed when we study the charge coupling

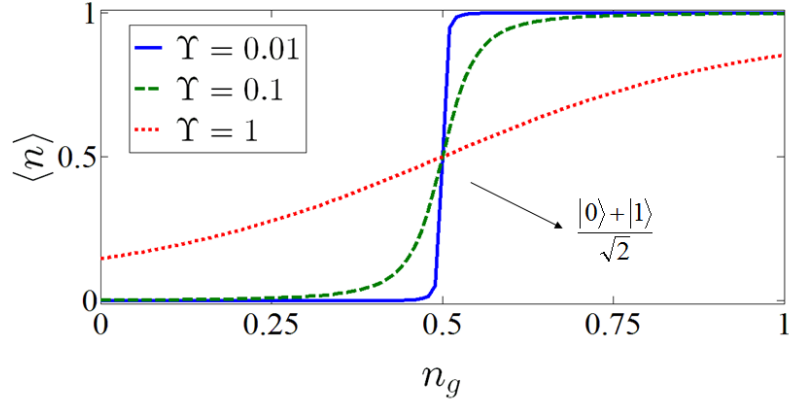


Figure 2.7: The average number value of excess Cooper pairs on the island as a function of n_g , with different $\Upsilon = 0.01, 0.1, 1$.

between a charge qubit and a transmission line in chapter 5. In matrix form, it reads

$$Q + C_g V_g = 2e \begin{pmatrix} \langle 0 | \hat{n} - n_g | 0 \rangle & \langle 0 | \hat{n} - n_g | 1 \rangle \\ \langle 1 | \hat{n} - n_g | 0 \rangle & \langle 1 | \hat{n} - n_g | 1 \rangle \end{pmatrix} = -e \sigma_z, \quad (2.22)$$

where we dropped the constant term $(1 - 2n_g)$.

We showed that the Cooper pair box reduces to an effective charge qubit in the strongly nonlinear regime. The interplay between the charging effects and the Josephson coupling results in a coherent quantum superposition of two charge states. Experimentally, this was first realized by the Saclay group [98], where they used a single-electron transistor coupled to a Cooper pair box and the average value of the charge of the box was measured. Their results provided the direct evidence that the ground state of a Cooper pair box can be a coherent superposition of only two charge states. Later, the NEC group [99] applied a short voltage pulse via a gate electrode, shown in Fig. 2.9. The applied pulse modified the energies of the two charge states non-adiabatically, and brought them into resonance. The resulting superposition of the two charge states was detected by a tunnelling current through a probe junction. It was shown that the coherent oscillations can be observed in the time domain. Their results demonstrated electrical coherent control of a charge qubit.

2.2.3 Summary

The Cooper pair box, as a controllable nonlinear device, was discussed in two different regimes. On the one hand, it can be used to realize a weakly anharmonic oscillator in the weakly nonlinear regime. Moreover, this weak nonlinearity

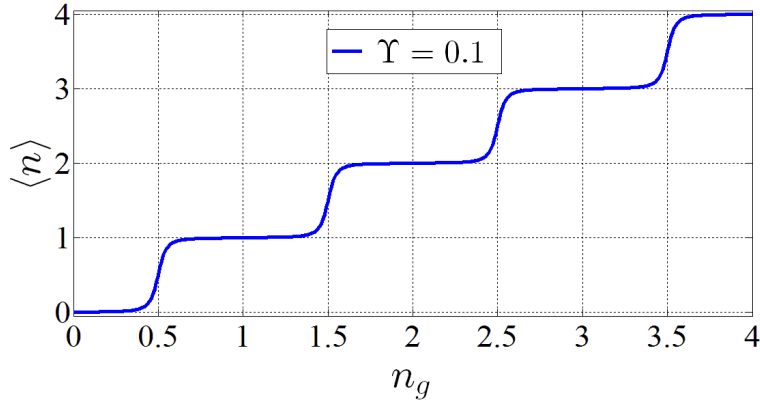


Figure 2.8: The average number of excess Cooper pairs on the island as a function of n_g with $\Upsilon = 0.1$.

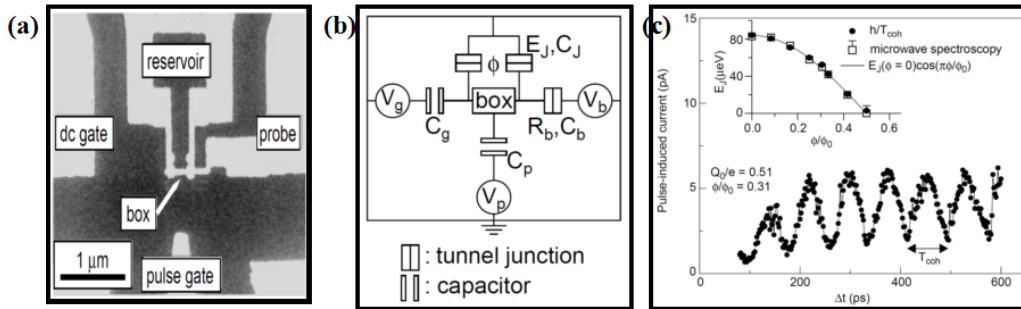


Figure 2.9: (a) Micrograph of the sample: Single Cooper pair box with a probe junction. (b) Circuit diagram of the device. (c) Pulse-induced current dependent of the pulse length. Inset: Josephson energy E_J as a function of the magnetic flux Φ penetrating through the loop. (from reference [99])

renormalizes the resonance frequency of the oscillator. On the other hand, in the strongly nonlinear regime, the Cooper pair box effectively reduces to a charge qubit. The relative energy of the two levels can be controlled through the gate voltage.

2.3 LC transmission line

An LC transmission line consists of a chain of discrete components: inductances L and capacitances C_0 , as shown in Fig. 2.10. It is a discrete model of a one dimension waveguide which is usually used to transmit electromagnetic signals which are composed of microwave photons [100].

Assume the line is infinite and in the continuum limit, then the dispersion relation (the relationship between frequencies and wave vectors) of photons behaves linear [87], i.e., $\omega_k = \omega_0 ka$, where $\omega_0 = 1/\sqrt{LC_0}$, k is the wave vector, and a is the lattice parameter in this discrete model.

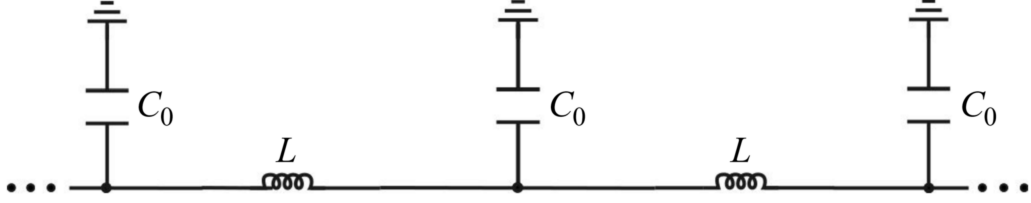


Figure 2.10: Schematic diagram of an LC transmission line. It consists of a set of discrete inductances L and ground capacitances C_0 .

The impedance of the infinite transmission line, $Z(\omega)$, which is defined as the ratio of the amplitudes of voltage and current of a single photon propagating along the line, is independent of frequency [87]. In this discrete model, we have the relation $Z(\omega) = Z_0$, where $Z_0 = \sqrt{L/C_0}$. Here, L and C_0 are only determined by geometrical factors, as well as the dielectric constant and permeability of the materials that are used to make them. Assuming that they do not deviate much from vacuum constant, we find $Z_0 \sim 100 \Omega$. One can see it is of the order of vacuum impedance². As $Z_{\text{vac}} \approx 377 \Omega$ and the quantum resistance $R_Q = 6.45 \text{ k}\Omega$, we find that the impedance of a normal transmission line is much smaller than the quantum resistance.

As stated in chapter 1, a transmission line with higher impedance (approaching the quantum resistance) is needed, since we want to characterize a strongly dissipative electromagnetic environment. Apparently, the normal transmission line can not meet this requirement. As an alternative way, a chain of Josephson junctions, which benefit from a large kinetic inductance [101] [$L_k = (\Phi_0/2\pi)^2/E_J$]. By decreasing E_J , a large L_k can be achieved], are demonstrated to be a high impedance transmission line under certain conditions. In addition to this point, another advantage is that Josephson junctions are controllable. We can get the desired impedance by tuning the relevant parameters of the chain.

In the following, we first briefly review the physics and modelling of Josephson junction chain. In particular, the superconducting-insulating transition of the chain is discussed. Next, we pay special attention to the superconducting regime where the chain reduces to an effective transmission line for microwave photons.

²The vacuum impedance, $Z_{\text{vac}} = \sqrt{\mu_0/\epsilon_0}$, where μ_0 is vacuum permeability and ϵ_0 is vacuum permittivity.

2.3.1 Josephson junction chain

A Josephson junction chain consists of superconducting islands (green boxes), connected to each other by Josephson junctions (cross boxes), shown in Fig 2.11 (a). We consider a chain made out of N homogeneous Josephson junctions. Each Josephson junction has a Josephson energy E_J and a capacitance C , and the island between two Josephson junctions has a capacitance C_0 to ground. As in Sec. 2.2, we take the superconducting gap energy to be the largest energy in the problem. With this condition, quasiparticle tunnelling is suppressed and only Cooper pairs tunnel between the superconducting islands via the Josephson junctions. The degrees of the freedom on the islands are described by the conjugate variables: phases ϕ_n and charges Q_n . They satisfy the commutation relation $[\phi_n, Q_m] = 2ie\delta_{nm}$. Here, the charge factor is $2e$ because we concentrate on Cooper pair tunnelling.

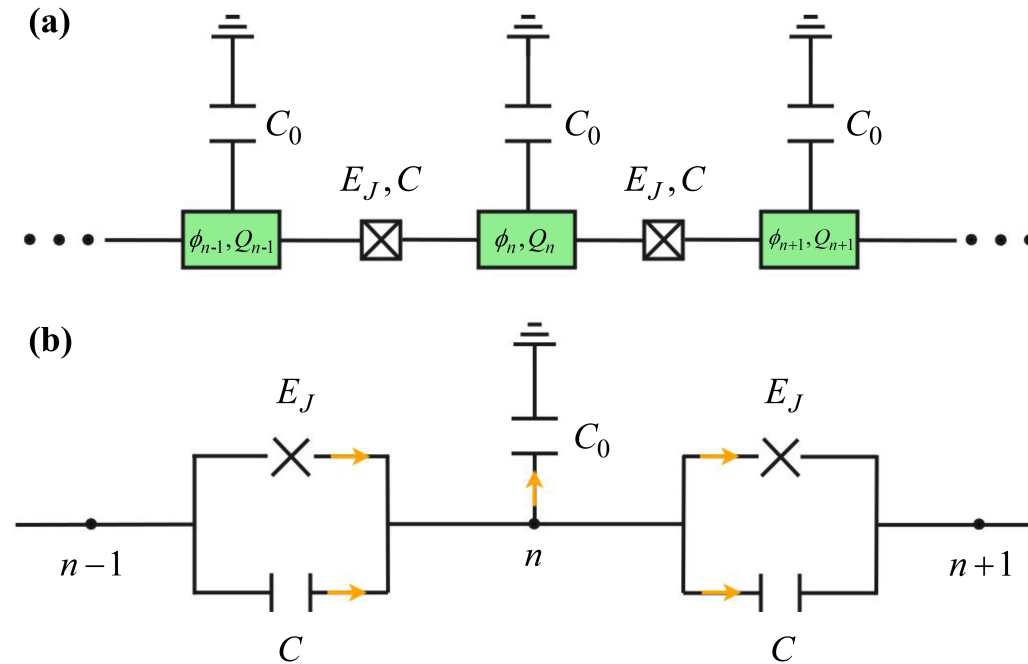


Figure 2.11: (a) Three islands of a homogeneous Josephson junction chain. Each Josephson junction has a Josephson energy E_J and a capacitance C , whereas the superconducting island between two junctions is capacitively connected to the ground by means of the capacitance C_0 . The phase and charge in the n -th island are denoted as ϕ_n and Q_n , respectively. (b) Kirchhoff's current conservation law (2.23) is applied at node n . The arrows indicate the direction of the current.

To derive the system Hamiltonian, we use the standard way: the method

allows us to write down the Hamiltonian of any quantum circuits consisting of capacitors, inductors and Josephson junctions, which was first proposed by Yurke and Denker [102], and then analyzed in detail by Devoret [103]. The procedure is as follows: present the equations of motion of the phase, write down the Lagrangian of the circuit, check the Lagrangian is fine, and finally obtain the Hamiltonian. Here, we present only the key steps. The complete derivation is shown in Appendix A.

First of all, the equation of motion is derived by applying Kirchhoff's current conservation law at node n : namely the sum of currents flowing into the node is equal to the sum of currents flowing out of that node [see Fig 2.11 (b)]. Thus,

$$\begin{aligned} I_c \sin(\phi_{n-1} - \phi_n) + \frac{\hbar}{2e} C (\ddot{\phi}_{n-1} - \ddot{\phi}_n) &= I_c \sin(\phi_n - \phi_{n+1}) \\ &+ \frac{\hbar}{2e} C (\ddot{\phi}_n - \ddot{\phi}_{n+1}) + \frac{\hbar}{2e} C_0 \ddot{\phi}_n, \end{aligned} \quad (2.23)$$

where we used that the current flowing through a capacitor is expressed as $(\hbar/2e)C\ddot{\phi}$, as the voltage across the capacitor is $U = (\hbar/2e)\dot{\phi}$. Indeed, the latter relation is the dynamic equation (2.2) of the superconducting phase evolution. Besides, the critical current of the Josephson Junction is related to the Josephson coupling energy $I_c = 2eE_J/\hbar$.

Then, the Lagrangian that yields Eq. (2.23) as its equation of motion is given by

$$L_{\text{chain}} = \sum_n \left[\left(\frac{\hbar}{2e} \right)^2 \frac{C_0}{2} \dot{\phi}_n^2 + \left(\frac{\hbar}{2e} \right)^2 \frac{C}{2} (\dot{\phi}_n - \dot{\phi}_{n+1})^2 + E_J \cos(\phi_n - \phi_{n+1}) \right]. \quad (2.24)$$

From Eq. (2.24), we find the charge Q_n , conjugate to the node phase ϕ_n , as

$$Q_n = \frac{2e}{\hbar} \frac{\partial L}{\partial \dot{\phi}_n} = \frac{\hbar}{2e} [(C_0 + 2C)\dot{\phi}_n - C\dot{\phi}_{n-1} - C\dot{\phi}_{n+1}]. \quad (2.25)$$

Furthermore, one can rewrite it in matrix form,

$$Q_n = \frac{\hbar}{2e} \sum_m C_{n,m} \dot{\phi}_m, \quad (2.26)$$

where the capacitance matrix $C_{n,m}$ is defined as

$$C_{n,m} = (C_0 + 2C)\delta_{n,m} - C\delta_{n+1,m} - C\delta_{n-1,m}. \quad (2.27)$$

In terms of the matrix $C_{n,m}$, the Lagrangian (2.24) becomes

$$L_{\text{chain}} = \frac{1}{2} \left(\frac{\hbar}{2e} \right)^2 \sum_{n,m} \dot{\phi}_n C_{n,m} \dot{\phi}_m + \sum_n E_J \cos(\phi_n - \phi_{n+1}). \quad (2.28)$$

Finally it is straightforward to obtain the Hamiltonian of the Josephson junction chain³,

$$H_{\text{chain}} = \sum_n \dot{\phi}_n Q_n - L_{\text{chain}} = \frac{1}{2} \sum_{n,m} Q_n C_{n,m}^{-1} Q_m - \sum_n E_J \cos(\phi_n - \phi_{n+1}). \quad (2.29)$$

In the Hamiltonian (2.29), the first term is the electrostatic energy which is the energy needed to add extra Cooper pairs to a neutral island; while the second one represents the Josephson energy, associated with the tunnelling of Cooper pairs between neighbouring islands.

The competition between these two energy scales leads to a variety of phenomena, for instance, superconductor-insulator transitions [104–106]. In particular, the charging energy want to localize the charge on each islands. As a result, the chain behaves as a Mott insulator. To transport charges from one island to another one, it require an activation energy of the order of charging energy. The Josephson energy plays an inverse role, i.e., delocalizing the charge from the island. Therefore, the chain turns to superconducting when the Josephson energy dominates.

Indeed, the mutual capacitance C and the grounding capacitance C_0 play different role in the transition. In the regime $C \ll C_0$, the superconductor-insulator transition occurs as a function of the ratio E_J/E_{C_0} , where $E_{C_0} = e^2/(2C_0)$ is the Coulomb charging energy of the island. In particular, the transition to the insulating state occurs when E_J/E_{C_0} becomes smaller than ~ 1 . Actually, this transition condition can also be characterized in terms of the impedance $Z_0/R_Q = \sqrt{E_{C_0}/E_J}$. As long as the impedance Z_0 do not exceeds the quantum impedance, the chain shows superconducting behavior. However, this is not the case when the mutual capacitance C is involved. In such chains, the phase slips due to C is unavoidable. This leads to superconductor-insulator transition in the thermodynamic limit, even when $E_J/E_{C_0} \geq 1$.

In our project, we focus on the superconducting regime which requires the Josephson energy to dominate over the charging energy. In this regime, the Josephson junction chain behaves as an effective transmission line [60, 61]. In addition, the impedance of the line can reach quantum resistance but still keep in superconducting state, if we consider that the grounding capacitance is much larger than the mutual capacitance.

2.3.2 Transmission line

In the superconducting regime, the Josephson junctions of the chain behave as inductors (see Fig. 2.12), the relation between the critical current of the junction and the inductance is $L = \hbar/(2eI_c)$. As a result, the Josephson junction chain

³For details see Appendix A

reduces effectively to a LCC_0 transmission line. The properties of dispersion relation and impedance of the line are now analysed.

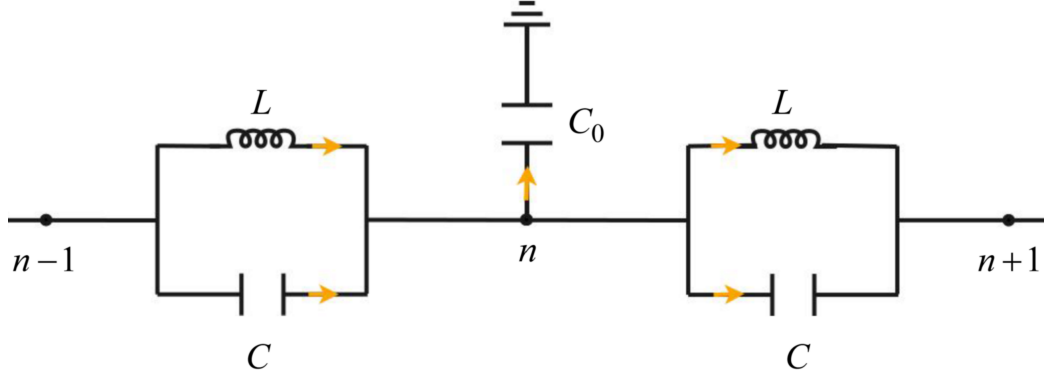


Figure 2.12: Three nodes of a transmission line with inductance L , capacitance C , and the ground capacitance C_0 . Kirchhoff's current conservation law (2.30) is applied at node n . The arrows indicate the direction of the current.

As before, we apply Kirchhoff's current conservation law at node n , obtaining the equation of motion

$$\frac{\phi_{n-1} - \phi_n}{L} + C(\ddot{\phi}_{n-1} - \ddot{\phi}_n) = \frac{\phi_n - \phi_{n+1}}{L} + C(\ddot{\phi}_n - \ddot{\phi}_{n+1}) + C_0\ddot{\phi}_n, \quad (2.30)$$

where the terms on the left hand represent the currents flowing in the node, while the right terms are means the currents flowing out the node (see Fig. 2.12).

For later convenience, the equation above is rewritten as

$$(\phi_{n-1} - \phi_{n+1} - 2\phi_n) + \frac{1}{\omega_p^2} (\ddot{\phi}_{n-1} - \ddot{\phi}_{n+1} - 2\ddot{\phi}_n) - \frac{1}{\omega_0^2} \ddot{\phi}_n = 0, \quad (2.31)$$

where we define the plasma frequency $\omega_p = 1/\sqrt{LC}$, and $\omega_0 = 1/\sqrt{LC_0}$. The next step is solving this equation of motion.

Supposing the transmission line is semi-infinite ($n \geq 0$), namely the total number of nodes $N \rightarrow \infty$, we may assume that the propagating modes, which are described by the equation of motion (2.31), have a plane wave form. Namely

$$\phi_{n,t} = \phi_0 e^{i(kn - \omega t)} + \phi'_0 e^{i(-kn - \omega t)}, \quad (2.32)$$

where these two terms represent modes travelling to the right and left, respectively. The prefactors ϕ_0 and ϕ'_0 are the amplitude of the modes. Here, k is measured in units of $1/a$.

Dispersion relation

Substituting Eq. (2.32) into Eq. (2.31), we obtain the dispersion relation, relating the frequency ω_k and k . It reads

$$\omega_k^2 = \omega_p^2 \frac{1 - \cos k}{1 - \cos k + C_0/2C}. \quad (2.33)$$

Taking different parameters $\Lambda = \sqrt{C_0/C}$, we plot the dispersion relation, ω as a function of the wave vector k , shown in Fig. 2.13. When $\Lambda = 0$, i.e., in the absence of the ground capacitance, Eq. (2.33) reduces to the dispersionless limit $\omega_k = \omega_p$ which is independent of k . When the ratio Λ has a finite value, the dispersion relation exhibits a linear behaviour for small k and then reaches a maximum value $\omega_{\max} = \omega_p / \sqrt{1 + (\Lambda/2)^2}$ which is always below the plasma frequency. By increasing the ratio, the linear dispersion regime becomes wider, but ω_{\max} decreases.

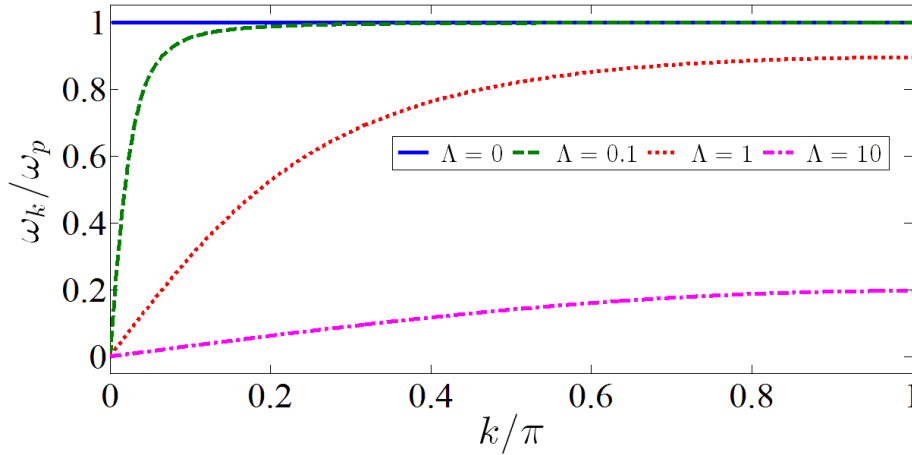


Figure 2.13: Plot of the dispersion relation (2.33) of a semi-infinite transmission line with different values of the parameter $\Lambda = 0, 0.1, 1, 10$. In the regime $k \ll \min[1, \Lambda]$, the dispersion relation is linear ($\omega_k = \omega_0|k|$).

At $k \ll 1$, the dispersion (2.33) reduces to

$$\omega_k^2 = \omega_p^2 \frac{k^2}{k^2 + \Lambda^2}. \quad (2.34)$$

For $k \ll \Lambda$, the dispersion relation behaves linear, i.e., $\omega_k = \omega_0|k|$ as anticipated above. The condition for linear regime (i.e., $k \ll \min[1, \Lambda]$) corresponds to a cut-off high frequency, i.e., $\omega \ll \min[\omega_0, \omega_p]$.

Impedance

Now we compute the impedance of the semi-infinite transmission line “seen” at node $n = 0$: $Z(\omega) \equiv V(\omega)/I(\omega)$. With this condition, we only have modes travelling to the right, i.e., ϕ'_0 in Eq. (2.32) equals zero. Therefore the voltage of the node n is

$$V_n(\omega) \equiv \frac{\hbar}{2e} \dot{\phi}_n = i\omega \frac{\hbar}{2e} \phi_0 e^{i(kn - \omega t)}. \quad (2.35)$$

Then, the current flowing through the line is connected with the voltage drop along the chain through the total impedance of the inductor L and the capacitor C ,

$$Z_{LC} = \frac{1}{\frac{1}{i\omega L} + i\omega C} = \frac{i\omega L}{1 - \frac{\omega^2}{\omega_p^2}}, \quad (2.36)$$

so

$$I_n(\omega) \equiv \frac{V_n - V_{n+1}}{Z_{LC}} = \frac{\hbar}{2e} \frac{1}{L} \left(1 - \frac{\omega^2}{\omega_p^2}\right) (1 - e^{ik}) \phi_0 e^{i(kn + \omega t)}. \quad (2.37)$$

Using Eqs. (2.35) and (2.37), we get the impedance of the transmission line,

$$Z(\omega) \equiv \frac{V(\omega)}{I(\omega)} = \frac{i\omega L}{\left(1 - \frac{\omega^2}{\omega_p^2}\right) (1 - e^{ik})}. \quad (2.38)$$

Using the dispersion relation (2.33) and the definition of ω_{\max} , the equation above can be rewritten in a simple form. It reads

$$Z(\omega) = \frac{Z_0}{\sqrt{1 - \left(\frac{\omega}{\omega_{\max}}\right)^2} + i \frac{\Lambda/2}{\sqrt{1 + (\Lambda/2)^2}} \frac{\omega}{\omega_{\max}}}, \quad (2.39)$$

from which the real part of the impedance (see Fig. 2.14) is formulated as

$$\text{Re}[Z(\omega)] = Z_0 \frac{\sqrt{1 - \left(\frac{\omega}{\omega_{\max}}\right)^2}}{1 - \frac{1}{1 + (\Lambda/2)^2} \left(\frac{\omega}{\omega_{\max}}\right)^2}. \quad (2.40)$$

In the linear dispersion relation regime, the frequency ω is always much below the maximum frequency, i.e., $\omega \ll \omega_{\max}$, which can be seen clearly from Fig. 2.13. As a consequence, the impedance of the transmission line keeps Z_0 (see Fig. 2.14).

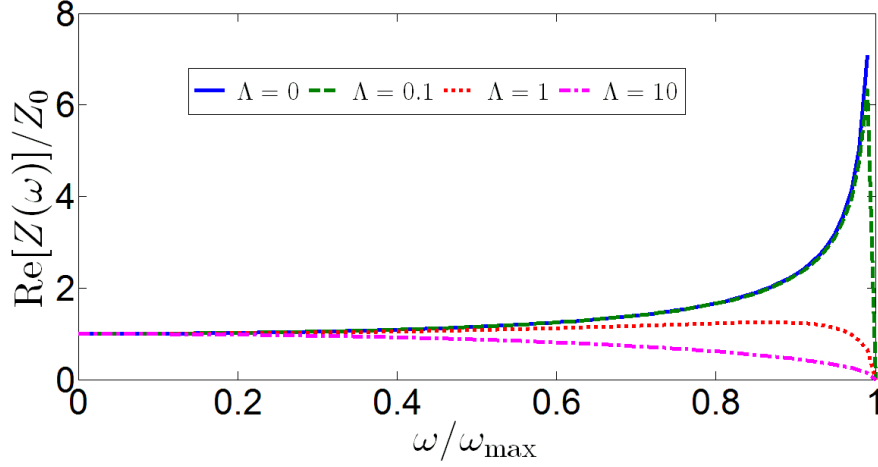


Figure 2.14: The real part of the impedance of the transmission line dependent of the frequency for $k \ll 1$. In linear dispersion relation regime, the impedance is a constant Z_0 .

Impedance of a Josephson junction chain

As we mentioned before, the impedance of the transmission line is of the order of the vacuum impedance (much smaller than the quantum resistance) if one uses only geometrical inductors and capacitors. By contrast, we now estimate how large an impedance can be achieved if the line is realized using a chain of Josephson junctions.

Basically, Josephson junction chains have three controllable parameters: the critical current I_c , the mutual capacitance C , and the ground capacitance C_0 . It should be noticed that I_c and C of a Josephson junction cannot be varied independently because both of them are proportional to the junction area. The critical current is given as $I_c = (\pi\Delta/2e)G_N \propto \mathcal{A}$ (G_N is the normal conductance of Josephson junction) and as the capacitance $C \propto \mathcal{A}$, where \mathcal{A} is the cross-section of the junctions, respectively. Therefore, it is reasonable to have a relation

$$I_c/C = \alpha. \quad (2.41)$$

Actually, α cannot be much varied. In most of the experiments, the junction is made of Al/AIO_xAl. Using realistic parameters [90–92], the dimensional constant α is estimated in the range of $\sim 10^7$ A/F.

By contrast, using different geometries, the mutual and ground capacitances C and C_0 are tuned independently. Then, the chain impedance normalized by the

quantum resistance can be rewritten as

$$\frac{Z_0}{R_Q} = \frac{1}{2\pi} \sqrt{\frac{C}{C_0}} \sqrt{\frac{L}{C}} \frac{(2e)^2}{\hbar}. \quad (2.42)$$

Using the relation $L = \hbar/(2eI_c)$ and Eq. (2.41), we further obtain

$$\frac{Z_0}{R_Q} = \frac{1}{2\pi} \sqrt{\frac{C}{C_0}} \frac{I_{\text{typ}}}{I_c}, \quad (2.43)$$

where we defined the typical current $I_{\text{typ}} = \sqrt{(2e)^3 \alpha / \hbar}$. Using the constant α , we may estimate I_{typ} as tens of nA. As we argued before, we need a larger impedance transmission line. From Eq. (2.43), we see that the impedance can approach the quantum resistance by controlling either the rate C/C_0 or the critical current I_c . In the regime $C/C_0 \ll 1$, the impedance Z_0 is restricted to not exceed quantum impedance⁴. This condition $Z_0 \leq R_Q$ require that the critical current I_c should be a smaller values. In the opposite regime, i.e., $C/C_0 \gg 1$, the suitable parameters for the critical current under the same condition are relatively flexible. But, the chain maybe turn to insulating regime.

The Hamiltonian

The Hamiltonian of the transmission line is obtained by expanding the Josephson energy in Eq. (2.29) up to the second order in ϕ_n :

$$H_T = \frac{1}{2} \sum_{n,m} \left[Q_n C_{n,m}^{-1} Q_m + \left(\frac{\hbar}{2e} \right)^2 \phi_n L_{n,m}^{-1} \phi_m \right], \quad (2.44)$$

where we define an inverse inductance matrix L^{-1} that is similar to the capacitance matrix C^{-1} ,

$$L_{n,m}^{-1} = \frac{2}{L} \delta_{n,m} - \frac{1}{L} \delta_{n+1,m} - \frac{1}{L} \delta_{n-1,m}. \quad (2.45)$$

It is known that electromagnetic signals are always composed of photons, although in the circuit domain those signals are carried as voltages and currents on the elements, and the discreteness of the photon's energy is usually not evident. Theoretically, the photons modes are apparent when we diagonalize the Hamiltonian (2.44) to the standard form (see details in appendix B)

$$H_T^{\text{diag}} = \sum_k \hbar \omega_k \left(a_k^\dagger a_k + \frac{1}{2} \right), \quad (2.46)$$

⁴For $Z_0 > R_Q$, the chain behaves as a Mott insulator. This is not our interested regime.

by using the following expansions with respect to photon operators a_k^\dagger, a_k

$$\phi_n = \frac{1}{\sqrt{N}} \sum_k \alpha_k e^{ikn} (a_k + a_{-k}^\dagger), \quad Q_n = \frac{e}{\sqrt{N}} \sum_k \frac{1}{i\alpha_k} e^{ikn} (a_k - a_{-k}^\dagger) \quad (2.47)$$

with

$$\alpha_k^2 = \frac{e^2}{\hbar} \sqrt{\frac{L}{C}} \sqrt{\frac{1}{1 - \cos k + C_0/2C} \frac{1}{1 - \cos k}}. \quad (2.48)$$

In linear regime, i.e., $k \ll \min[1, \Lambda]$, the amplitude α_k^2 reduces to

$$\alpha_k^2 = \pi \frac{Z_0}{R_Q} \frac{1}{|k|}. \quad (2.49)$$

The photon operators above satisfy the commutation relation $[a_{k_1}, a_{k_2}^\dagger] = \delta_{k_1, k_2}$. And, we find that ω_k in Eq. (2.46) is consistent with the dispersion relation (2.33). In linear regime, $\omega_k = \omega_0 |k|$.

2.3.3 Summary

A high-impedance (compared to vacuum impedance) transmission line can be realized by using Josephson junction chains in the superconducting regime. We derived the Hamiltonian of the transmission line, as well as its diagonal form. At low frequency, we obtained a linear spectrum for microwave photons, corresponding to an ohmic environment. This provides a good background for studying the scattering problems in chapter 4 and chapter 5.

Dynamical Coulomb blockade theory in Josephson junctions

In this chapter, the dynamical Coulomb blockade theory [or $P(E)$ -theory] is reviewed. We start with the description of the Coulomb blockade phenomenon in tunnelling junctions. Then, we restrict ourselves to a Josephson junction in the Cooper pair tunnelling regime in Sec. 3.1. We study how the current-voltage characteristic of a Josephson junction is influenced by its environment which is described by the Hamiltonian H_{env} . We show in detail the derivation of the Cooper pair tunnelling rates in Sec. 3.2. At zero temperature, the tunnelling rates are proportional to the $P(E)$ function, which is the probability for the Josephson junction to emit photons with total energy E in the electromagnetic environment. The resulting $P(E)$ function is the Fourier transform of a phase-phase correlator. To compute this correlator, we consider two different cases: 1) If H_{env} is quadratic, the correlator can be evaluated with the $P(E)$ function which can be calculated exactly, cf., in Sec. 3.3. Taking an infinite transmission line as the electromagnetic environment, we study how the current-voltage characteristic of the Josephson junction is influenced by the line impedance. 2) If H_{env} is not quadratic, it is impossible to compute the exponential phase-phase correlator exactly. Thus other methods are needed. We propose two methods in Sec. 3.4: Green's function perturbation theory and path integral method.

3.1 Introduction

The concept of Coulomb blockade was first proposed by Gorter [107] in 1951 as an explanation for the observation [108, 109] of an anomalous increase of the resistance of thin granular metallic films as temperature is reduced. He assumed that the films consisted of separate grains or blocks. When the temperature was decreased to a certain value such that thermal energy was smaller than the charging energy, which was associated with the separation between a pos-

itive and a negative charge located on a grain, the electron flowing in the film was suppressed. As a result, the resistance increased. Thanks to the advance of modern lithography which allows to fabricate capacitances in the range $C \leq 1\text{fF}$, such charging effects in ultra-small multiple-junctions were observed by Fulton and Dolan [110] thirty years later. The striking electric-field-induced oscillations were seen in the current-voltage characteristic of the junctions arranged in a low-capacitance multiple-junction configuration.

In ultra-small junctions, new effects emerge due to charging effects. The essential physics is that the tunnelling electron gains energy eV at bias voltage V , but must pay a charging cost of E_c . This leads to interesting consequences including the Coulomb blockade [111, 112], the Coulomb staircase [113, 114], and various oscillatory and dynamic effects [110, 115, 116]. These behaviours arise from the tunnelling of individual electrons, charging and discharging the capacitance. At the beginning, the charging effects were observed only in multiple-junctions due the difficulties associated with stray capacitances. As for single normal-metal junction, one can see only the suppression of the tunnelling current at voltage $V < e/2C$; and for higher voltages, the $I - V$ characteristic is offset by the Coulomb gap, i.e., $e/2C$. But, the direct features of Coulomb blockade at voltage $V < e/2C$ was hard seen experimentally. Indeed, it was realized soon that the charging effect was influenced strongly by the nature of the environment (e.g., the metallic leads and pads) coupled to the junction. Quantum fluctuations of the environment may smear out the Coulomb gap [117–119]. As a consequence, the behaviour of the system, e.g., the current-voltage characteristic, may change quantitatively or even qualitatively. This phenomenon, called dynamical Coulomb blockade, has been investigated widely in different kinds of junctions (see a review [87]).

In addition to normal metal junctions, the dynamical Coulomb blockade was also studied in Josephson junctions [120–123] (see Fig. 3.1). In this case we have two kinds of charge carriers: quasi-particles and Cooper pairs. We will restrict ourselves to the Cooper pair tunnelling regime. In a voltage-biased Josephson junction, this regime can be achieved at low temperature ($T < T_c$, the superconducting critical temperature) and weak bias ($eV < 2\Delta$, the energy gap). Within this regime, the current-voltage characteristic of an ideal Josephson junction is shown in Fig. 2.2 (a), where we can see that no current flows through the junction. However, the characteristic will be changed when the influence of the environment is involved. In particular, the supercurrent provides a direct mean to access the properties of the environmental.

As shown in Fig. 3.2 (a), we now consider a Josephson junction (with capacitance C_J and Josephson energy E_J) coupled to a voltage source V via an external circuit which is described by its impedance $Z(\omega)$. The environment [see the dashed box of Fig. 3.2 (a)] seen by the junction consists of the external circuit

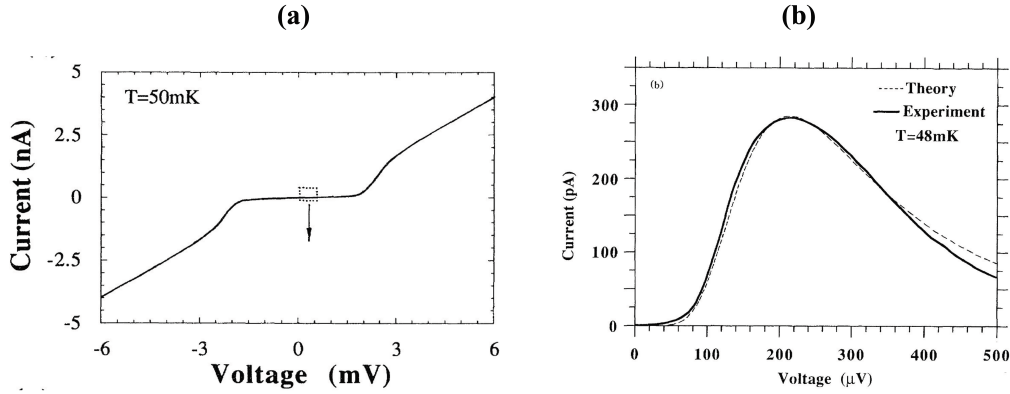


Figure 3.1: The experimental $I - V$ characteristic of submicron-size Pb-alloy single Josephson junction attached to thin-film NiCr leads [120]. (a) the attached leads with low impedance $22\text{k}\Omega$. (b) the attached leads with high impedance $200\text{k}\Omega$.

and the capacitance. When a voltage V is applied, the Cooper pairs can tunnel inelastically across the junction by dissipating the gained energy $2eV$ to the electromagnetic environment via emitting (or absorbing) one or several photons. These excitations, in turn, affect the tunnelling of Cooper pairs. As a result, the current-voltage characteristic of the junction will be modified.

In the following, we first show how the $I - V$ characteristic of the Josephson junction is modified by the environment. To do so, Cooper pair tunnelling rates are derived using perturbation theory. Next, we discuss not only linear environments which are described by a quadratic Hamiltonian; but also we extend the theory to nonlinear environments (with a non-quadratic Hamiltonian). As for the latter one, Green's function perturbation theory and the path integral method are introduced to handle the non-linearity.

3.2 Cooper pair tunnelling rates

In order to determine the current-voltage characteristic, one needs to calculate the tunnelling rates from both directions [see the arrows in Fig. 3.2 (b)] through the Josephson junction while taking into account the environment. First of all, the circuit is described by the Hamiltonian

$$H = -E_J \cos \phi + H_{\text{env}}, \quad (3.1)$$

where the first term is the coupling free energy [see Eq. (2.4)] of the Josephson junction, and ϕ the phase difference across the junction. The environment is described by the Hamiltonian H_{env} . The phase of the coupling node between the

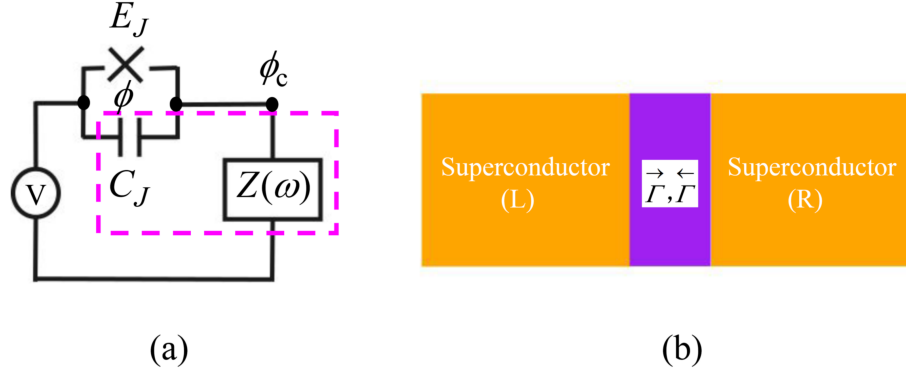


Figure 3.2: (a) A voltage-biased Josephson junction with Josephson energy E_J coupled to an electromagnetic environment [which is described by the impedance $Z(\omega)$]. The Josephson junction capacitance C_J and the external circuit make up the environment (see the dashed box). (b) Schematic drawing of a single Josephson junction. The arrows indicate forward (from left to right) and backward (from right to left) Cooper pair tunnelling through the barrier.

junction and the environment is denoted as ϕ_c . The relation of the two phases reads

$$\phi = 2eVt - \phi_c. \quad (3.2)$$

In the framework of circuit QED, the dissipative environment is usually modelled as a set of LC -oscillators [124] (with degrees of freedom: phase ϕ_n and charge Q_n , n represents the nodes) which are linearly coupled to ϕ . This can be seen more clearly from the system Hamiltonian involving a term $(2L_n)(\phi_n - \phi)^2$ (see details in reference [87]). Indeed, this is not the only case. The coupling between the junction and the environment can also be local. We will give an example in the next section.

In order to clearly see the physical processes of the Cooper-pair tunnelling, we rewrite the Josephson term as

$$E_J \cos \phi = \frac{E_J}{2} e^{-i\phi} + H.c.. \quad (3.3)$$

Physically, the operator $e^{-i\phi}$ changes the charge Q on the junction by $2e$ according to the commutator (2.6). This process is related to the tunnelling of a Cooper pair from the left lead to the right one and exchanging energy $2eV$ with the environment. Next, we show in detail the derivation of the Cooper pair tunnelling rate in the Josephson junction.

Before the calculation, we point out that the $P(E)$ -theory described below is valid only for incoherent tunnelling of Cooper pairs, namely, one by one across

the junction. Moreover, we consider the regime where Josephson energy E_J is small in the problem. It means that charge is well defined. Then, we can regard the tunnelling Hamiltonian $-E_J \cos \phi$ as a perturbation, and use the Fermi golden rule to calculate the tunnelling rates:

$$\Gamma_{i \rightarrow f} = \frac{\pi E_J^2}{2\hbar} |\langle f | e^{-i\phi} + e^{i\phi} | i \rangle|^2 \delta(E_i - E_f). \quad (3.4)$$

Equation above gives the rates for transitions between the initial states $|i\rangle$ and the final states $|f\rangle$. In the absence of the Josephson junction tunnelling Hamiltonian, we may write the states of the environment H_{env} , i.e., the reservoir states $|R\rangle$ with energy E_R . The initial states and final states are written as $|i\rangle = |R\rangle$ and $|f\rangle = |R'\rangle$, with energies E_R and E'_R , respectively. Hence, the matrix element in Eq. (3.4) naturally becomes

$$\langle f | e^{-i\phi} + e^{i\phi} | i \rangle = \langle R' | e^{-i\phi} | R \rangle + \langle R' | e^{i\phi} | R \rangle. \quad (3.5)$$

In order to compute the total rate, one has to sum up all the possible initial and final states weighted by the thermal probability. Since we are considering the tunnelling processes from the left lead to the right lead, only the first term of Eq. (3.5) plays a role while the second term describes the inverse processes. Hence, we write the total tunnelling rates as

$$\vec{\Gamma}(V) = \frac{\pi E_J^2}{2\hbar} \sum_{R,R'} |\langle R' | e^{-i\phi} | R \rangle|^2 P_\beta(R) \delta(E_R - E'_R), \quad (3.6)$$

where $E_R - E'_R$ is the energy difference of Cooper pairs associated with the tunnelling process, and the probability to find the initial reservoir states $|R\rangle$ reads

$$P_\beta(R) = \langle R | \rho_\beta | R \rangle. \quad (3.7)$$

The equilibrium density matrix at inverse temperature $\beta = 1/(k_B T)$ is

$$\rho_\beta = \frac{e^{-\beta H_{\text{env}}}}{Z}, \quad (3.8)$$

with the partition function of the environment, $Z = \text{Tr}[e^{-\beta H_{\text{env}}}]$. Therefore, the average of an operator X over the environmental equilibrium distribution takes the form $\langle X \rangle_{H_{\text{env}}} = \langle R | X e^{-\beta H_{\text{env}}} | R \rangle_{H_{\text{env}}} / Z$.

In order to simplify Eq. (3.6), we rewrite the delta function as

$$\delta(E_R - E'_R) = \frac{1}{2\pi\hbar} \int_{-\infty}^{\infty} dt e^{i(E_R - E'_R)t/\hbar}. \quad (3.9)$$

Upon substituting Eq. (3.9) into Eq. (3.6), replacing the junction phase ϕ by ϕ_c [using Eq. (3.2)], and transforming the result into the Heisenberg picture¹, finally, Eq. (3.6) becomes

$$\begin{aligned}\vec{\Gamma}(V) &= \frac{E_J^2}{4\hbar^2} \int_{-\infty}^{\infty} dt e^{i2eVt/\hbar} \sum_{R,R'} \langle R | e^{i\phi_c(t)} | R' \rangle \langle R' | e^{-i\phi_c(0)} | R \rangle P_\beta(R) \\ &= \frac{E_J^2}{4\hbar^2} \int_{-\infty}^{\infty} dt e^{i2eVt/\hbar} \sum_R \langle R | e^{i\phi_c(t)} e^{-i\phi_c(0)} | R \rangle P_\beta(R).\end{aligned}\quad (3.10)$$

Substituting Eqs. (3.7) and (3.8) into Eq. (3.10), we obtain naturally

$$\sum_R \langle R | e^{i\phi_c(t)} e^{-i\phi_c(0)} | R \rangle P_\beta(R) = \langle e^{i\phi_c(t)} e^{-i\phi_c(0)} \rangle_{H_{\text{env}}}.\quad (3.11)$$

Now, we obtain the expression for the total tunnelling rates from the left lead to the right lead

$$\vec{\Gamma}(V) = \frac{E_J^2}{4\hbar^2} \int_{-\infty}^{\infty} dt e^{i2eVt/\hbar} \langle e^{i\phi_c(t)} e^{-i\phi_c(0)} \rangle_{H_{\text{env}}}.\quad (3.12)$$

Mathematically, it will be quite convenient to introduce a new function $P(E)$, which is the Fourier transform of the exponential phase-phase correlation function,

$$P(E) = \frac{1}{2\pi\hbar} \int_{-\infty}^{\infty} dt e^{iEt/\hbar} \langle e^{i\phi_c(t)} e^{-i\phi_c(0)} \rangle_{H_{\text{env}}}.\quad (3.13)$$

With this definition, Eq. (3.12) is rewritten in a simple form,

$$\vec{\Gamma}(V) = \frac{\pi}{2\hbar} E_J^2 P(2eV).\quad (3.14)$$

Here, we interpret $P(E)$ as the probability to release energy E ($E > 0$)² to the environment via emitting one or several photons. Indeed, this is already verified experimentally by Hofheinz, et al. [88]. They measured the radiation emitted by a small voltage biased Josephson junction embedded in a microwave resonator. In this experiment, the Cooper pair current and the photon emission rate are measured simultaneously at the resonance frequency of the resonator. When the Cooper

¹The time-dependent operators take the form $e^{i\phi_c(t)} = e^{iH_{\text{env}}t/\hbar} e^{i\phi_c} e^{-iH_{\text{env}}t/\hbar}$.

²Reversely, for negative energy ($E < 0$), it describes the absorption of energy $|E|$ from the environment.

pair tunnel inelastically through the Josephson junction, it emits either one or two photons into the resonator.

The backward tunnelling rates $\overleftarrow{\Gamma}$ from the right lead to the left lead can be computed the same way. However, it is much easier to obtain the result from the symmetry of a voltage-biased single junction as

$$\overleftarrow{\Gamma}(V) = \overrightarrow{\Gamma}(-V). \quad (3.15)$$

Note that Eq.(3.15) is valid when $\langle e^{i\phi_c(t)} e^{-i\phi_c(0)} \rangle_{H_{\text{env}}} = \langle e^{-i\phi_c(t)} e^{i\phi_c(0)} \rangle_{H_{\text{env}}}$. This relation requires that the environmental Hamiltonian H_{env} has symmetry in phase ϕ and charge Q [125]. One can easily certify it as follows: $\langle e^{i\phi_c(t)} e^{-i\phi_c(0)} \rangle_{H_{\text{env}}} = (1/Z) \int D[\phi(t)] \int D[Q(t)] e^{i\phi_c(t)} e^{-i\phi_c(0)} e^{-s}$, where $Z = \int D[\phi(t)] \int D[Q(t)] e^{-s}$ is the partition function. The term $-s = \int_0^\infty dt \{iQ(t)\dot{\phi}(t) - H_{\text{env}}[\phi(t), Q(t)]\}$ is the action. If we have $\phi \rightarrow -\phi$, and $Q \rightarrow -Q$ in H_{env} , then Eq.(3.15) is verified.

Finally, the total current flowing through the Josephson junction is given by the tunnelling Cooper pair charge $2e$ (corresponding to each tunnelling process) multiplied with the difference of the forward and backward tunnelling rates,

$$I(V) = 2e \left[\overrightarrow{\Gamma}(V) - \overleftarrow{\Gamma}(V) \right] = \frac{e\pi E_J^2}{\hbar} [P(2eV) - P(-2eV)]. \quad (3.16)$$

At zero temperature, the thermal fluctuations of the environment are completely suppressed. Thus, there is no absorption from the environment, i.e., $P(E < 0) = 0$. Only the emission processes contribute. Consequently, Eq. (3.16) immediately reduces to

$$I(V) = \frac{e\pi E_J^2}{\hbar} P(2eV). \quad (3.17)$$

The current is proportional to the $P(E)$ function, which enables us to measure the properties of the environment directly. We will apply this idea in chapter 4 and chapter 5.

So far, we have introduced the dynamical Coulomb blockade theory of Josephson junctions in the Cooper pair tunnelling regime. The current flowing through the junction is influenced by the environment. In particular, the current-voltage characteristic is directly related to the $P(E)$ function, which is the Fourier transform of phase-phase correlation function $\langle e^{i\phi_c(t)} e^{-i\phi_c(0)} \rangle_{H_{\text{env}}}$. Next, the task is to compute this correlator. Though $P(E)$ -theory is usually presented in the context of a linear environment (H_{env} is assumed to be quadratic) [87, 126–128], Eqs. (3.13) and (3.16) hold more generally for a nonlinear environment [129]. In the following, we will discuss the linear and the nonlinear environment, respectively.

3.3 Phase-phase correlator: linear regime

We consider a linear environment which is described by the quadratic Hamiltonian $H^{(0)}$, given by Eq. (2.44). Then the operator ϕ_c is expressed in terms of a linear combination of creation and annihilation operators [see Eq. (2.47)]. As a result, the phase-phase correlator can be simplified by exploiting the Wick's theorem. To do so, we first construct a function $f(\gamma) = \langle e^{i\gamma\phi_c(t)} e^{-i\gamma\phi_c(0)} \rangle_{H^{(0)}}$, then

$$\frac{df(\gamma)}{d\gamma} = i \left[\langle \phi_c(t) e^{i\gamma\phi_c(t)} e^{-i\gamma\phi_c(0)} \rangle_{H^{(0)}} - \langle e^{i\gamma\phi_c(t)} \phi_c(0) e^{-i\gamma\phi_c(0)} \rangle_{H^{(0)}} \right]. \quad (3.18)$$

Expanding the exponentials on the right hand side of Eq. (3.18), and applying the Wick's theorem, we obtain

$$\frac{df(\gamma)}{d\gamma} = 2\gamma \langle [\phi_c(t) - \phi_c(0)] \phi_c(0) \rangle_{H^{(0)}} f(\gamma), \quad (3.19)$$

where we used $\langle \phi_c^2(t) \rangle_{H^{(0)}} = \langle \phi_c^2(0) \rangle_{H^{(0)}}$ (valid under stationary and equilibrium conditions).

Solving the differential equation (3.19), and using the initial condition $f(0) = 1$, we arrive at a general expression³ for the exponential phase-phase correlation function:

$$\langle e^{i\phi_c(t)} e^{-i\phi_c(0)} \rangle_{H^{(0)}} \equiv f(1) = \exp \left\{ \langle \phi_c(0) [\phi_c(t) - \phi_c(0)] \rangle_{H^{(0)}} \right\}. \quad (3.20)$$

For later convenience, we introduce the abbreviation

$$J_0(t) = \langle \phi_c(0) [\phi_c(t) - \phi_c(0)] \rangle_{H^{(0)}} \quad (3.21)$$

for the two-point phase-phase correlation function, namely, the average taken over the environmental degrees of freedom. To compute the correlator $J_0(t)$, we use the retarded Green's function $G_R^{(0)}(\phi_c, \phi_c; t) = i/\hbar \Theta(t) \langle [\phi_c(t), \phi_c(0)] \rangle_{H^{(0)}}$, where $\Theta(t)$ is the Heaviside step function. The relation between the two is written in frequency space (see details in Appendix ??):

$$J_0(t) = \frac{\hbar}{\pi} \int_0^\infty d\omega \operatorname{Im} \left[G_R^{(0)}(\phi_c, \phi_c; \omega) \right] [(\cos \omega t - 1) \cosh(\hbar\omega\beta/2) - i \sin \omega t]. \quad (3.22)$$

At zero temperature, it reduces to

$$J_0(t) = \frac{\hbar}{\pi} \int_0^\infty d\omega \operatorname{Im} \left[G_R^{(0)}(\phi_c, \phi_c; \omega) \right] (e^{-i\omega t} - 1). \quad (3.23)$$

³Eq. (3.20) is also verified later using the path integral method [see Eq. (3.87)].

Normally, the retarded Green's function $G_R^{(0)}(\phi_c, \phi_c; \omega)$ is solved from its equation of motion, which can be derived with the given Hamiltonian $H^{(0)}$. We will show this in detail using a specific electromagnetic environment in the next subsection.

3.3.1 Electromagnetic environment: the transmission line

As shown in Fig. 3.3, we now apply the $P(E)$ -theory to a probe Josephson junction with Josephson energy E_J and capacitance C_J connected (at node m) to a transmission line. We constrict to the case of low frequency regime where the transmission line behaves as an ohmic environment (see Sec. 2.3). To simplify the calculation, we further concentrate on the case that the ground capacitance C_0 is much larger than the mutual capacitance C .

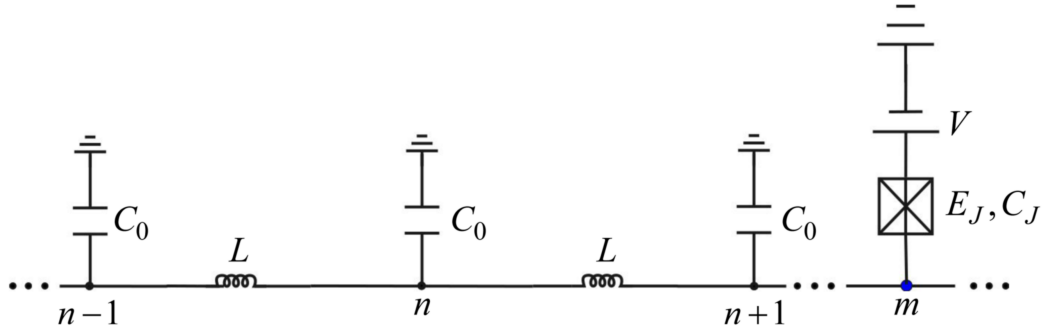


Figure 3.3: The system consists of a voltage-biased (voltage source V) Josephson junction with Josephson energy E_J and capacitance C_J side-coupled with an infinite transmission line at node m . The transmission line is realized using identical LC_0 oscillators. At low frequency, the line behaves as an ohmic environment.

First of all, the Hamiltonian of the transmission line is obtained from Eq. (2.44) by taking the condition $C \ll C_0$:

$$H_T = \sum_n \frac{Q_n^2}{2C_0} + \left(\frac{\hbar}{2e} \right)^2 \frac{(\phi_n - \phi_{n+1})^2}{2L}. \quad (3.24)$$

The environment seen by the Josephson junction consists of the transmission line and the capacitance C_J . The charging energy associated with the capacitance C_J is located at node m , so the linear environmental Hamiltonian reads

$$H^{(0)} = \sum_n \frac{Q_n^2}{2(C_0 + C_J \delta_{n,m})} + \left(\frac{\hbar}{2e} \right)^2 \frac{(\phi_n - \phi_{n+1})^2}{2L}. \quad (3.25)$$

Then, the local retarded Green's function $G_R^{(0)}[\phi_m, \phi_m; \omega]$ is needed according to the discussion above.

The equation of motion of the retarded Green's function $G_R^{(0)}[\phi_n(t), \phi_m(0)]$ can be derived. The first derivation with respect to time is

$$\begin{aligned}\partial_t G_R^{(0)}[\phi_n(t), \phi_m(0)] &= \frac{i}{\hbar} \delta(t) \langle [\phi_n(t), \phi_m(0)] \rangle_{H^{(0)}} + \frac{i}{\hbar} \Theta(t) \langle [\partial_t \phi_n(t), \phi_m(0)] \rangle_{H^{(0)}} \\ &= \frac{i}{\hbar} \Theta(t) \langle [\partial_t \phi_n(t), \phi_m(0)] \rangle_{H^{(0)}}.\end{aligned}\quad (3.26)$$

Substituting $\partial_t \phi_n(t)$ ⁴ into Eq. (3.26),

$$\partial_t G_R^{(0)}[\phi_n(t), \phi_m(0)] = \frac{i}{\hbar} \frac{2e}{C_0 + C_J \delta_{n,m}} \Theta(t) \langle [Q_n(t), \phi_m(0)] \rangle_{H^{(0)}}. \quad (3.27)$$

The second derivation with respect to time is

$$\begin{aligned}\partial_t^2 G_R^{(0)}[\phi_n(t), \phi_m(0)] &= \frac{i}{\hbar} \frac{2e}{C_0 + C_J \delta_{n,m}} [\delta(t) \langle [Q_n(t), \phi_m(0)] \rangle_{H^{(0)}} \\ &\quad + \Theta(t) \left\langle \left[\frac{\partial Q_n(t)}{\partial t}, \phi_m(0) \right] \right\rangle_{H^{(0)}}].\end{aligned}\quad (3.28)$$

Substituting $\partial_t Q_n(t)$ ⁵ into Eq. (3.28),

$$\begin{aligned}\partial_t^2 G_R^{(0)}[\phi_n(t), \phi_m(0)] &= \frac{1}{\hbar} \frac{(2e)^2}{C_0 + C_J \delta_{n,m}} \delta(t) \delta_{n,m} - \frac{1}{L(C_0 + C_J \delta_{n,m})} \\ &\quad \left\{ 2G_R^{(0)}[\phi_n(t), \phi_m(0)] - G_R^{(0)}[\phi_{n-1}(t), \phi_m(0)] - G_R^{(0)}[\phi_{n+1}(t), \phi_m(0)] \right\}.\end{aligned}\quad (3.29)$$

Taking the Fourier transform of Eq. (3.29) with respect to time, we obtain the equation of motion of the retarded Green's function in frequency space,

$$\begin{aligned}\omega^2 G_R^{(0)}(\phi_n, \phi_m; \omega) &- \frac{1}{L(C_0 + C_J \delta_{n,m})} \left\{ 2G_R^{(0)}(\phi_n, \phi_m; \omega) - G_R^{(0)}(\phi_{n-1}, \phi_m; \omega) \right. \\ &\quad \left. - G_R^{(0)}(\phi_{n+1}, \phi_m; \omega) \right\} + \frac{1}{\hbar} \frac{(2e)^2}{C_0 + C_J \delta_{n,m}} \delta_{n,m} = 0.\end{aligned}\quad (3.30)$$

Eq. (3.30) describes that photons (excited by the inelastic tunnelling of Cooper pairs) are emitted from the Josephson junction at node m , and then propagate along the transmission line in both left and right directions (see Fig. 3.4).

⁴It equals $(i/\hbar)[H^{(0)}, \phi_n(t)] = (2e/\hbar)Q_n(t)/(C_0 + C_J \delta_{n,m})$.

⁵It equals $(i/\hbar)[H^{(0)}, Q_n(t)] = -(1/2e)[2\phi_n(t) - \phi_{n-1}(t) - \phi_{n+1}(t)]/L$.

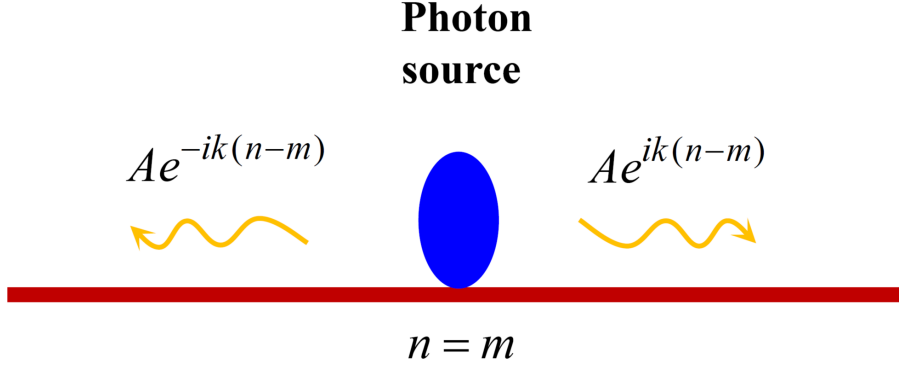


Figure 3.4: Inelastic tunnelling of Cooper pairs excites the electromagnetic environment. The resulting photons propagate down the transmission line, as described by the equation of motion (3.31).

The solution of Eq. (3.30) can be written using a plane wave basis,

$$G_R^{(0)}(\phi_n, \phi_m; \omega) = Ae^{ik(n-m)}\Theta(n-m) + Ae^{-ik(n-m)}\Theta(m-n), \quad (3.31)$$

where we already used the boundary condition⁶ at $n = m$. The coefficient A needs to be determined. Substituting Eq. (3.31) into Eq. (3.30) and taking $n = m$, we obtain

$$A\omega^2 - \frac{\hbar}{L(C_0 + C_J)}(2A - Ae^{ik} - Ae^{-ik}) + \frac{1}{\hbar} \frac{(2e)^2}{C_0 + C_J} = 0. \quad (3.32)$$

At low frequencies that requires $k \ll 1$, the coefficient A is obtained from Eq. (3.32) as

$$A = i \frac{\pi}{\hbar\omega} \frac{Z_t(\omega)}{R_Q}, \quad (3.33)$$

where the total impedance is $Z_t^{-1}(\omega) = 1/Z_0 + i\omega C_J$ with $Z_0 = \sqrt{L/C_0}$ as the impedance of the transmission line. The impedance can be computed in different ways. Here, we choose Green's functions since it is a convenient tool to study the nonlinear case. The result of a transmission line can be easily generalized to other complex cases. Physically, the total impedance seen by the probe junction can be regarded as the impedance of the line in parallel with the capacitance of the probe. For later convenience, we normalize the total impedance by the quantum resistance, namely

$$\frac{Z_t(\omega)}{R_Q} = \frac{Z_0}{R_Q} \frac{1}{1 + i\omega/\omega_{\text{cut-off}}}, \quad (3.34)$$

⁶At $n = m$, the Heaviside function $\Theta(n - m) = 1/2$. Thus, we have $G_R^{(0)}(\phi_{m+0^+}, \phi_m; \omega) = G_R^{(0)}(\phi_{m+0^-}, \phi_m; \omega) = A$.

where the frequency $\omega_{\text{cut-off}} = 1/(Z_0 C_J)$ describes the effective cut-off of the total impedance due to the existence of the junction capacitance C_J .

Substituting the coefficient (3.33) into Eq. (3.31), and taking $n = m$, we get the local retarded Green's function at node m

$$G_R^{(0)}(\phi_m, \phi_m; \omega) = i \frac{\pi}{\hbar \omega} \frac{Z_t(\omega)}{R_Q}. \quad (3.35)$$

Using the relation (3.22), we obtain the correlation function

$$J_0(t) = \int_0^\infty \frac{d\omega}{\omega} \frac{\text{Re}[Z_t(\omega)]}{R_Q} \left[\cosh \frac{\beta \omega}{2} (\cos \omega t - 1) - i \sin \omega t \right]. \quad (3.36)$$

Integral equation for the $P(E)$ -function

Substituting Eq. (3.20) into Eq. (3.13), we simplify $P(E)$ as

$$P(E) = \frac{1}{2\pi\hbar} \int_{-\infty}^{\infty} dt \exp[J_0(t) + iEt/\hbar]. \quad (3.37)$$

Generally, it is impossible to calculate $P(E)$ analytically. In the zero temperature limit, $P(E)$ can be solved numerically from an integral equation inspired by the idea of Minnhagen [130]. Using Eq. (3.36), the phase-phase correlation function at $T = 0$ reads

$$J_0(t) = \int_0^\infty \frac{d\omega}{\omega} \frac{\text{Re}[Z_t(\omega)]}{R_Q} (e^{-i\omega t} - 1). \quad (3.38)$$

Taking the time derivative of $\exp[J_0(t)]$, we get

$$\frac{d e^{J_0(t)}}{dt} = -2i e^{J_0(t)} \int_0^\infty d\omega \frac{\text{Re}[Z_t(\omega)]}{R_Q} e^{-i\omega t}. \quad (3.39)$$

Taking the Fourier transform on both sides of Eq. (3.39), yields

$$\int_{-\infty}^{\infty} dt e^{i\frac{E}{\hbar}t} \frac{d e^{J_0(t)}}{dt} = -2i \int_0^\infty d\omega \frac{\text{Re}[Z_t(\omega)]}{R_Q} \int_{-\infty}^{\infty} dt e^{i\frac{E-\hbar\omega}{\hbar}t} e^{J_0(t)}. \quad (3.40)$$

Then, we make use of the convolution on the left hand side, and use the definition of $P(E)$ [see Eq. (3.37)] to write

$$-i \frac{E}{\hbar} P(E) = -2i \int_0^\infty d\omega \frac{\text{Re}[Z_t(\omega)]}{R_Q} P(E - \hbar\omega). \quad (3.41)$$

Next, we change the variable on the right hand side, i.e., $E - \hbar\omega = E'$. Moreover, considering the fact that $P(E)$ vanishes for negative E at zero temperature, we obtain the integral equation for $P(E)$:

$$EP(E) = 2 \int_0^E dE' \frac{\text{Re} \left[Z_t \left(\frac{E-E'}{\hbar} \right) \right]}{R_Q} P(E'). \quad (3.42)$$

Finally, we can solve this equation numerically. Technically, we start with an arbitrary value $P(0)$ and then use the normalization condition $\int_0^{E_{\text{cut-off}}} dE P(E) = 1$ to complete the numerical evaluation. $E_{\text{cut-off}}$ is a cut-off energy corresponding to the cut-off frequency $\omega_{\text{cut-off}}$ in Eq. (3.34).

The current-voltage characteristic

We obtain numerically the current-voltage characteristic for various values of the normalized impedance Z_0/R_Q by substituting Eq. (3.34) into the integral equation (3.42) and ensuing numerical calculation. The result is shown in Fig. 3.5. In the weak impedance regime, i.e., $Z_0/R_Q < 0.5$, the current is peaked at $V = 0$ and then decreases with voltage. As for the opposite case of high impedance, the current increases with voltage for small voltage, and has a peak centered around $2eV = 4E_c$. In addition, Coulomb blockade appears for large impedance (e.g., $Z_0/R_Q = 40$).

To better understand the results, we discuss further two extreme impedance regimes.

When the impedance Z_0 is much larger than the quantum resistance R_Q , the real part of the total impedance (3.34) becomes a delta function:

$$\frac{\text{Re}[Z_t(\omega)]}{R_Q} = \lim_{Z_0/R_Q \rightarrow \infty} \frac{Z_0/R_Q}{1 + [\pi(Z_0/R_Q)\hbar\omega/(4E_c)]^2} \approx \frac{4E_c}{\hbar} \delta(\omega). \quad (3.43)$$

Plugging Eq. (3.43) into Eq. (3.38), we obtain the phase correlation $J(t)$ which is formulated at low frequencies means that the short time expansion

$$J_0(t) = \frac{4E_c}{\hbar} \int_0^\infty d\omega \delta(\omega) (-it) = -4iE_c t / \hbar. \quad (3.44)$$

Substituting it into Eq. (3.17), we obtained the current

$$I(V) = \frac{e\pi E_J^2}{\hbar} \delta(2eV - 4E_c). \quad (3.45)$$

Equation above shows that the current is sharply peaked at $V = 4E_c/2e$ [e.g., $Z_0/R_Q = 40$ in Fig. 3.5]: the tunnelling of Cooper pair with charge $2e$ gains energy

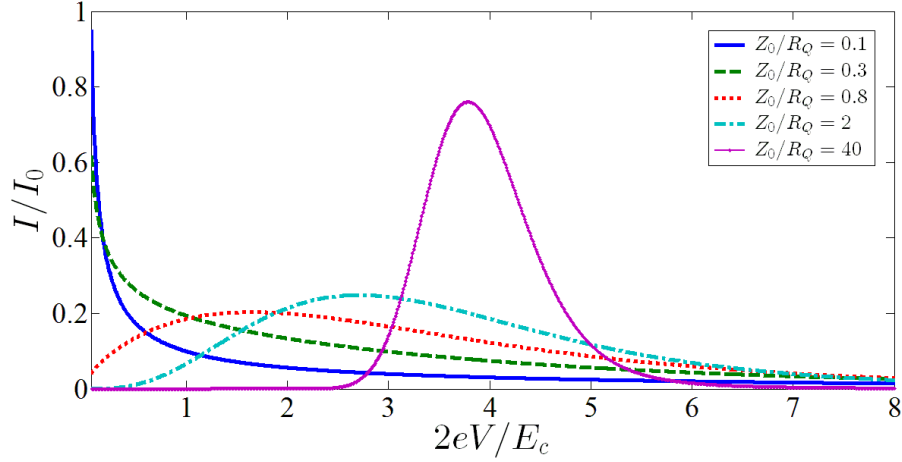


Figure 3.5: The current-voltage characteristic of a voltage-biased Josephson junction. The junction is coupled to an infinite transmission line with five different impedance values $Z_0/R_Q = 0.1, 0.3, 0.8, 2, 40$. The current is normalized by $I_0 = e\pi E_J^2/\hbar E_c$.

$2eV$, but must pay a cost $4E_c = (2e)^2/C_J$ to charge the capacitance C_J , which leads to Coulomb blockade.

Now we consider the case with a weak impedance, i.e., $Z_0/R_Q \ll 1$. In such a situation, we may write approximately the term $e^{J(t)}$ as $1 + J(t)$, since $J(t)$ is proportional to Z_0/R_Q [see Eq. (3.38)]. Using the expression with Eqs. (3.37) and (3.17), the current at finite V is obtained at zero temperature:

$$I(V) = \frac{Z_0}{R_Q} \frac{\pi E_J^2}{2\hbar V}. \quad (3.46)$$

At voltage $V \rightarrow 0$, the current goes divergent. Indeed, this is due to the limitation of the $P(E)$ -theory. The range of validity⁷ is given by $V \gg (1/2\pi)I_c Z_0$, where I_c is the critical current of the Josephson junction. Beyond this voltage, the theory is correct and Cooper pair tunnels incoherently through the Josephson junction. Otherwise Cooper pair tunnels coherently and results in a supercurrent. In some sense, the peak (at low voltage) in the current-voltage characteristic can be seen as a precursor of the supercurrent branch. Comparing with the strong impedance

⁷In the derivation of $P(E)$ -theory, we assumed that the Josephson energy E_J is small. From an analysis of higher order term, one can obtain that the theory is valid only if $E_J P(2eV) \ll 1$. Obviously, the condition depends on the voltage as well as the impedance of the environment. Taking the ohmic environment discussed in this section as an example, we find the condition becomes $V \gg (1/2\pi)I_c Z_0$.

regime, the Coulomb blockade effect disappears. This is due to the quantum fluctuation of the environment that activate the charge transfer across the junction. It smears the Coulomb charging effect. With increasing voltage, the current starts to decrease as $1/V$. In chapter 4, we will concentrate on this regime.

3.3.2 Summary

In this section, we solved the current flowing through the Josephson junction with $P(E)$ -function which characterize the influence of the environment. Taking the transmission line as the electromagnetic environment, we discussed the current-voltage characteristic of the junction. At high impedances of the line, charging effect dominated and the Coulomb blockade manifested at voltage below that charging energy. At low impedances, the current increased inversely with the voltage, which is a precursor of the supercurrent branch in an ideal Josephson junction.

3.4 Phase-phase correlator: nonlinear regime

We now switch to nonlinear electromagnetic environments which are described by a non-quadratic Hamiltonian H_{nl} . Then the phase-phase correlator in Eq. (3.13) is impossible to compute exactly. The Green's function perturbation theory and path integral method offer a possibility to obtain the results. In the following, we first present the ideas of Green's function perturbation theory, and then introduce the Feynman diagrams which are a valuable tool for organizing and understanding the perturbative calculations. Next, we introduce the path integral method. In order to see how it works, we apply it to a specific (quadratic) environment, i.e., a transmission line.

3.4.1 Green's function perturbation theory

To use the Green's function perturbation theory, we write the Hamiltonian of the nonlinear system as

$$H_{\text{nl}} = H^{(0)} + V, \quad (3.47)$$

where $H^{(0)}$, is a solvable quadratic Hamiltonian; and the interaction V includes all remaining parts of H_{nl} . Starting with a system described by $H^{(0)}$, we then add perturbatively the effect of V to see how it changes the relevant property.

The Hamiltonian H_{nl} describes an interacting system, therefore the phase-phase correlation function in Eq. (3.13) can no longer be written as a simple closed

form expression [e.g., Eq. (3.20)]. Instead we expand it in powers of ϕ_c as follows:

$$\begin{aligned}
\langle e^{i\phi_c(t)} e^{-i\phi_c(0)} \rangle_{H_{\text{nl}}} &= 1 + i \langle \phi_c(t) - \phi_c(0) \rangle_{H_{\text{nl}}} \\
&+ \langle [\phi_c(t) - \phi_c(0)] \phi_c(0) \rangle_{H_{\text{nl}}} \\
&+ \frac{i}{2} \langle \phi_c(t) \phi_c(0) [\phi_c(t) - \phi_c(0)] \rangle_{H_{\text{nl}}} \\
&+ \frac{1}{4} \langle [\phi_c^2(t) - \phi_c^2(0)] \phi_c^2(0) \rangle_{H_{\text{nl}}} \\
&- \frac{1}{6} \langle [\phi_c^3(t) - \phi_c^3(0)] \phi_c(0) \rangle_{H_{\text{nl}}} \\
&- \frac{1}{6} \langle [\phi_c(t) - \phi_c(0)] \phi_c^3(0) \rangle_{H_{\text{nl}}} \\
&+ \mathcal{O}(\phi_c^5). \tag{3.48}
\end{aligned}$$

As before, we still use Green's functions to evaluate the correlators in Eq. (3.48). Indeed, the relation (3.22) can be extended to compute multiple-point correlators. In addition to the two-point retarded Green's function $G_R(\phi_c, \phi_c; \omega)$ we used for linear cases, we may need one-point retarded Green's function $G_R(\phi_c; \omega)$, three-point retarded Green's functions $G_R(\phi_c^2, \phi_c; \omega)$ and $G_R(\phi_c, \phi_c^2; \omega)$, as well as four-point retarded Green's functions $G_R(\phi_c^2, \phi_c^2; \omega)$, $G_R(\phi_c^3, \phi_c; \omega)$, and $G_R(\phi_c, \phi_c^3; \omega)$. In order to be able to use perturbation theory to evaluate these Green's functions, we switch to imaginary-time-ordered or Matsubara Green's functions, \mathcal{G} . When the nonlinear Hamiltonian H_{nl} is symmetric in phase and charge, the odd-point retarded Green's functions will vanish (this can be verified using the argument given in Sec. 3.2). We will check the specific cases in Chapter 4 and Chapter 5.

For convenience, we write the needed Green's functions in a uniform formalism, i.e., $\mathcal{G}[\phi_c^\alpha(\tau), \phi_c^\beta(0)]$ ($\alpha + \beta \geq 1$, α, β are non-negative integers). At zero temperature, we define

$$\mathcal{G}[\phi_c^\alpha(\tau), \phi_c^\beta(0)] = \langle T_\tau \phi_c^\alpha(\tau) \phi_c^\beta(0) \rangle_{H_{\text{nl}}}, \tag{3.49}$$

where T_τ is the time-ordering operator. And $\langle \dots \rangle_{H_{\text{nl}}} \equiv \langle |\dots\rangle_{H_{\text{nl}}} | \dots \rangle_{H_{\text{nl}}}$ refers to averaging over eigenstates $|\dots\rangle_{H_{\text{nl}}}$ of the system. Initially, $|\dots\rangle_{H_{\text{nl}}}$ is of course not known since that is exactly what is to be determined by using the Green's functions.

To compute the Green's function (3.49) which is based on the unknown ground states $|\dots\rangle_{H_{\text{nl}}}$, we use the interaction representation⁸. It allows us to isolate the effect of the interacting Hamiltonian from the unperturbed Hamiltonian. The idea is to treat the main Hamiltonian $H^{(0)}$ in the Heisenberg representation,

⁸Such choice does not change the results of problem comparing with using Schrödinger or Heisenberg representations.

but to handle the interaction V in the Schrödinger representation. As a result, the operators have a time dependence, e.g., $\phi_c(\tau) = e^{H^{(0)}\tau}\phi_c e^{-H^{(0)}\tau}$, while the wave functions $\psi(\tau)$ vary as

$$\frac{\partial}{\partial \tau} \psi(\tau) = -V(\tau)\psi(\tau). \quad (3.50)$$

Indeed, the wave function at $\tau = 0$, i.e., $\psi(0)$, describes the state $|\rangle_{H_{\text{nl}}}$.

For later convenience, we introduce the S matrix as the operator $S(\tau, \tau')$ which connects the wave function $\psi(\tau')$ and $\psi(\tau)$, namely

$$\psi(\tau) = S(\tau, \tau')\psi(\tau'). \quad (3.51)$$

Using Eq. (3.50), we obtain

$$\frac{\partial}{\partial \tau} S(\tau, \tau') = -V(\tau)S(\tau, \tau'), \quad (3.52)$$

from which the solution is obtained by a couple of steps: integrate both sides of the equation above with respect to time, iterate repeatedly the obtained solution, introduce the time-ordering operator, and rewrite the result⁹. It is expressed as

$$S(\tau, \tau') = T_\tau \exp \left[- \int_{\tau'}^{\tau} d\tau_1 V(\tau_1) \right]. \quad (3.53)$$

Using the S matrix, we now establish the relation between the ground states of perturbed and the unperturbed Hamiltonian: $|\rangle_{H_{\text{nl}}} = S(0, -\infty)|\rangle_{H^{(0)}}$ [132], where $|\rangle_{H^{(0)}}$ is defined as the ground state of the unperturbed Hamiltonian $H^{(0)}$. We used the assertion that $|\rangle_{H^{(0)}}$ is equal to $\psi(-\infty)$. The argument is that one starts in the past ($\tau = -\infty$) with a unperturbed state $|\rangle_{H^{(0)}}$, then the operator $S(0, -\infty)$ brings the state to the present ($\tau = 0$), i.e., $|\rangle_{H_{\text{nl}}}$. It is the ground state of H_{nl} which contains the effects of the interaction V . As argued before, $|\rangle_{H^{(0)}}$ is solvable, therefore one can get $|\rangle_{H_{\text{nl}}}$ and further compute the trace in Eq. (3.49). We finally obtain [131]

$$\mathcal{G} \left[\phi_c^\alpha(\tau), \phi_c^\beta(0) \right] = \frac{\langle T_\tau \phi_c^\alpha(\tau) \phi_c^\beta(0) S(\infty, -\infty) \rangle_{H^{(0)}}}{\langle S(\infty, -\infty) \rangle_{H^{(0)}}}, \quad (3.54)$$

where we used the relation ${}_{H^{(0)}}\langle S(-\infty, 0) | = {}_{H^{(0)}}\langle S(\infty, 0) | / {}_{H^{(0)}}\langle | S(-\infty, \infty) \rangle | \rangle_{H^{(0)}}$. It is seen that the expectation values in the unknown ground states $|\rangle_{H_{\text{nl}}}$ are now expressed in terms of the expectation values in the solvable ground state $|\rangle_{H^{(0)}}$.

⁹The details can be found in the book [131], page 68.

In the absence of the interaction, i.e., $V = 0$, the S matrix is unity according to Eq. (3.53). Thus, Eq. (3.54) reduces to a unperturbed time-ordered Green's function,

$$\mathcal{G}^{(0)} \left[\phi_c^\alpha(\tau) \phi_c^\beta(0) \right] = \langle T_\tau \phi_c^\alpha(\tau) \phi_c^\beta(0) \rangle_{H^{(0)}}. \quad (3.55)$$

Indeed, we will see later that this equation corresponds to the zeroth order contribution of a perturbation series.

When the interaction is involved, the Green's function (3.54) is evaluated by expanding the S matrix in a series, namely

$$\begin{aligned} \mathcal{G} \left[\phi_c^\alpha(\tau), \phi_c^\beta(0) \right] &= \sum_{n=0}^{\infty} \frac{1}{n!} \int_{-\infty}^{\infty} d\tau_1 \int_{-\infty}^{\infty} d\tau_2 \cdots \int_{-\infty}^{\infty} d\tau_n \\ &\times \frac{\langle T_\tau \phi_c^\alpha(\tau) \phi_c^\beta(0) V(\tau_1) V(\tau_2) \cdots V(\tau_n) \rangle_{H^{(0)}}}{\langle V(\tau_1) V(\tau_2) \cdots V(\tau_n) \rangle_{H^{(0)}}}. \end{aligned} \quad (3.56)$$

As $H^{(0)}$ is quadratic, we can use Wick's theorem to evaluate the time-ordered brackets. The operators in the bracket are paired and aligned according to the time order.

In order to see in detail the way of constructing pairings, to introduce the Feynman diagrams, and to understand the relevant physical meaning, we introduce a simple case: the unperturbed Hamiltonian $H^{(0)}$ is given by a quadratic form with phase and charge [e.g., Eq. (2.44)]; and the interaction is added to the coupling node [see Fig. 3.2 (a), the coupling node was labelled by ϕ_c] between the Josephson junction and the environment. We do not specify the interaction but only state that it reads as a quartic form, namely

$$V = \frac{\lambda}{4!} \phi_c^4, \quad (3.57)$$

where the constant λ describes the coupling strength. Such choice was indeed inspired by the well-known quartic self-interacting scalar field theory [133, 134], which is frequently used to study interacting problems.

For a quartic interaction, the odd orders in Eq. (3.48) do not contribute while only even orders are left. In the following, we use Eqs. (3.56) and (3.57) to evaluate the two-point Green's function $\mathcal{G}[\phi_c(\tau), \phi_c(0)]$ as well as the four-point Green's function $\mathcal{G}[\phi_c^2(\tau), \phi_c^2(0)]$. Of course, the results can be generalized to other theories of interest. As the interaction considered in chapter 4 will be quartic as well, we will see the method addressed below can be conveniently mapped to the problem.

Two-point Green's function

Substituting Eq. (3.57) into Eq. (3.56), and taking $\alpha = \beta = 1$, we now look at the first few terms of the expansion [see Eq. (3.56)] of the two-point Green's function $\mathcal{G}[\phi_c(\tau), \phi_c(0)]$.

To zeroth order in λ , namely by taking $n = 0$ in Eq. (3.56), the numerator reduces to $\langle T_\tau \phi_c(\tau) \phi_c(0) \rangle_{H^{(0)}}$, while the denominator is equal to one. Therefore we obtain

$$\mathcal{G}[\phi_c(\tau), \phi_c(0)] = \mathcal{G}^{(0)}[\phi_c(\tau), \phi_c(0)] + \mathcal{O}(\lambda), \quad (3.58)$$

where we used the definition of unperturbed Green's function (3.55).

To first order in λ , namely taking $n = 1$ in Eq. (3.56), the numerator becomes

$$\langle T_\tau \phi_c(\tau) \phi_c(0) \rangle_{H^{(0)}} - \frac{\lambda}{4!} \int_{-\infty}^{\infty} d\tau_1 \langle T_\tau \phi_c(\tau) \phi_c(0) \phi_c^4(\tau_1) \rangle_{H^{(0)}}. \quad (3.59)$$

Since $H^{(0)}$ is quadratic, we can use Wick's theorem to simplify the time-ordered bracket of the second term. According to the rules, the bracket can be rewritten as the summation of all the possible pairings, and each of these pairings will either be a time-ordered Green's function (different time) or number operator (same time). Moreover, the time ordering of each pair is given by the proper time ordering to get the entire result. Using these rules, we get

$$\begin{aligned} \langle T_\tau \phi_c(\tau) \phi_c(0) \phi_c^4(\tau_1) \rangle_{H^{(0)}} &= 3 \langle T_\tau \phi_c(\tau) \phi_c(0) \rangle_{H^{(0)}} [\langle \phi_c^2(\tau_1) \rangle_{H^{(0)}}]^2 \\ &+ 12 \langle T_\tau \phi_c(\tau) \phi_c(\tau_1) \rangle_{H^{(0)}} \langle \phi_c^2(\tau_1) \rangle_{H^{(0)}} \langle T_\tau \phi_c(\tau_1) \phi_c(0) \rangle_{H^{(0)}}. \end{aligned} \quad (3.60)$$

In Eq. (3.60) above, the two terms correspond to two different types of pairings. For the first term, the operators of the interaction pair with each other, while they pair with $\phi_c(\tau)$ and $\phi_c(0)$ for the second one. The difference will be seen more clearly in the representation of Feynman diagrams. Besides, the pre-factors 3 and 12 count the number of ways that the same time-ordered pairings repeat. For the similar pre-factors appearing in the following calculations, we do not explain this any more it is due to the same reason.

Plugging Eq. (3.60) into Eq. (3.59), we obtain the numerator of Eq. (3.56) up to first order in λ :

$$\begin{aligned} \langle T_\tau \phi_c(\tau) \phi_c(0) \rangle_{H^{(0)}} - \frac{3\lambda}{4!} \langle T_\tau \phi_c(\tau) \phi_c(0) \rangle_{H^{(0)}} \int_{-\infty}^{\infty} d\tau_1 [\langle \phi_c^2(\tau_1) \rangle_{H^{(0)}}]^2 \\ - \frac{12\lambda}{4!} \int_{-\infty}^{\infty} d\tau_1 \langle T_\tau \phi_c(\tau) \phi_c(\tau_1) \rangle_{H^{(0)}} \langle \phi_c^2(\tau_1) \rangle_{H^{(0)}} \langle T_\tau \phi_c(\tau_1) \phi_c(0) \rangle_{H^{(0)}} \end{aligned} \quad (3.61)$$

Similarly, the denominator of the Eq. (3.56) is expanded to the first order in λ as

$$1 - \frac{3\lambda}{4!} \int_{-\infty}^{\infty} d\tau_1 [\langle \phi_c^2(\tau_1) \rangle_{H^{(0)}}]^2 + \mathcal{O}(\lambda^2). \quad (3.62)$$

Substituting Eqs. (3.61) and (3.62) into Eq. (3.56), we find it is hard to further simplify. However, if we expand the interaction of the numerator beyond the first order, it comes to:

$$\begin{aligned} & \left\{ 1 - \frac{3\lambda}{4!} \int_{-\infty}^{\infty} d\tau_1 [\langle \phi_c^2(\tau_1) \rangle_{H^{(0)}}]^2 + \mathcal{O}(\lambda^2) \right\} \times [\langle T_\tau \phi_c(\tau) \phi_c(0) \rangle_{H^{(0)}}] \\ & - \frac{12\lambda}{4!} \int_{-\infty}^{\infty} d\tau_1 \langle T_\tau \phi_c(\tau) \phi_c(\tau_1) \rangle_{H^{(0)}} \langle \phi_c^2(\tau_1) \rangle_{H^{(0)}} \langle T_\tau \phi_c(\tau_1) \phi_c(0) \rangle_{H^{(0)}} \\ & + \mathcal{O}(\lambda^2)]. \end{aligned} \quad (3.63)$$

We now collect the two equations above, i.e., the results of numerator and denominator, the denominator cancel exactly one part of the numerator. Later we will see that this part corresponds to the disconnected Feynman diagrams which do not contribute. Thus, the two-point Green's function to the first order in λ reads

$$\begin{aligned} \mathcal{G}[\phi_c(\tau), \phi_c(0)] &= \mathcal{G}^{(0)}[\phi_c(\tau)\phi_c(0)] - \frac{\lambda}{2} \int_{-\infty}^{\infty} d\tau_1 \mathcal{G}^{(0)}[\phi_c(\tau)\phi_c(\tau_1)] \\ & \quad \times \langle \phi_c^2(\tau_1) \rangle_{H^{(0)}} \mathcal{G}^{(0)}[\phi_c(\tau_1)\phi_c(0)] + \mathcal{O}(\lambda^2). \end{aligned} \quad (3.64)$$

Making Fourier transform with respect to time upon the equation above, we rewrite it in Matsubara frequency space:

$$\begin{aligned} \mathcal{G}[\phi_c, \phi_c; i\omega_V] &= \mathcal{G}^{(0)}[\phi_c; \phi_c; i\omega_V] \\ & \quad - \mathcal{G}^{(0)}[\phi_c, \phi_c; i\omega_V] \left[\frac{\lambda}{2} \langle \phi_c^2 \rangle_{H^{(0)}} \right] \mathcal{G}^{(0)}[\phi_c, \phi_c; i\omega_V] + \mathcal{O}(\lambda^2). \end{aligned} \quad (3.65)$$

When the second order is much smaller than the first one, the first order expansion is enough for the result. Otherwise, the result is no longer true. Indeed, it is possible to go beyond the first order expansion by realizing that $(-\lambda/2)\langle \phi_c^2 \rangle_{H^{(0)}}$ is the lowest term of the self-energy¹⁰ Σ . The Dyson's equation is expressed as:

$$\mathcal{G}[\phi_c, \phi_c; i\omega_V] = \mathcal{G}^{(0)}[\phi_c; \phi_c; i\omega_V] + \mathcal{G}^{(0)}[\phi_c, \phi_c; i\omega_V] \Sigma \mathcal{G}[\phi_c, \phi_c; i\omega_V]. \quad (3.66)$$

¹⁰The self-energy is summation of an infinite number of series, and it is defined as an irreducible part of the Green's function. Normally, it is impossible to get exactly, and one must be content with an approximate result.

Dyson's equation state that the time-ordered Green's functions \mathcal{G} can be obtained from Eq. (3.66) by simply knowing the unperturbed time-ordered Green's function $\mathcal{G}^{(0)}$ and the self-energy Σ . Basically, Dyson's equation is useful only in weak coupling theory where the perturbation is sufficiently weak that an adequate approximation is obtained with a few terms in Σ . In our case, when $\lambda \ll 1$, $\Sigma \approx (-\lambda/2)\langle\phi_c^2\rangle_{H^{(0)}}$.

Feynman diagrams for two-point Green's function

The Feynman diagrams are both an exact mathematical representation of perturbation theory to infinite order and a powerful pictorial method that elucidates the physical content of the complicated expressions. We now introduce the Feynman diagrams for the two-point Green's functions.

As a starting point, the basic graphical vocabulary is defined in Fig. 3.6. We use thick lines and thin lines to represent the full ($\mathcal{G}[\phi_c(\tau)\phi_c(0)]$) and unperturbed ($\mathcal{G}^{(0)}[\phi_c(\tau)\phi_c(0)]$) time-ordered Green's functions, respectively. An arrow is often included to represent the direction. Note that the arrow does not mean $\tau > 0$. We use a closed circle, which starts and terminates at the same time point (e.h., τ_1), representing the term $\langle\phi_c^2(\tau_1)\rangle_{H^{(0)}}$. Using these basic diagrams, we can interpret the calculations above using the language of Feynman diagrams.

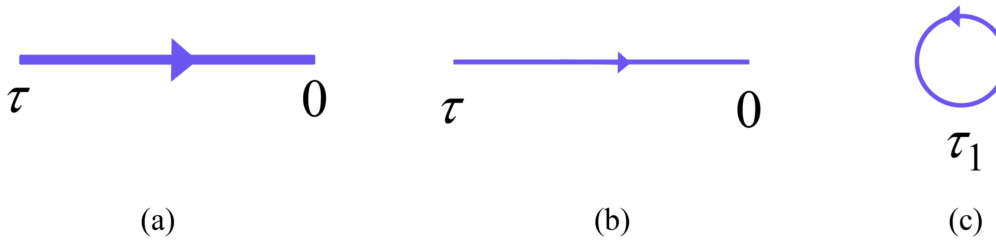


Figure 3.6: The Feynman diagrams of (a) the full time-ordered Green's function $\mathcal{G}(\tau, 0)$, (b) the unperturbed time-ordered Green's function $\mathcal{G}^{(0)}(\tau, 0)$, and (c) the term $\langle\phi_c^2(\tau_1)\rangle_{H^{(0)}}$.

Collecting the numerator [see Eq. (3.61)] and the denominator [see Eq. (3.62)], we obtain the Feynman diagrams for the two-point Green's function to the first order in λ . The denominator represents the vacuum fluctuation and the first order correction; while the numerator consists of both connected diagrams and disconnected diagram. In order to see clearly which parts of the diagrams play a role, we expand λ beyond the first order, then the numerator becomes Eq. (3.63). The corresponding Feynman diagrams are shown in Fig. 3.7. We can see the diagrams of

the dominator cancel¹¹ exactly the disconnected diagrams of the numerator, and only the connected diagrams are left. Indeed, this conclusion can be generalized into an important theorem that the vacuum polarization terms $\langle S(\infty, -\infty) \rangle_{H(0)}$ will exactly cancel the disconnected diagrams in the numerator expression. Consequently, only connected diagrams are necessary in the calculation of time-ordered Green's function. For the evaluation of the four-point Green's function, we will directly use this theorem.

$$\begin{array}{c} \tau \\ \longrightarrow \\ 0 \end{array} = \frac{\left(1 + \text{loop}_{\tau_1} + o(\lambda^2) \right) \left(\begin{array}{c} \tau \longrightarrow 0 \\ \tau \longrightarrow \text{loop}_{\tau_1} \longrightarrow 0 \\ + o(\lambda^2) \end{array} \right)}{1 + \text{loop}_{\tau_1} + o(\lambda^2)}$$

Figure 3.7: The Feynman diagrams of the two-point Green's function $\mathcal{G}[\phi_c(\tau), \phi_c(0)]$ beyond the first order contribution. The numerator corresponds to Eq. (3.63).

The Feynman diagram of Dyson's equation (3.66) is shown in Fig. 3.8.

$$\begin{array}{c} \longrightarrow \\ \wp \end{array} = \begin{array}{c} \longrightarrow \\ \wp^{(0)} \end{array} + \begin{array}{c} \longrightarrow \\ \wp^{(0)} \end{array} \textcircled{\Sigma} \begin{array}{c} \longrightarrow \\ \wp \end{array}$$

Figure 3.8: The Feynman diagrams of the Dyson's equation Eq. (3.66). In weak coupling limit, the self-energy Σ can be approximated as the lowest term $(-\lambda/2)\langle \phi_c^2 \rangle_{H(0)}$.

In summary, two-point Green's function was evaluated. The perturbed Green's function can be expressed in terms of the unperturbed Green's function and the self-energy. Moreover, we introduced the Feynman diagrams. It was verified the visual clarity is obtained without loss of mathematical rigour. When Green's functions are used to handle the specific problems in chapter 4 and chapter 5, we will try to use the Feynman diagrams instead of the complex integral formalisms.

¹¹Note that the pre-factors of each diagram are shown in Eqs. (3.61) and (3.63).

Four-point Green's function

We now switch to evaluate the four-point Green's function $\mathcal{G}[\phi_c^2(t)\phi_c^2(0)]$. As before, substituting Eq. (3.57) into Eq. (3.56), but taking $\alpha = \beta = 2$, we study the first few terms of the expansion [see Eq. (3.56)]. We already learned that the terms in the dominator cancel exactly those with disconnected Feynman diagrams in the numerator. Therefore, only the terms with connected Feynman diagrams in the numerator should be kept. The numerator of Eq. (3.56) takes the form:

$$\sum_{n=0}^{\infty} \left(\frac{\lambda}{4!}\right)^n \frac{1}{n!} \int_{-\infty}^{\infty} d\tau_1 \int_{-\infty}^{\infty} d\tau_2 \cdots \int_{-\infty}^{\infty} d\tau_n \quad (3.67)$$

$$\langle T_{\tau} \phi_c^2(\tau)\phi_c^2(0)\phi_c^4(\tau_1)\phi_c^4(\tau_2)\cdots\phi_c^4(\tau_n) \rangle_{H^{(0)}}.$$

To zeroth order in λ , i.e., taking $n = 0$ in Eq. (3.67), the equation above reduces to $\langle T_{\tau} \phi_c^2(\tau)\phi_c^2(0) \rangle_{H^{(0)}}$. Using Wick's theorem, it is expressed in terms of two-point functions, i.e., $2[\langle T_{\tau} \phi_c(\tau)\phi_c(0) \rangle_{H^{(0)}}]^2$. In the representation in terms of Feynman diagrams (see Fig. 3.9), it consists of two thin lines.

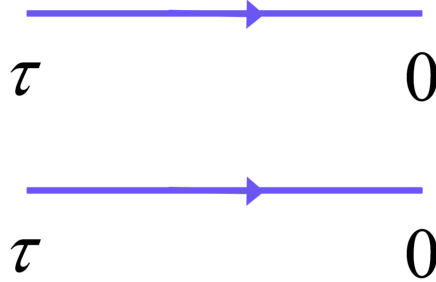


Figure 3.9: The Feynman diagrams of four-point Green's function to the zeroth order in λ . It reads in term of two-point Green's functions.

To first order in λ , i.e., taking $n = 1$ in Eq. (3.67), becomes

$$\langle T_{\tau} \phi_c^2(\tau)\phi_c^2(0) \rangle_{H^{(0)}} + \frac{\lambda}{4!} \int_{-\infty}^{\infty} d\tau_1 \langle T_{\tau} \phi_c^2(\tau)\phi_c^2(0)\phi_c^4(\tau_1) \rangle_{H^{(0)}}. \quad (3.68)$$

The time-ordered bracket of the first order correction [the second term of Eq. (3.68)] can be simplified using Wick's theorem. According to the rules argued before, we now have two possible ways for pairing:

i) the interaction term $\phi_c^4(\tau_1)$ pairs only with two of the operators $\phi_c^2(\tau)\phi_c^2(0)$, i.e., $\phi_c(\tau)$ and $\phi_c(0)$; while the other two operators pair with each other, consisting

of a two-point time-ordered correlator $\langle T_\tau \phi_c(\tau)\phi_c(0) \rangle_{H^{(0)}}$. Thus, we obtain¹²

$$48 \langle T_\tau \phi_c(\tau)\phi_c(0) \rangle_{H^{(0)}} \langle T_\tau \phi_c(\tau)\phi_c(\tau_1) \rangle_{H^{(0)}} \langle \phi_c^2(0) \rangle_{H^{(0)}} \langle T_\tau \phi_c(\tau_1)\phi_c(0) \rangle_{H^{(0)}}, \quad (3.69)$$

The corresponding Feynman diagrams of the equation above is shown in Fig. 3.10 (a). Comparing with the Feynman diagrams [Fig. 3.9] of the zeroth order contribution, the interaction corrects only one of the lines.

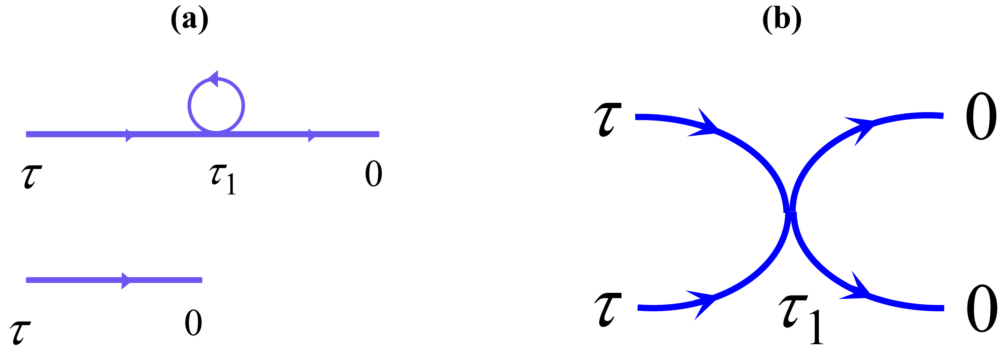


Figure 3.10: The Feynman diagrams of four-point Green's function to the first order in λ , with the pairing way *i*) (a) and *ii*) (b).

ii) the interaction term pairs with each operator of $\phi_c^2(\tau)\phi_c^2(0)$. As a result, the time-ordered bracket becomes

$$24 [\langle T_\tau \phi_c(\tau)\phi_c(\tau_1) \rangle_{H^{(0)}} \langle T_\tau \phi_c(\tau_1)\phi_c(0) \rangle_{H^{(0)}}]^2. \quad (3.70)$$

The corresponding Feynman diagram is shown in Fig. 3.10 (b). It is seen that the interaction couples the two lines together.

Plugging Eqs. (3.69) and (3.70) into Eq. (3.68), and recovering the correlators by the time-ordered Green's functions, we obtain the four-point Green's function to the first order in λ :

$$\begin{aligned} \mathcal{G}[\phi_c^2(\tau)\phi_c^2(0)] &= 2\mathcal{G}^{(0)}[\phi_c(\tau)\phi_c(0)] + 2\lambda\mathcal{G}^{(0)}[\phi_c(\tau)\phi_c(0)] \quad (3.71) \\ &\quad \times \int_{-\infty}^{\infty} d\tau_1 \mathcal{G}^{(0)}[\phi_c(\tau)\phi_c(\tau_1)] \langle \phi_c^2(0) \rangle_{H^{(0)}} \mathcal{G}^{(0)}[\phi_c(\tau_1)\phi_c(0)] \\ &\quad + \lambda \int_{-\infty}^{\infty} d\tau_1 \left\{ \mathcal{G}^{(0)}[\phi_c(\tau)\phi_c(\tau_1)] \mathcal{G}^{(0)}[\phi_c(\tau_1)\phi_c(0)] \right\}^2 \\ &\quad + \mathcal{O}(\lambda^2). \end{aligned}$$

¹²The pre-factors 48 count the number of ways that the same time-ordered pairings repeat. The same reason for the pre-factor in Eq. (3.70).

In summary, four-point Green's function $\mathcal{G}[\phi_c^2(\tau)\phi_c^2(0)]$ was evaluated. Comparing with the two-point Green's function, there were two different pairing ways, results in two kinds of contributions. For the first one, the interaction term only interacts with one of the lines; while the left two operators paired with each other. As for the second one, the interaction term interacts with both lines. As a result, the two lines couple together. In many-particle physics, it represents particle-particle interaction.

3.4.2 Path integral method

Green's function perturbation theory offers a solution to compute the phase-phase correlation functions if we consider a nonlinear system. However, the computational complexity of the multiple-point correlators increases dramatically with the perturbation theory. Nevertheless, the path integral method provides a convenient way to compute the time-ordered Green's functions. Especially for the exponential phase-phase correlator, e.g., $\langle e^{i\phi_c(t)}e^{-i\phi_c(0)} \rangle_{H_{\text{nl}}}$ in Eq. (3.13), other methods are tough, but the path integral method can simplify the calculations. Another aspect is that it allows obtaining some relations between two objects that one of them is hard to compute while the other one is already known well.

As before, the task is to compute the phase-phase correlator $\langle e^{i\phi_c(t)}e^{-i\phi_c(0)} \rangle_{H_{\text{nl}}}$. In order to be able to use path integral, one needs to switch to the imaginary time-ordered representation, namely, $\langle T_\tau e^{i\phi_c(\tau)}e^{-i\phi_c(0)} \rangle_{H_{\text{nl}}}$. Here, we do not present the derivation of the path integral but directly use the method to evaluate time-ordered correlators. The derivation can be found in details in reference [135] and book [136].

First of all, we take the nonlinear electromagnetic environment [described by H_{nl}] characterized by two canonically conjugate variables: the phase ϕ and the charge Q .

Taking advantage of the path integral representation [136], the partition function $Z = \text{Tr}[e^{-\beta H_{\text{nl}}}]$ (β is the inverse temperature) is expressed via a functional integral

$$Z = \int D\phi(\tau) \int DQ(\tau) e^{-s}, \quad (3.72)$$

where $\int D\phi(\tau)$ [$\int DQ(\tau)$] means the integration over all possible functions $\phi(\tau)$ [$Q(\tau)$]. They can be thought of as a ‘‘function of a function’’ acting as functional over a continuous range of functions. The action term reads

$$-s = \frac{1}{\hbar} \int_0^{\beta\hbar} d\tau [iQ(\tau)\dot{\phi}(\tau) - H_{\text{nl}}(\phi_c(\tau), Q_c(\tau))]. \quad (3.73)$$

Then the time-ordered phase-phase correlator is expressed as [136]

$$\langle T_\tau e^{i\phi(\tau)} e^{-i\phi(0)} \rangle_{H_{nl}} = \frac{1}{Z} \int D\phi(\tau) \int DQ(\tau) e^{i\phi(\tau)} e^{-i\phi(0)} e^{-s}. \quad (3.74)$$

For computing the equation above, we need a cornerstone formula: a Gaussian integral over N complex variables u ,

$$\left(\prod_i \int \frac{du_i du_i^*}{2\pi i} \right) \exp \left[- \sum_{i,j} u_i^* C_{ij} u_j + \sum_i (h_i^* u_i + h_i u_i^*) \right] = \frac{\exp \left[\sum_{i,j} h_i (C^{-1})_{ij} h_j^* \right]}{\det(C)} \quad (3.75)$$

where C is an $N \times N$ matrix.

In order to further show how to use path integrals to evaluate correlation functions, we consider a specific case which was discussed in subsection 3.3.1 but with the approach of Green's functions. Indeed, the linear case constitutes a good starting point to present the generic process and technique of the calculation. As for the nonlinear system, we will postpone the calculation to chapter 5. The basic procedures will be the same, we just have to add the nonlinearity.

Here, we do not repeat the relevant physical things but only take care of the mathematical calculations. The task now is to compute the local phase-phase correlator, i.e., $\langle e^{i\phi_m(t)} e^{-i\phi_m(0)} \rangle_{H_T}$, where H_T was given in Eq. (3.24).

Using the path integral representation, the phase-phase correlator is expressed as the functional integral

$$\langle T_\tau e^{i\phi_m(\tau)} e^{-i\phi_m(0)} \rangle_{H_T} = \frac{1}{Z} \int D\phi_n(\tau) DQ_n(\tau) e^{i\phi_m(\tau)} e^{-i\phi_m(0)} e^{-s}, \quad (3.76)$$

where the partition function is $\int D\phi_n(\tau) DQ_n(\tau) e^{-s}$ with the action,

$$-s = \frac{1}{\hbar} \int_0^{\beta\hbar} d\tau \sum_n iQ_n(\tau) \frac{\hbar}{2e} \dot{\phi}_n(\tau) - H_T. \quad (3.77)$$

In order to solve Eq. (3.76), we introduce two useful relations:

$$\phi_n(\tau) = (1/\beta\mathcal{L}) \sum_q e^{iq\tau} \phi_q, \quad Q_n(\tau) = (1/\beta\mathcal{L}) \sum_q e^{iq\tau} Q_q, \quad (3.78)$$

where $q \equiv (k, \omega_n)$, $r \equiv (n, \tau)$ and $qr \equiv kn - \omega_n \tau$; and \mathcal{L} represents the length of the transmission line.

Substituting the two relations above into Eq. (3.77), we obtain the action in q -space:

$$-s = \frac{1}{\beta\mathcal{L}\hbar} \sum_q \left[\omega_n Q_{-q} \frac{\hbar}{2e} \phi_q - \frac{Q_q Q_{-q}}{2C_0} - \left(\frac{\hbar}{2e} \right)^2 k^2 \frac{\phi_q \phi_{-q}}{2L} \right]. \quad (3.79)$$

It is useful to rewrite the action in matrix form, namely

$$\begin{aligned} -s &= \frac{1}{\beta \mathcal{L} \hbar} \sum_q (\phi_{-q} \quad Q_{-q}) M^{-1} \begin{pmatrix} \phi_q \\ Q_q \end{pmatrix} \\ &= -\frac{1}{2} \frac{1}{\beta \mathcal{L} \hbar} \sum_q (\phi_{-q} \quad Q_{-q}) \begin{pmatrix} (\frac{\hbar}{2e})^2 \frac{k^2}{L} & \frac{\hbar}{2e} \omega_n \\ -\frac{\hbar}{2e} \omega_n & \frac{1}{C_0} \end{pmatrix} \begin{pmatrix} \phi_q \\ Q_q \end{pmatrix}, \end{aligned} \quad (3.80)$$

where the matrix M reads

$$M = \begin{pmatrix} (\frac{\hbar}{2e})^2 \frac{k^2}{L} & \frac{\hbar}{2e} \omega_n \\ -\frac{\hbar}{2e} \omega_n & \frac{1}{C_0} \end{pmatrix}^{-1} = \frac{1}{\omega_n^2 + (k\omega_0)^2} \begin{pmatrix} (\frac{2e}{\hbar})^2 \frac{1}{C_0} & -\frac{2e}{\hbar} \omega_n \\ \frac{2e}{\hbar} \omega_n & \frac{k^2}{L} \end{pmatrix}. \quad (3.81)$$

In the same way, the exponential correlators in q space are formulated as

$$e^{i\phi_m(\tau)} e^{-i\phi_m(0)} = \exp \left[\frac{1}{\beta \mathcal{L}} \sum_q A_{-q} \phi_q \right], \quad (3.82)$$

where the amplitude

$$A_{-q} = e^{ikm} (e^{-i\omega_n \tau} - 1). \quad (3.83)$$

Plugging Eqs. (3.80) and (3.82) into Eq. (3.76), we obtain

$$\begin{aligned} \langle T_\tau e^{i\phi_m(\tau)} e^{-i\phi_m(0)} \rangle_{H_T} &= \frac{1}{Z} \int D\phi_q(\tau) DQ_q(\tau) \exp \left\{ -\frac{1}{2} \frac{1}{\beta \mathcal{L} \hbar} \sum_q [(\phi_{-q} \quad Q_{-q}) \right. \\ &\cdot M^{-1} \begin{pmatrix} \phi_q \\ Q_q \end{pmatrix} - (iA_{-q} \hbar \quad 0) \begin{pmatrix} \phi_q \\ Q_q \end{pmatrix} - (\phi_{-q} \quad Q_{-q}) \begin{pmatrix} -iA_q \hbar \\ 0 \end{pmatrix}] \left. \right\}, \end{aligned} \quad (3.84)$$

where the partition function Z is rewritten in matrix form as well, namely

$$Z = \int D\phi_q(\tau) DQ_q(\tau) \exp \left[-\frac{1}{2} \frac{1}{\beta \mathcal{L} \hbar} \sum_q (\phi_{-q} \quad Q_{-q}) M^{-1} \begin{pmatrix} \phi_q \\ Q_q \end{pmatrix} \right]. \quad (3.85)$$

Combining the two equations above, and using the Gaussian integral, i.e., Eq. (3.75), we straightforwardly obtain

$$\langle e^{i\phi_m(\tau)} e^{-i\phi_m(0)} \rangle_{H_T} = \exp \left[-\frac{1}{2} \frac{1}{\beta \mathcal{L} \hbar} \sum_q (iA_{-q} \hbar \quad 0) M \begin{pmatrix} -iA_q \hbar \\ 0 \end{pmatrix} \right]. \quad (3.86)$$

Substituting the matrix (3.81) into Eq. (3.86), we further get

$$\langle e^{i\phi_m(\tau)} e^{-i\phi_m(0)} \rangle_{H_T} = \exp [J_0(\tau)], \quad (3.87)$$

where

$$J_0(\tau) = -\frac{1}{\beta\mathcal{L}} \frac{(2e)^2}{\hbar} \sum_q \frac{1}{C_0} \frac{1 - \cos \omega_n \tau}{\omega_n^2 + (k\omega_0)^2}. \quad (3.88)$$

The next step is to compute $J_0(\tau)$. At zero temperature, and for an infinite transmission line, i.e., $\mathcal{L} \rightarrow \infty$, Eq. (3.88) can be rewritten as

$$J_0(\tau) = -\int_{-\infty}^{\infty} \frac{dk}{2\pi} \int_{-\infty}^{\infty} \frac{d\omega}{2\pi} \frac{(2e)^2}{\hbar} \frac{1}{C_0} \frac{1 - \cos \omega \tau}{\omega^2 + (k\omega_0)^2}. \quad (3.89)$$

where the function $f(k)$ consists of three integrals:

$$\int_{-\infty}^{\infty} \frac{d\omega}{2\pi} \frac{1}{\omega^2 + (k\omega_0)^2} - \int_{-\infty}^{\infty} \frac{d\omega}{4\pi} \frac{e^{i\omega\tau}}{\omega^2 + (k\omega_0)^2} - \int_{-\infty}^{\infty} \frac{d\omega}{4\pi} \frac{e^{-i\omega\tau}}{\omega^2 + (k\omega_0)^2}. \quad (3.90)$$

Using the residue theorem, we get

$$J_0(\tau) = \frac{Z_0}{R_Q} \int_0^{\infty} \frac{dk}{k} (e^{-k\omega_0|\tau|} - 1). \quad (3.91)$$

Finally, we need to transform the result back to the real time space, i.e., to find $J_0(t)$. This can be directly obtained from $J(\tau)$ by just doing the Wick's rotation, i.e., $\tau = it + \eta \text{Sign}(t)$, where $\eta = 0^+$ and $\text{Sign}(t)$ is the sign function. For $t > 0$, we get

$$J_0(t) = \frac{Z_0}{R_Q} \int_0^{\infty} \frac{dk}{k} (e^{-ik\omega_0 t} - 1) \equiv \frac{Z_0}{R_Q} \int_0^{\infty} \frac{dk}{k} (e^{-ikt} - 1). \quad (3.92)$$

This matches well with the result [see Eq. (3.38), taking $C_J = 0$] we obtained before using the approach of Green's functions.

Furthermore, Eq. (3.87) can be rewritten in real time space as well, namely

$$\langle e^{i\phi_m(t)} e^{-i\phi_m(0)} \rangle_{H_T} = \exp[J_0(t)]. \quad (3.93)$$

The result verifies Eq. (3.20). As we argued before, Eq. (3.93) is valid as long as H_T is quadratic.

In summary, the path integral method was introduced. In particular, we applied it to a linear system, i.e., an infinite transmission line. The resulting phase-phase correlator matched well with the results obtained from Green's function approach.

3.4.3 Summary

Green's function perturbation theory and the path integral method were introduced to compute the phase-phase correlator in a (nonlinear) system. We briefly explained the ideas of the theory and method, as well as introduced the Feynman diagrams. Using perturbation theory, we may choose the nonlinear term (interaction) as the perturbation, and then sum up the perturbation to the leading order (and sometimes all the orders). With the help of the path integral, the phase-phase correlators were expressed by functional integrals. Moreover, we used the path integral method to verify the simplification of exponential phase-phase correlator with a quadratic Hamiltonian.

So far, we have introduced all the needed elements as well as the adopted theories and methods. In the next two chapters, we will use them to analyze special problems. In particular, in chapter 4 we will deal with a weakly nonlinear environment. The strongly nonlinear regime will be studied in chapter 5.

Detecting photon-photon interactions in a transmission line side-coupled with a weakly anharmonic oscillator

A local interaction between photons can be engineered by coupling a nonlinear system to a transmission line. In the framework of superconducting circuits, the transmission line can be conveniently formed from a chain of Josephson junctions; while the nonlinearity is generated by side-coupling this chain to a Cooper pair box. We propose to probe the resulting photon-photon interactions via their effect on the current-voltage characteristic of a voltage-biased Josephson junction connected to the transmission line. This chapter is organized as follows. In Sec. 4.1, we introduce the Hamiltonian that describe the environment seen by the probe junction. The current-voltage characteristic of the probe junction is characterized by the dynamical Coulomb blockade theory. Then, we calculate the current-voltage characteristic in two different regimes, respectively. 1) the linear regime in Sec. 4.2: considering the Cooper pair box to be in the harmonic regime, the environment is thus described by a quadratic Hamiltonian. 2) the nonlinear regime in Sec. 4.3: considering the Cooper pair box to be in the weak anharmonic regime, we include a nonlinear correction and study the effect of the resulting photon-photon interaction on the current-voltage characteristic. Finally, we summarize our results in Sec. 4.4.

4.1 The studied circuit

We are interested in the interaction of photons propagating in a nonlinear electromagnetic environment. In particular, we study a transmission line, consisting of a chain of Josephson junctions, to which a Cooper pair box acting as the nonlinear element is side-coupled at node $n = 0$ as shown in Fig. 4.1 (dashed box). We assume weak coupling, namely the coupling capacitance, C_c , is much smaller

than the characteristic capacitances of the chain and the nonlinear element.

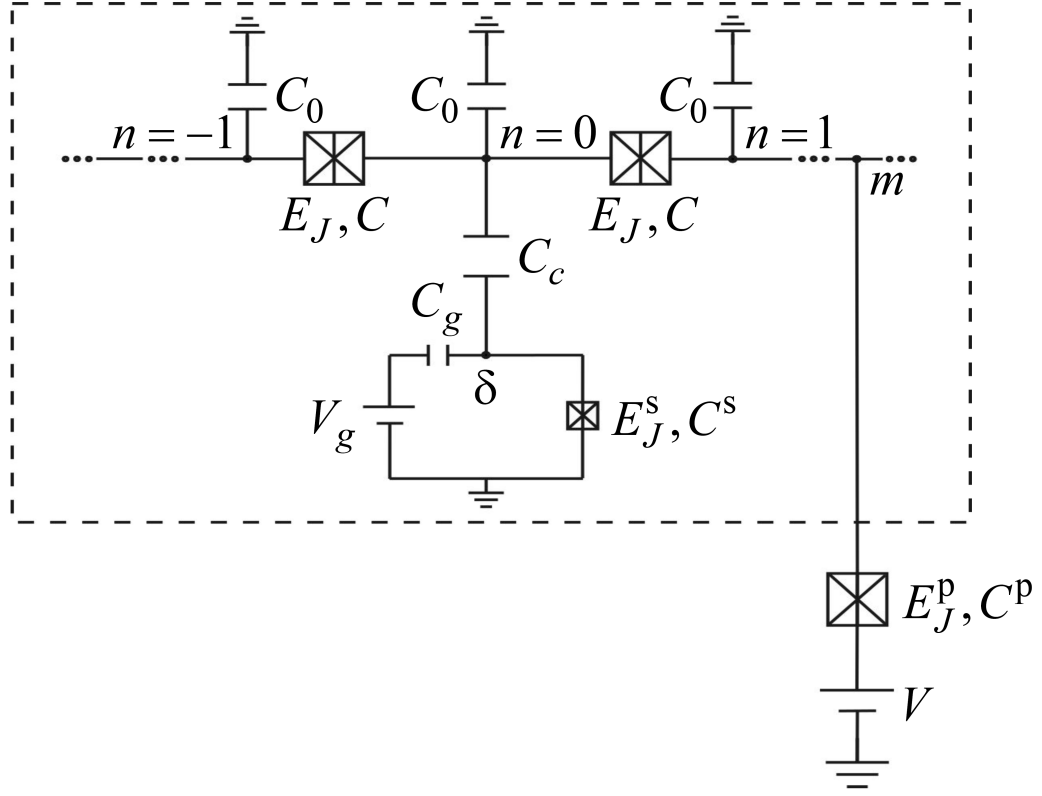


Figure 4.1: The system consists of a transmission line that is capacitively coupled (capacitor C_c) to a Cooper pair box, shown inside the dashed box. The transmission line is realized using a chain of Josephson junctions with Josephson energy E_J much larger than the charging energy E_C . The system is probed at node m using another Josephson junction (outside the dashed box) whose current-voltage characteristic is sensitive to the properties of the system.

The Hamiltonian of the system is, thus, assembled from three parts,

$$H = H_T + H_J + H_c, \quad (4.1)$$

where H_T is the Hamiltonian of the transmission line, H_J is the Hamiltonian of the side-coupled Josephson junction, and H_c is the coupling Hamiltonian.

As we argued in Sec. 2.3, a transmission line with large impedance can be realized using a chain of Josephson junctions in the limit where the Josephson energy E_J is much larger than the charging energy E_C . We further consider the case where the capacitance to the ground C_0 is much larger than the mutual capacitance C . Then, for frequencies much smaller than the plasma frequency of Josephson

junctions in the chain, the Hamiltonian takes the simple form, namely Eq. (3.24). For ease of reference, we write it down again.

$$H_T = \sum_n \left[\frac{Q_n^2}{2C_0} + \left(\frac{\hbar}{2e} \right)^2 \frac{(\phi_n - \phi_{n+1})^2}{2L} \right], \quad (4.2)$$

where the inductance is $L = \hbar^2 / (4e^2 E_J)$. At frequencies $\omega \ll \omega_0$, where $\omega_0 \equiv 1/\sqrt{LC_0}$, the transmission line has a linear spectrum (see Fig. 2.13), corresponding to a frequency-independent impedance, i.e., $Z(\omega) = Z_0$. Such impedance provides a good background for studying the scattering effect when the side-coupling element is involved.

The side-coupled Cooper pair box with Josephson energy E_J^s is described by the Hamiltonian [see Eq. (2.5)]

$$H_J = \frac{(Q_\delta + C_g V_g)^2}{2C_\Sigma} - E_J^s \cos \phi_\delta, \quad (4.3)$$

where Q_δ and ϕ_δ are the conjugate charge and phase operators at node δ (see Fig. 4.1). Furthermore, C_g and V_g are the gate capacitance and gate voltage, respectively, and $C_\Sigma = C^s + C_g$ is the total capacitance of the side-coupled Cooper pair box.

Finally, we turn to the coupling Hamiltonian H_c . When the coupling capacitance is small, $C_c \ll C_0, C_\Sigma$, the coupling Hamiltonian reads¹

$$H_c = \frac{C_c}{C_0 C_\Sigma} Q_0 (Q_\delta + C_g V_g), \quad (4.4)$$

where we used the fact that for $C \ll C_0$ the coupling is local², i.e., the side-coupled Josephson junction couples only to the charge Q_0 at $n = 0$. The Hamiltonian H fully describes our nonlinear system.

As a next step, we introduce the probe circuit used to characterize the photon-photon interactions generated by the nonlinear system. The probe circuit consists of yet another Josephson junction, with Josephson energy E_J^p and in series with a voltage source as shown in Fig. 4.1, coupled to the transmission line at node m [129, 137]. The current-voltage characteristic of the probe Josephson junction is influenced by the correlations of the phase $\phi_m(t)$ at node m , correlations that depend on the fluctuations in the nonlinear environment. The I - V characteristic may, thus, be used to characterize the photon-photon interactions in the nonlinear system.

¹More details are shown in Appendix A.

²This can be seen from the Eq. (A.20).

In particular, using dynamical Coulomb blockade theory introduced in chapter 3, it can be shown that at zero temperature the current flowing through the probe Josephson junction takes the form [see Eq. (3.17)]

$$I(V) = \frac{\pi e (E_J^p)^2}{\hbar} P(2eV), \quad (4.5)$$

for voltages $eV < 2\Delta$, where Δ is the superconducting gap, and

$$P(E) = \frac{1}{2\pi\hbar} \int_{-\infty}^{\infty} dt e^{iEt/\hbar} \langle e^{i\phi_m(t)} e^{-i\phi_m(0)} \rangle_{H_{\text{env}}} \quad (4.6)$$

is the probability of the probe Josephson junction to emit energy E to its environment, described by the Hamiltonian H_{env} . In general, the environment seen by the probe junction consists of both the nonlinear system and the capacitance C^p . However, the Hamiltonian of the environment in Eq. (4.6) may be replaced by the Hamiltonian H of the nonlinear system we want to characterize, if the capacitance of the probe Josephson junction is sufficiently small. In particular, the probe capacitance is side-coupled (at node m , see Fig. 4.1) to the chain, so its charging energy modifies the first term of Eq. (4.2) to $Q_n^2/[2(C_0 + \delta_{nm}C^p)]$. As $C^p \ll C_0$, we have $H_{\text{env}} = H$. Indeed, this condition guarantees that we are in the photonic regime of the dynamical Coulomb blockade. Our task is then to compute the phase correlator $\langle e^{i\phi_m(t)} e^{-i\phi_m(0)} \rangle_H$.

4.2 The linear regime

As a first step, we will consider the system in the linear regime, where photons do not interact. That is, we assume $E_J^s \gg e^2/(2C_\Sigma)$ and approximate the junction Hamiltonian H_J in Eq. (4.3) by

$$H_J^{(0)} = \frac{(Q_\delta + C_g V_g)^2}{2C_\Sigma} + \frac{E_J^s}{2} \phi_\delta^2. \quad (4.7)$$

In this section, we study the behavior of this simplified system described by $H^{(0)} = H_T + H_J^{(0)} + H_c$ to set the basis for investigating interaction effects, the main focus of our work, in the following section. In this regime, the gate voltage V_g can be gauged out of the Hamiltonian, and the side-coupled circuit behaves as an harmonic oscillator with plasma frequency $\omega_s \equiv (2e/\hbar)\sqrt{E_J^s/C_\Sigma}$. We will assume that $\omega_s \ll \omega_0$, associated with a linear spectrum and frequency-independent impedance.

As the system is non-interacting, the system Hamiltonian $H^{(0)}$ is harmonic, the phase-phase correlator $\langle e^{i\phi_m(t)} e^{-i\phi_m(0)} \rangle_{H^{(0)}}$ can be simplified. Using Eq. (3.20), it reduces as $e^{J_0(t)}$ with $J_0(t) \equiv \langle [\phi_m(t) - \phi_m(0)] \phi_m(0) \rangle_{H^{(0)}}$. To evaluate the two-point correlator $J_0(t)$, we use the retarded Green's function referred in Sec. 3.3. The relation between the two was easily written in frequency space [see Eq. (3.22)]. As a result, we need to first evaluate the local Green's function $G_R^{(0)}(\phi_m, \phi_m; \omega)$. This can be done by deriving its equation of motion and using scattering theory.

4.2.1 Two-point Green's function

Taking the same procedures as we did on the case of a pure transmission line (see details in subsection 3.3.1), we derived the coupled equations of motion for $G_R^{(0)}(\phi_n, \phi_m; \omega)$ and $G_R^{(0)}(\phi_\delta, \phi_m; \omega)$:

$$\omega^2 G_R^{(0)}(\phi_n, \phi_m; \omega) - \omega_0^2 \left(1 + \frac{C_c^2}{C_0 C_\Sigma} \delta_{n0} \right) \quad (4.8)$$

$$\begin{aligned} & \times \left[2G_R^{(0)}(\phi_n, \phi_m; \omega) - G_R^{(0)}(\phi_{n+1}, \phi_m; \omega) - G_R^{(0)}(\phi_{n-1}, \phi_m; \omega) \right] \\ & - \frac{C_c}{C_0} \omega_s^2 G_R^{(0)}(\phi_\delta, \phi_m; \omega) \delta_{n0} + \left(\frac{2e}{\hbar} \right)^2 \frac{1}{C_0} \delta_{nm} = 0, \\ & \frac{C_c}{C_\Sigma} \omega_0^2 \left[2G_R^{(0)}(\phi_0, \phi_m; \omega) - G_R^{(0)}(\phi_1, \phi_m; \omega) - G_R^{(0)}(\phi_{-1}, \phi_m; \omega) \right] \quad (4.9) \\ & = (\omega^2 - \omega_s^2) G_R^{(0)}(\phi_\delta, \phi_m; \omega). \end{aligned}$$

Combining Eqs. (4.8) and (4.9) then yields the equation for $G_R^{(0)}(\phi_n, \phi_m; \omega)$,

$$\begin{aligned} & \omega^2 G_R^{(0)}(\phi_n, \phi_m; \omega) - \omega_0^2 \left(1 + \frac{C_c^2}{C_0 C_\Sigma} \frac{\omega^2}{\omega^2 - \omega_s^2} \delta_{n0} \right) \left[2G_R^{(0)}(\phi_n, \phi_m; \omega) \right. \\ & \left. - G_R^{(0)}(\phi_{n+1}, \phi_m; \omega) - G_R^{(0)}(\phi_{n-1}, \phi_m; \omega) \right] = - \left(\frac{2e}{\hbar} \right)^2 \frac{1}{C_0} \delta_{nm}. \quad (4.10) \end{aligned}$$

In absence of the side-coupling, i.e., $C_c = 0$, Eq. (4.10) recovers Eq. (3.30) (taking $C_J = 0$, namely neglecting the charging effect). It describes photons propagating freely along the transmission line. At low frequencies, i.e., $\omega \ll \min[\omega_0, \omega_p]$ ³, the solution is $G_R^{(0)}(\phi_n, \phi_m; \omega) = i[\pi/(\hbar\omega)](Z_0/R_Q)e^{ik|n-m|}$.

When the side-coupling is involved, it leads to scattering of photons at the node $n = 0$. The transport processes are simply shown in Fig. 4.2. Then, for

³It corresponds to the linear dispersion, which was argued in chapter 2

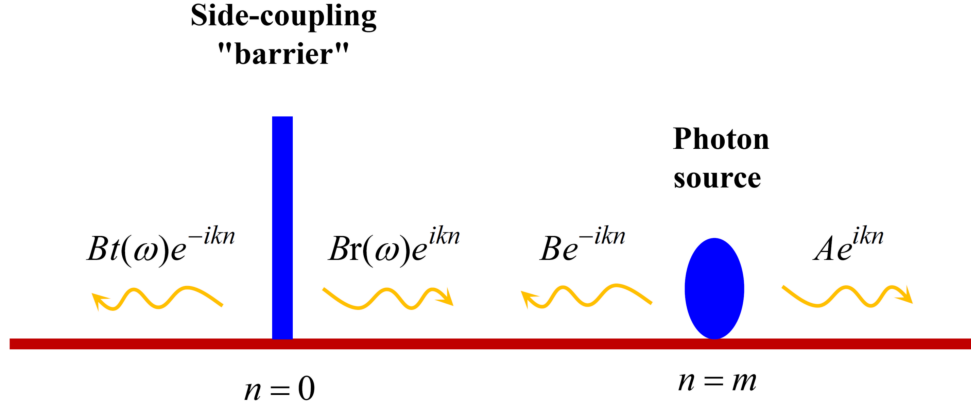


Figure 4.2: Photons are emitted from the source at node $n = m$, some of them propagate in the right direction; while others propagate in the left direction. The side-coupling “barrier” leads to the reflection and transition of photons at the node $n = 0$. The process can be mathematically described by Eq. (4.11).

$m > 0$, the solution may be written in the form

$$G_R^{(0)}(\phi_n, \phi_m; \omega) = Ae^{ikn}\Theta(n-m) + B \left[e^{-ikn} + r(\omega)e^{ikn} \right] \Theta(n-m)\Theta(n) + Bt(\omega)e^{-ikn}\Theta(-n), \quad (4.11)$$

where the reflection and transmission coefficients, $r(\omega)$ and $t(\omega)$, and the amplitudes A and B have to be determined using the boundary conditions at $n = 0$ and $n = m$.

One finds $t(\omega) = 1 + r(\omega)$ with $r(\omega)$ given as,

$$r(\omega) = - \left[1 - 2i \frac{\omega_0}{\omega} \left(1 + \frac{C_0 C_\Sigma}{C_c^2} \frac{\omega^2 - \omega_s^2}{\omega^2} \right) \right]^{-1}. \quad (4.12)$$

Under the conditions specified above, $C_0 C_\Sigma / C_c^2 \gg 1$ and $\omega_s \ll \omega_0$, the reflection coefficient has a narrow resonance at $\omega = \omega_s$ with width

$$\Gamma = \frac{1}{4} \frac{C_c^2}{C_0 C_\Sigma} \frac{\omega_s}{\omega_0}. \quad (4.13)$$

Close to the resonance, we can approximate Eq. (4.12) as $r(\omega) = -1/[1 - i(\omega - \omega_s)/\Gamma]$.

Furthermore,

$$B = i \frac{\pi}{\hbar \omega} \frac{Z_0}{R_Q} e^{ikm}, \quad (4.14)$$

$$A = B \left[e^{-2ikm} + r(\omega) \right]. \quad (4.15)$$

The result is obtained by substituting Eqs. (4.12), (4.14), and (4.15) into Eq. (4.11). Generalizing to arbitrary m , we find

$$G_R^{(0)}(\phi_n, \phi_m; \omega) = i \frac{\pi}{\hbar \omega} \frac{Z_0}{R_Q} \left[e^{ik|n-m|} + r(\omega) e^{ik(|n|+|m|)} \right]. \quad (4.16)$$

In particular, the local Green's function needed to evaluate $P(E)$ reads

$$G_R^{(0)}(\phi_m, \phi_m; \omega) = i \frac{\pi}{\hbar \omega} \frac{Z_0}{R_Q} \left[1 + r(\omega) e^{2ik|m|} \right]. \quad (4.17)$$

While this is the only Green's function needed in the linear case, more Green's functions will be required in the non-linear case. Using Eq. (4.9), we obtain

$$G_R^{(0)}(\phi_\delta, \phi_m; \omega) = -2 \frac{\pi}{\hbar \omega} \frac{1}{R_Q C_c \omega} r(\omega) e^{ik|m|}. \quad (4.18)$$

Similarly, the Green's functions $G_R^{(0)}(\phi_m, \phi_\delta; \omega)$ and $G_R^{(0)}(\phi_\delta, \phi_\delta; \omega)$ obey coupled equations of motion. One may show that $G_R^{(0)}(\phi_m, \phi_\delta; \omega) = G_R^{(0)}(\phi_\delta, \phi_m; \omega)$, whereas the equation of motion for $G_R^{(0)}(\phi_\delta, \phi_\delta; \omega)$ is derived in the same way.

$$\begin{aligned} (\omega^2 - \omega_s^2) G_R^{(0)}(\phi_\delta, \phi_\delta; \omega) - \frac{C_c}{C_\Sigma} \omega_0^2 \left[2G_R^{(0)}(\phi_0, \phi_\delta; \omega) - G_R^{(0)}(\phi_1, \phi_\delta; \omega) \right. \\ \left. - G_R^{(0)}(\phi_{-1}, \phi_\delta; \omega) \right] = - \left(\frac{2e}{\hbar} \right)^2 \frac{1}{C_\Sigma}. \end{aligned} \quad (4.19)$$

Using Eq. (4.18), one obtains

$$G_R^{(0)}(\phi_\delta, \phi_\delta; \omega) = -4i \frac{\pi}{\hbar \omega} \frac{1}{R_Q Z_0 (C_c \omega)^2} r(\omega). \quad (4.20)$$

Using the explicit expression for $r(\omega)$, Eq. (4.20) may be rewritten as

$$G_R^{(0)}(\phi_\delta, \phi_\delta; \omega) = - \frac{2\pi}{\hbar R_Q C_\Sigma} \frac{1}{\omega^2 - \omega_s^2 + i \frac{C_c^2}{2C_0 C_\Sigma} \frac{\omega^2}{\omega_0} (\omega - 2i\omega_0)}. \quad (4.21)$$

Finally, using the fact that $C_c^2/(C_0 C_\Sigma) \ll 1$, we approximate

$$G_R^{(0)}(\phi_\delta, \phi_\delta; \omega) \simeq - \frac{2\pi}{\hbar R_Q C_\Sigma} \frac{1}{\omega^2 - (\omega_s - i\Gamma)^2}. \quad (4.22)$$

This result also allows us to evaluate

$$\langle \phi_\delta^2 \rangle_{H^{(0)}} = \frac{\hbar}{\pi} \int_0^\infty d\omega \operatorname{Im} \left[G_R^{(0)}(\phi_\delta, \phi_\delta; \omega) \right] = \frac{\hbar \omega_s}{2E_J^s}. \quad (4.23)$$

4.2.2 Phase-phase correlator

Using the local Green's function (4.17) and the relation Eq. (3.23), one obtains

$$J(t) = \frac{2}{R_Q} \int_0^\infty \frac{d\omega}{\omega} \text{Re}[Z(\omega)] (e^{-i\omega t} - 1), \quad (4.24)$$

as expected from $P(E)$ -theory, with the impedance

$$Z(\omega) = \frac{Z_0}{2} \left[1 + r(\omega) e^{2i\frac{\omega}{\omega_0} m} \right]. \quad (4.25)$$

The prefactor $1/2$ corresponds to the fact that the probe junction ‘sees’ an environment consisting of *two* half-infinite transmission lines. As shown in Fig. 4.3, the impedance is unaffected by the side-coupled Josephson junction as $r(\omega) \rightarrow 0$ when it is far from the resonance at ω_s . In contrast, at the resonance, photons are strongly scattered. In particular when the probe and the scatterer are coupled to the same node ($m = 0$), $r(\omega_s) = -1$ so that transport is completely blocked due to destructive interference. Changing the distance between the probe and the scatterer modulates the phase difference between incoming and reflected photons and, thus, creates an interference pattern.

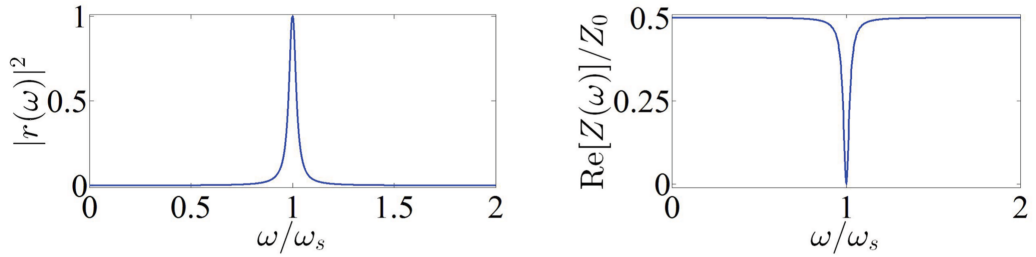


Figure 4.3: The reflection probability (left) and the impedance (right) depend of the frequency when placed at $m = 0$. The parameters are $\Gamma/\omega_s = 0.02$. At the resonance frequency ω_s , the reflection probability is one. Photons are completely blocked due to destructive interference.

4.2.3 Current-voltage characteristic

To compute the current-voltage characteristic, we need to determine $P(E)$. This can be done numerically using the integral equation [see Eq. (3.42)] as before.

The resulting current-voltage characteristic is plotted in Fig. 4.4 for several values of the impedance of the transmission line. The characteristic current is given by

$$I_0 = \frac{\pi e (E_J^P)^2 Z_0}{\hbar^2 \omega_s R_Q}. \quad (4.26)$$

The background current decreases with increasing voltage. In addition, there is a clear resonance feature at $2eV = \hbar\omega_s$.

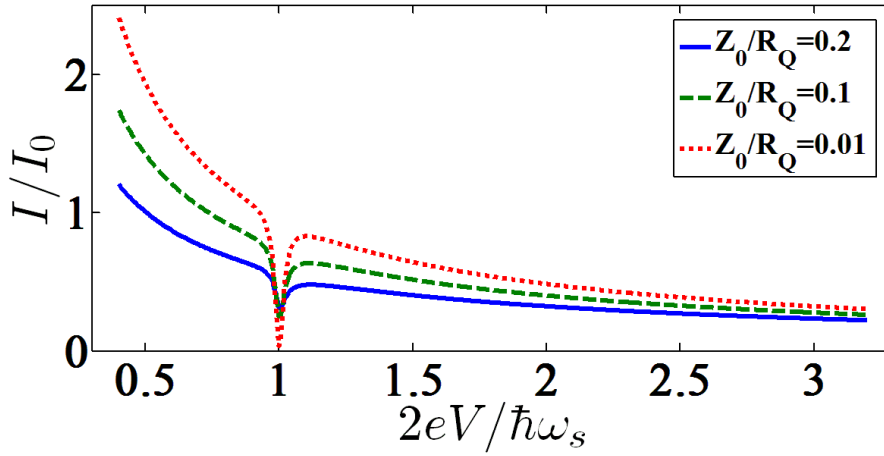


Figure 4.4: The linear regime: current-voltage characteristic of the probe Josephson junction when placed at $m = 0$. The parameters are $\Gamma/\omega_s = 0.02$, $E_{\text{cut-off}}/(\hbar\omega_s) = 20$, and different Z_0 ($Z_0/R_Q = 0.01, 0.1, 0.2$). The side-coupled Josephson junction causes a resonance at $2eV = \hbar\omega_s$. In the limit $Z_0/R_Q \rightarrow 0$, the current vanishes at the resonance.

This result can be understood as follows. The starting point is to recognize that when a bias voltage V is applied, Cooper pairs can flow through the probe junction provided that they can release their energy by emitting one or several photons into the environment.

First, let us concentrate on the regime $Z_0/R_Q \ll 1$. In that case, multi-photon processes are suppressed, and we can expand $e^{J(t)} \simeq 1 + J(t)$. Thus, the current is proportional to the Fourier transform of $J(t)$ at frequency $2eV$. It is straightforward to show that for a constant impedance this yields a current that decays with increasing voltage as $I(V) \propto 1/V$. This is apparent in Fig. 3.5, where we consider the case of a pure transmission line with a constant impedance. On top of this, the resonance in the impedance at ω_s due to the side-coupled Josephson junction leads to a resonance in the current-voltage characteristic at $2eV = \hbar\omega_s$. Namely,

the correction to the current $\delta I_1(\delta V)$ at voltages $V = \hbar\omega_s/(2e) + \delta V$ takes the form

$$\frac{\delta I_1(\delta V)}{I_0} = \frac{-\Gamma^2}{(2e\delta V)^2 + \Gamma^2} \left(\cos \alpha - \frac{2e\delta V}{\Gamma} \sin \alpha \right), \quad (4.27)$$

where $\alpha = 2m\omega_s/\omega_0$. This leads to a complete extinction of the current at $\delta V = 0$ (at the one photon level) when the probe is coupled to the same node as the side-coupled Josephson junction ($m = 0$). The shape of the resonance for different α is shown in Fig. 4.5; note the sensitivity to the placement of the probe produced by interference effects. The width of the resonance is given by $W_1 = \Gamma/e$ where Γ is given in Eq. (4.13).

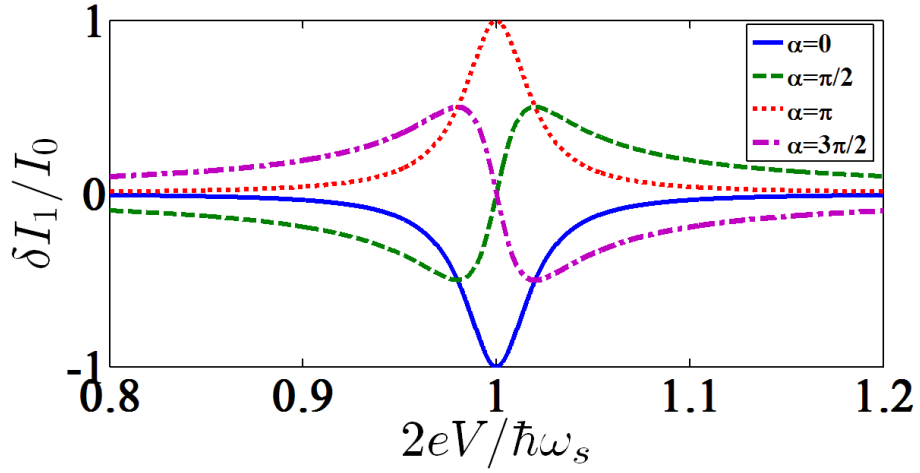


Figure 4.5: The resonance in the current-voltage characteristic for different values of the distance between the side-coupled Josephson junction and the probe Josephson junction, $\alpha = 2m\omega_s/\omega_0$. Results in the single-photon, linear regime are plotted [Eq. (4.27)] with $\Gamma/\omega_s = 0.02$. Note the effect of interference on the shape of the resonance.

Let us now turn to multi-photon processes corresponding to higher order terms in $J(t)$. These processes modify the resonance at $2eV = \hbar\omega_s$. In particular, while the scattering from the side-coupled Josephson junction may completely block the single-photon process at that voltage, this is not the case for the multi-photon processes: at most one photon can be on resonance, whereas the other photons will be off resonance and therefore propagate freely. Thus, the multi-photon processes lead to a finite current at the resonance. As an n -photon process yields a current contribution proportional to $(Z_0/R_Q)^n$, the resonant structure weakens with increasing Z_0/R_Q due to the increasing importance of multi-photon processes.

In addition, one might expect that multi-photon processes lead to higher order resonances at voltages $2eV = n\hbar\omega_s$ ($n \geq 2$). We find, however, that this is not the case. While $2eV = n\hbar\omega_s$ is indeed a resonance condition for an n -photon process, the non-resonant background from the entire frequency range is large enough to completely overwhelm that contribution.

Thus, in the linear regime where photons do not interact, the side-coupled Josephson junction leads to a single resonance in the current-voltage characteristic at $2eV = \hbar\omega_s$. As we will show in next section, additional features at $2eV = n\hbar\omega_s$ with $n \geq 2$ are a signature of photon-photon interactions.

4.3 The weakly nonlinear regime

To investigate photon-photon interactions, we now take into account the non-linearity of the side-coupled Josephson junction. In particular, we concentrate on the case of weak nonlinearity in the regime $E_J^s \gg e^2/(2C_\Sigma)$. To do so, we expand Eq. (4.3) up to fourth order in ϕ_δ ,

$$H_J \approx H_J^{(0)} + V, \quad (4.28)$$

where

$$V = -\frac{E_J^s}{24}\phi_\delta^4. \quad (4.29)$$

In the following, we treat V as a perturbation. Since we are considering a quartic interaction, the results of the perturbation theory developed in Sec. 3.4 can be used. The only difference is that the interaction $-(E_J^s/24)\phi_\delta^4$ originates from the side-coupling element.

As the Hamiltonian $H_{\text{wnl}} \doteq H^{(0)} + V$ describes an interacting system, we can no longer write a closed form expression for the phase-phase correlator in Eq. (4.6) in terms of $\langle \phi_n(t)\phi_m(0) \rangle_{H_{\text{wnl}}}$. Instead we expand the correlator in powers of ϕ_m [see Eq. (3.48)]. As we argued in Sec. 3.4, only the even-point correlators contribute if the weakly nonlinear Hamiltonian has symmetry in phase and charge. In this regime, it is clearly seen that H_{wnl} satisfies the symmetry: $\phi_n \rightarrow -\phi_n$, $Q_n \rightarrow -Q_n$, and $Q_\delta \rightarrow -Q_\delta$ (note that the gate voltage does not play a role in weakly nonlinear regime).

Here, we concentrate on only the two-point phase-phase correlator and four-point phase-phase correlators. The former correlator represents single photon processes, whereas the latter ones correspond to two photon processes. As before, we still use Green's functions to evaluate the correlators. In addition to the two-point Green's function $G_R(\phi_m, \phi_m; \omega)$, we now also need the four-point Green's

functions $G_R(\phi_m^2, \phi_m^2; \omega)$, $G_R(\phi_m^3, \phi_m; \omega)$, and $G_R(\phi_m, \phi_m^3; \omega)$. To be able to facilitate doing perturbation theory in the interaction V , we switch to imaginary-time-ordered or Matsubara Green's functions, \mathcal{G} .

4.3.1 Two-point Green's function

Let us first evaluate the two-point Green's function $\mathcal{G}[\phi_n(\tau)\phi_m(0)]$, corresponding to single photon processes.

Consider only first order in the perturbation V and using Wick's theorem yields

$$\begin{aligned} \mathcal{G}[\phi_n(\tau)\phi_m(0)] &\simeq \mathcal{G}^{(0)}[\phi_n(\tau)\phi_m(0)] \\ &+ \int_0^\infty d\tau_1 \mathcal{G}^{(0)}[\phi_n(\tau)\phi_\delta(\tau_1)] \frac{E_J^s}{2} \langle \phi_\delta^2 \rangle_{H^{(0)}} \mathcal{G}^{(0)}[\phi_\delta(\tau_1)\phi_m(0)]. \end{aligned} \quad (4.30)$$

After Fourier transformation and analytical continuation, one obtains the corresponding retarded Green's function,

$$G_R(\phi_n, \phi_m; \omega) \simeq G_R^{(0)}(\phi_n, \phi_m; \omega) + G_R^{(0)}(\phi_n, \phi_\delta; \omega) \frac{E_J^s}{2} \langle \phi_\delta^2 \rangle_{H^{(0)}} G_R^{(0)}(\phi_\delta, \phi_m; \omega). \quad (4.31)$$

While far from the resonance at $\omega = \omega_s$, the second term is much smaller than the first one, this is no longer true close to the resonance. Thus, this first order expansion is not sufficient to describe the modifications to the resonance due to the perturbation. According to the discussion in Sec. 3.4, it is possible to go beyond the first order expansion and sum up the perturbation series to all orders in the interactions by realizing that $E_J^s \langle \phi_\delta^2 \rangle_{H^{(0)}} / 2$ is a local self-energy, $\Sigma(\phi_\delta, \phi_\delta)$. Thus, one obtains the Dyson's equation

$$G_R(\phi_n, \phi_m; \omega) = G_R^{(0)}(\phi_n, \phi_m; \omega) + G_R^{(0)}(\phi_n, \phi_\delta; \omega) \frac{E_J^s}{2} \langle \phi_\delta^2 \rangle_{H^{(0)}} G_R(\phi_\delta, \phi_m; \omega), \quad (4.32)$$

A similar equation can be written for the Green's function $G_R(\phi_\delta, \phi_m; \omega)$. Namely,

$$G_R(\phi_\delta, \phi_m; \omega) = G_R^{(0)}(\phi_\delta, \phi_m; \omega) + G_R^{(0)}(\phi_\delta, \phi_\delta; \omega) \frac{E_J^s}{2} \langle \phi_\delta^2 \rangle_{H^{(0)}} G_R(\phi_\delta, \phi_m; \omega). \quad (4.33)$$

The representation in terms of Feynman diagrams is shown in Fig. 4.6.

Combining Eqs. (4.32) and (4.33), we obtain the result

$$G_R(\phi_n, \phi_m; \omega) = G_R^{(0)}(\phi_n, \phi_m; \omega) + \frac{G_R^{(0)}(\phi_n, \phi_\delta; \omega) \frac{E_J^s}{2} \langle \phi_\delta^2 \rangle_{H^{(0)}} G_R^{(0)}(\phi_\delta, \phi_m; \omega)}{1 - \frac{E_J^s}{2} \langle \phi_\delta^2 \rangle_{H^{(0)}} G_R^{(0)}(\phi_\delta, \phi_\delta; \omega)}. \quad (4.34)$$

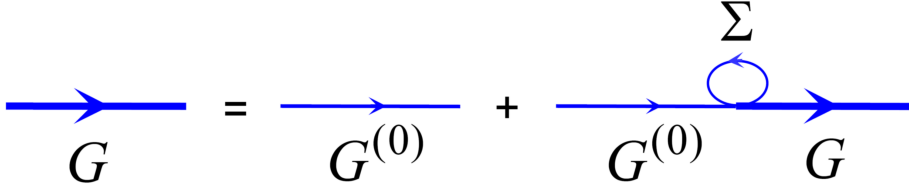


Figure 4.6: Dyson equation for the two-point Green's function. The non-linearity results in a self energy, $\Sigma = E_J^s \langle \phi_\delta^2 \rangle_{H^{(0)}} / 2$.

Then, using the Green's functions $G_R^{(0)}$ of the linear problem derived in Sec. 4.2, we find that the local Green's function preserves its form though with a shifted resonance frequency ω'_s . Namely,

$$G_R(\phi_m, \phi_m; \omega) = i \frac{\pi Z_0}{\omega R_Q} \left[1 + r'(\omega) e^{2i \frac{\omega}{\omega_0} m} \right], \quad (4.35)$$

where

$$r'(\omega) = - \left[1 - 2i \frac{\omega_0}{\omega} \left(1 + \frac{C_0 C_\Sigma}{C_c^2} \frac{\omega^2 - \omega_s'^2}{\omega^2} \right) \right]^{-1} \quad (4.36)$$

with $\omega'_s \approx \omega_s [1 - \omega_s / (8E_J^s)]$. In the same way, we can show that this is true for all two-point Green's functions. As we argued in Eq. (2.11), $\delta\omega_s = \omega_s^2 / (8E_J^s) \ll \omega_s$ coincides with the shift of the excitation energy between the ground and first excited states of the Hamiltonian (4.28).

4.3.2 Four-point Green's function

We turn to the four-point Green's functions, corresponding to two-photon processes. Using perturbation theory, we may express them in terms of the two-point Green's functions. As we saw in Sec. 3.4, it is essential to sum up the perturbation series to all orders in V to obtain these two-point Green's functions. By contrast, we will keep only the lowest order term in V accounting for interactions between the two photons. Then, the four-point Green's function $G_R(\phi_n^2, \phi_m^2; \omega)$ has two contributions: the first one describes the independent propagation of the two photons, whereas the second one describes the interaction effects. More precisely, the imaginary-time-ordered four-point Green's function may be written as $\mathcal{G}[\phi_n^2(\tau)\phi_m^2(0)] = 2\mathcal{G}^2[\phi_n(\tau)\phi_m(0)] + \delta\mathcal{G}^{\text{int}}[\phi_n^2(\tau)\phi_m^2(0)]$ with

$$\delta\mathcal{G}^{\text{int}}[\phi_n^2(\tau)\phi_m^2(0)] \simeq E_J^s \int_0^\infty d\tau_1 \{ \mathcal{G}[\phi_n(\tau)\phi_\delta(\tau_1)] \mathcal{G}[\phi_\delta(\tau_1)\phi_m(0)] \}^2. \quad (4.37)$$

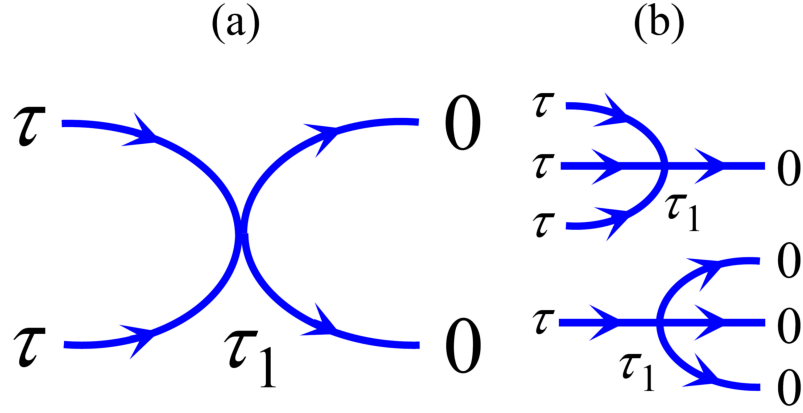


Figure 4.7: The Feynman diagrams for the interaction correction to the four-point Green's functions. (a) $\delta\mathcal{G}^{\text{int}}[\phi_n^2(\tau)\phi_m^2(0)]$. (b) $\mathcal{G}[\phi_n^3(\tau)\phi_m(0)]$ and $\mathcal{G}[\phi_n^3(\tau)\phi_m(0)]$.

The corresponding Feynman diagram is shown in Fig. 4.7(a).

Taking the Fourier transform upon Eq. (4.37) and then performing the analytical continuation from Matsubara to real frequencies, $i\omega_v \rightarrow \omega + i0^+$, and using standard methods of contour integration, we obtain the four-point retarded Green's function $\delta G_R^{\text{int}}(\phi_m^2, \phi_m^2; \omega)$, which is needed to further compute the interaction contribution to the current-voltage characteristic. As a result, the local retarded Green's function at zero temperature takes the form $\delta G_R^{\text{int}}(\phi_m^2, \phi_m^2; \omega) \simeq (E_J^s/\pi^2)f^2(\omega)$, where

$$f(\omega) = \sum_{\pm} \int_0^{\infty} d\omega_1 \text{Im}[G_R(\phi_m, \phi_{\delta}; \omega_1)] G_R(\phi_m, \phi_{\delta}; \omega \pm \omega_1). \quad (4.38)$$

The leading order term for the other four-point Green's functions $G_R(\phi_n^3, \phi_m; \omega)$ and $G_R(\phi_n, \phi_m^3; \omega)$ is linear in E_J^s . In particular, we find the local Green's functions

$$G_R(\phi_m^3, \phi_m; \omega) \simeq \frac{E_J^s}{\pi^2} G_R(\phi_{\delta}, \phi_m; \omega) \int_0^{\infty} d\omega_1 \int_0^{\infty} d\omega_2 \text{Im}[G_R(\phi_m, \phi_{\delta}; \omega_1)] \quad (4.39)$$

$$\times \text{Im}[G_R(\phi_m, \phi_{\delta}; \omega_2)] \sum_{s_1, s_2=\pm} G_R(\phi_m, \phi_{\delta}; \omega + s_1\omega_1 + s_2\omega_2)$$

and $G_R(\phi_m, \phi_m^3; \omega) = G_R(\phi_m^3, \phi_m; \omega)$. The Feynman diagrams for the corresponding time-ordered Green's functions are shown in Fig. 4.7(b).

4.3.3 Phase-phase correlator

With the above results we can now write the phase-phase correlator needed to compute $P(E)$ in the following form

$$\langle e^{i\phi_m(t)} e^{\phi_m(0)} \rangle_{H_{\text{wnl}}} \simeq e^{J'(t)} + \delta J^{\text{int}}(t), \quad (4.40)$$

with

$$J'(t) = \frac{\hbar}{\pi} \int_0^\infty d\omega \operatorname{Im} [G_R(\phi_m, \phi_m; \omega)] (e^{-i\omega t} - 1), \quad (4.41)$$

and the interaction part is derived with the help of the relation (3.23),

$$\begin{aligned} \delta J^{\text{int}}(t) \simeq & \frac{\hbar}{\pi} \int_0^\infty d\omega \left\{ \frac{1}{4} \operatorname{Im} [\delta G_R^{\text{int}}(\phi_m^2, \phi_m^2; \omega)] \right. \\ & \left. - \frac{1}{3} \operatorname{Im} [G_R(\phi_m^3, \phi_m; \omega)] \right\} (e^{-i\omega t} - 1). \end{aligned} \quad (4.42)$$

4.3.4 Current-voltage characteristic

Using Eq. (4.40) to compute $P(E)$, we obtain the current

$$\begin{aligned} I(V) \simeq & \frac{e}{\hbar} (E_J^{\text{p}})^2 \left\{ \frac{1}{2\hbar} \int_{-\infty}^\infty dt \exp [i2eVt + J'(t)] \right. \\ & \left. + \frac{1}{4} \operatorname{Im} [\delta G_R^{\text{int}}(\phi_m^2, \phi_m^2; 2eV)] - \frac{1}{3} \operatorname{Im} [G_R(\phi_m^3, \phi_m; 2eV)] \right\}. \end{aligned} \quad (4.43)$$

The first line describes the resonant structure discussed in Sec. 4.2. Here the only effect of the non-linearity is to shift the resonance from ω_s to ω'_s . The second line describes interaction effects between two photons. The current-voltage characteristic including these effects is shown in Fig. 4.8: it displays additional structure at $2eV = 2\omega'_s$.

The new peak at $2eV = 2\hbar\omega'_s$ comes from the contribution $\delta G_R^{\text{int}}(\phi_m^2, \phi_m^2; 2eV)$. This contribution describes a process in which a Cooper pair tunnels through the probe Josephson junction emitting two photons. When both photons are on resonance with the side-coupled Josephson junction, they interact strongly. This happens when each photon takes away half of the energy of the Cooper pair, $\omega = eV/\hbar \simeq \omega'_s$. The resulting correction to the current is obtained using Eq. (4.37). As shown in Appendix C, for voltages $V = \hbar\omega'_s/e + \delta V$, it takes the

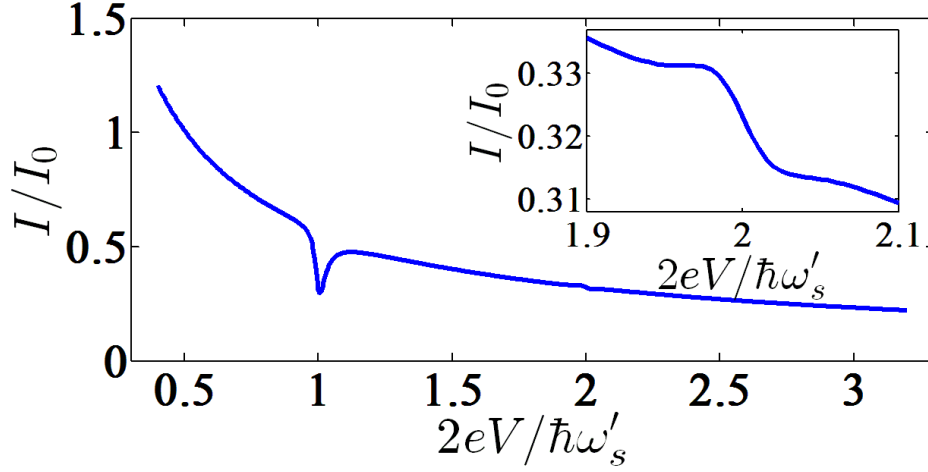


Figure 4.8: The weakly nonlinear regime: current-voltage characteristic of the probe Josephson junction when placed at $m = 0$. The parameters are $\hbar\omega'_s/E_J^s = 0.9$, $\Gamma/\omega'_s = 0.02$, $E_{\text{cut-off}}/(\hbar\omega'_s) = 20$, and $Z_0/R_Q = 0.2$. Photon-photon interactions lead to a second resonant feature at $2eV = 2\hbar\omega'_s$. A zoom on that feature with amplitude $\delta I_2/I_0 \propto (Z_0/R_Q)(\hbar\omega'_s/E_J^s)$ is shown in the inset.

form

$$\begin{aligned} \delta I_2(\delta V) = & -I_0 \frac{\pi}{32} \frac{Z_0}{R_Q} \frac{\hbar\omega'_s}{E_J^s} \frac{\Gamma^2}{[(e\delta V)^2 + \Gamma^2]^2} \\ & \times \left\{ \Gamma e\delta V \cos(2\alpha') - \frac{1}{2} [(e\delta V)^2 - \Gamma^2] \sin(2\alpha') \right\}, \end{aligned} \quad (4.44)$$

where $\alpha' = 2m\omega'_s/\omega_0$.

The characteristic amplitude A_2 of the change in current is, thus, much smaller than I_0 or the single-photon resonant structure δI_1 ,

$$A_2 = \frac{\pi}{64} \frac{Z_0}{R_Q} \frac{\hbar\omega'_s}{E_J^s} I_0 \ll I_0. \quad (4.45)$$

Here, the suppression factor Z_0/R_Q is due to the fact that it is a two-photon process, whereas the suppression factor $\hbar\omega'_s/E_J^s$ is due to the fact that it is an interaction effect. Notice that the widths of the resonances at $2eV = \hbar\omega'_s$ and $2eV = 2\hbar\omega'_s$ are the same. The dependence of the shape of the second resonance on the distance $\propto \alpha'$ between the side-coupled Josephson junction and the probe Josephson junction is shown in Fig. 4.9.

We finally consider the current contribution stemming from $G_R(\phi_m^3, \phi_m; \omega)$. While it is of the same order as the current contribution from $\delta G_R^{\text{int}}(\phi_m^2, \phi_m^2; \omega)$, i.e.,

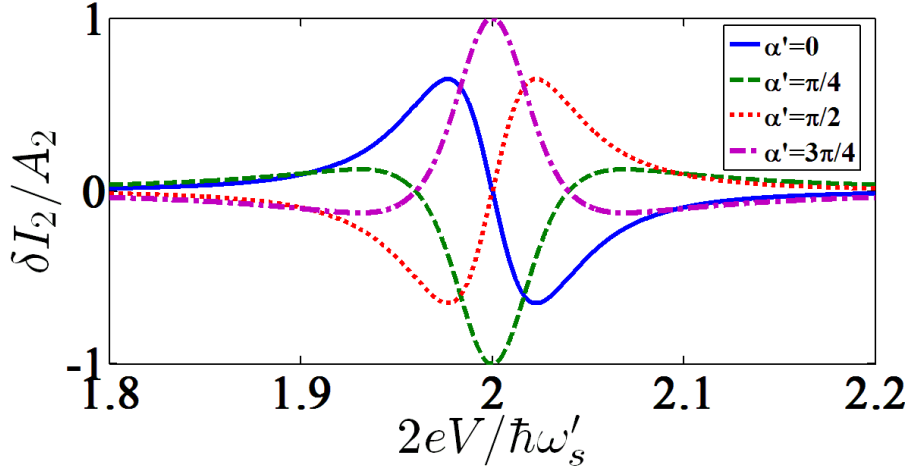


Figure 4.9: The second resonance in the current-voltage characteristic for different values of the distance between the side-coupled Josephson junction and the probe Josephson junction, $\alpha' = 2m\omega'_s/\omega_0$. Results are plotted near $2eV = 2\hbar\omega'_s$ in the two-photon, nonlinear regime [Eq. (4.44)] with $\Gamma/\omega'_s = 0.02$.

it is proportional to $(Z_0/R_Q)(\omega'_s/E_J^S)I_0$, in this case it is impossible to fulfill the resonance condition simultaneously for all the photons involved. Therefore, this contribution acquires an additional suppression factor Γ/ω'_s , and we can neglect it.

The main interaction effect is, thus, the appearance of a resonance at $2eV = 2\hbar\omega'_s$ due to two-photon processes. Higher order processes are expected to lead to additional features at $2eV = n\hbar\omega'_s$ ($n \geq 3$). However, their amplitude decreases rapidly with increasing n and may be estimated as $A_n \sim [(Z_0/R_Q)(\hbar\omega'_s/E_J^S)]^{n-1}I_0 \ll A_2$.

Taking typical parameters for realistic system [90–92], we may estimate the the amplitude A_2 . To do so, we needs the characteristic current I_0 according to Eq. (4.45). Furthermore, the characteristic current is restricted to be below than the minimum of the critical currents, including I_c (the chain junctions), I_c^S (the side-coupling junction), and I_c^P (the probe junction). We then examine these three current scales, respectively.

For I_c : as we argued in Sec. 2.3, the Josephson energy E_J and the mutual capacitance C of a junction depend mainly on the junction area and, thus, cannot be varied independently; and the capacitance to ground C_0 depends on the geometry and is therefore tunable. As a result, the impedance of the transmission line reads $Z_0/R_Q = 1/(2\pi)\sqrt{C/C_0}(I_{\text{typ}}/I_c)$ with the current I_{typ} is estimated on the order of

tens of nA. In the regime $C_0 \gg C$, the requirement that the impedance $Z_0 \leq R_Q$ ⁴ limits the critical current, thus one may have $I_c \sim I_{\text{typ}} \sim 10$ nA.

For I_c^s : the critical current of the side-coupled junction should be smaller than the chain junction, i.e., $I_c^s \ll I_c$ due to the two facts: *i*) the linear spectrum requires $\omega_s \ll \omega_0$, namely, $\sqrt{E_J^s E_{c_s}^s} \ll \sqrt{E_J E_{c_0}}$. *ii*) weakly nonlinear regime for the side-coupled junction, and linear regime for the Josephson junction chain. As a result, $E_J^s/E_{c_s}^s \ll E_J/E_{c_0}$.

For I_c^p : we have $I_0/I_c^p = (Z_0/R_Q)(E_J^p/E_J^s)(E_J^s/\hbar\omega_s) \leq 1$ [see Eq. (4.26)]. With the conditions $Z_0 \leq R_Q$ and $E_J^s \gg \omega_s$, the probe Josephson energy E_J^p must be smaller than the side-coupling junction E_J^s , therefore $I_c^p < I_c^s$.

With the analyses above, it is reasonable to estimate $I_0 \leq I_c^p \sim 100$ pA and $I_c^s \sim 1$ nA while $I_c \sim 10$ nA. Finally, we may estimate the amplitude A_2 as ~ 1 pA using Eq. (4.45). This is well within the reach of current experimental measuring techniques. In the opposite regime $C \gg C_0$, where one could use junctions with a much larger critical current. We may then estimate the critical currents as, $I_c \sim 1$ μ A, $I_c^s \sim 100$ nA, and $I_0 \leq I_c^p \sim 10$ nA. As a consequence, the amplitude A_2 may approach ~ 100 pA. In this regime, the coupling between the chain and the side-coupling junction is no local. This would make the theoretical analysis somewhat more complicated, but we expect that the results would not change qualitatively.

4.4 Summary

We have shown that the dc current-voltage characteristic of a Josephson junction provides a sensitive probe to study photon-photon interactions in a nonlinear environment. In particular, we investigated the case of a transmission line side-coupled to another Josephson junction whose non-linearity leads to local photon-photon interactions. Scattering of individual photons by the side-coupled Josephson junction results in a resonance feature in the current-voltage characteristic of the probe Josephson junction at $2eV = \hbar\omega'_s$, where ω'_s is the plasma frequency of the side-coupled Josephson junction. By contrast, the interactions due to the non-linearity yield an additional resonance feature at $2eV = 2\hbar\omega'_s$ due to two-photon processes. Such a feature is thus a clear indication of photon-photon interactions. The current amplitude of the feature is estimated on the order of pA which is well within the reach of current experimental measuring techniques. While we concentrated here on the regime of a weak non-linearity, it will be interesting to see how these features are modified in the strongly nonlinear regime. This will be discussed in chapter 5.

⁴In the regime $C \ll C_0$, Josephson junction chain transforms to the insulating state when the impedance larger than quantum resistance [138, 139].

Detecting photon-photon interactions in a transmission line side-coupled with a charge qubit

In this chapter, we still focus on detecting the photon-photon interaction created by a Cooper pair box in a transmission line. While the last chapter concentrated on the weakly nonlinear regime, we now switch to the strongly nonlinear regime. In this regime, the Cooper pair box provides a physical realization of a charge qubit. The system can be described using a spin-boson model that a qubit (spin) is linearly coupled with the travelling photons (boson). This chapter is organized as follows. We first introduce the spin-boson Hamiltonian that describes the strongly nonlinear system in Sec. 5.1. Then, the following task is to compute phase-phase correlators¹ in Sec. 5.2. To do so, we apply two kinds of methods: the first one uses Green's function perturbation theory to calculate the two-point correlator as well as the four-point correlator; while the second one uses path integral method to compute the entire phase-phase correlator. Both the resulting phase-phase correlators are expressed in terms of spin-spin correlators, which represents the influence of the side-coupled qubit. Next, spin-spin correlators are evaluated in Sec. 5.3. This can be mapped to the problem of a two-level system coupled to an ohmic bosonic bath. In particular, Bloch equations are used to compute the two-point spin-spin correlator. Furthermore, the current-voltage characteristic of the probe junction is discussed in Sec. 5.4. Finally, we summarize in Sec. 5.5.

5.1 Hamiltonian of the system

We consider the same superconducting circuit as in chapter 4 (see Fig. 4.1). The system Hamiltonian H was addressed in Eq. (4.1). It consists of the transmission line Hamiltonian H_T , the side-coupled Cooper pair box Hamiltonian H_J , and

¹The same as in the weakly nonlinear regime. See details in chapter 4.

the coupling Hamiltonian H_c . Before the following discussion, it should be mentioned that we are making the same approximations² as in chapter 4, except in the case of the nonlinear regime. In this chapter, we consider the strongly nonlinear regime.

Firstly, the transmission line Hamiltonian takes the form (4.2), namely

$$H_T = \sum_n \left[\frac{Q_n^2}{2C_0} + \left(\frac{\hbar}{2e} \right)^2 \frac{(\phi_n - \phi_{n+1})^2}{2L} \right]. \quad (5.1)$$

Next, for the side-coupled Cooper pair box, we are interested in the strongly nonlinear regime, i.e. when the charging energy $e^2/2C_\Sigma$ dominates over the Josephson coupling energy E_J^s . In this regime, the Cooper pair box is effectively reduced to a two-state quantum system (a charge qubit) when the dimensionless gate charge $C_g V_g/2e$ is close to a half-integer³. Correspondingly, the Cooper pair box Hamiltonian H_J is replaced by the charge qubit Hamiltonian (2.18). Specifically, at the degeneracy points, e.g., $C_g V_g/2e = 1/2$, the qubit Hamiltonian (2.18) reduces to

$$H_{\text{qb}} = -\frac{E_J^s}{2} \sigma_x. \quad (5.2)$$

For later convenience, we define the resonance frequency of the qubit as $\omega_{\text{qb}} = E_J^s/\hbar$.

Finally, the coupling Hamiltonian H_c is obtained from Eq. (4.4). It is necessary to rewrite the coupling charge term $Q_\delta + C_g V_g$ using the spin-1/2 representation. It reads $-e\sigma_z$ [see Eq. (2.22)]. Hence,

$$H_c = -\lambda Q_0 \sigma_z, \quad (5.3)$$

where $\lambda = eC_c/(C_0 C_\Sigma)$ is the coupling factor between the charge qubit and the transmission line.

Collecting Eqs. (5.1) - (5.3) together, we obtain a spin-boson model with an ohmic environment:

$$H_{\text{sb}} = H_T + H_{\text{qb}} + H_c. \quad (5.4)$$

The next step is the same as in chapter 4: computing the phase-phase correlator $\langle e^{i\phi_m(t)} e^{-i\phi_m(0)} \rangle_{H_{\text{sb}}}$. With the result, one can compute the $P(E)$ function and further obtain the current flowing through the probe junction.

²We take $C \ll C_0$, $E_{C_0} \ll E_J$, and $C_c \ll C_0, C_\Sigma$. See details in chapter 4.

³They corresponds to the charge degeneracy points in Fig. 2.4

5.2 Phase-phase correlator

Since the Hamiltonian H_{sb} is not quadratic, the phase-phase correlator cannot be simplified to the form expressed in Eq. (3.20). Instead, using the approach introduced in Sec. 3.4, we expand $\langle e^{i\phi_m(t)} e^{-i\phi_m(0)} \rangle_{H_{\text{sb}}}$ in powers of ϕ_m , cf., Eq. (3.48). The resulting phase-phase correlator is expressed in terms of a single-point correlator, two-point correlators, and n -point correlators.

Then, we use Green's function perturbation theory to compute each phase-phase correlator. The coupling term (5.3) is set as the interaction V , while the unperturbed Hamiltonian $H^{(0)}$ is contributed from the transmission line and the side-coupled qubit, namely

$$H^{(0)} = H_T + H_{\text{qb}} \quad (5.5)$$

At the degeneracy points, we find that the spin-boson Hamiltonian [Eq.(5.4)] has the following symmetry: $\phi_n \rightarrow -\phi_n$, $Q_n \rightarrow -Q_n$, and $\sigma_z \rightarrow -\sigma_z$. This leads to the odd-point phase-phase correlators vanishing and only the even-point correlators contributing according to the arguments specified in Sec. 3.4.

In the following, we first use Green's function perturbation theory to evaluate the two-point phase-phase correlator $\langle \phi_m(t) \phi_m(0) \rangle_{H_{\text{sb}}}$ (corresponding to single photon processes) as well as the four-point phase-phase correlators $\langle \phi_m^2(t) \phi_m^2(0) \rangle_{H_{\text{sb}}}$, $\langle \phi_m^3(t) \phi_m(0) \rangle_{H_{\text{sb}}}$, and $\langle \phi_m(t) \phi_m^3(0) \rangle_{H_{\text{sb}}}$ (two photon processes). When it comes to $2n$ ($n \geq 3$)-point phase-phase correlators (multiple photon processes), the calculations using perturbation theory become cumbersome. As an alternative we will use the path integral method.

5.2.1 Single photon processes

We now compute the two-point phase-phase correlator $\langle \phi_m(t) \phi_m(0) \rangle_{H_{\text{sb}}}$, which represents the single photon processes. For spin-boson systems, we will see that the boson-boson correlators can be expressed in terms of local spin-spin correlators. As for the latter correlators, they were often mapped to the well-studied problem [140, 141] where a two-level system couples with a bosonic bath.

As before, the phase-phase correlator is formulated using the corresponding retarded Green's function $G_R[\phi_n(t), \phi_m(0)]$. In order to be able to use perturbation theory, we switch to the imaginary-time Green's function formalism, \mathcal{G} .

Let us evaluate the two-point time-ordered Green's function $\mathcal{G}[\phi_n(t) \phi_m(0)]$. Using Eq. (3.56) and the pairing rules argued in Sec. 3.4, we expand the interaction V to the first few orders in λ . The interaction term V is bilinear in charge operator Q_0 and spin operator σ_z . As a result, only the even order remains in the expansion of the interaction since phase and charge operators must appear in

pairs in the bracket. One more thing we specify is that the spin operators do not obey a Wick's theorem, thus they can not be decoupled into two-point spin-spin correlators. Considering these rules, the Green's function reads⁴

$$\begin{aligned}
\mathcal{G}[\phi_n(\tau)\phi_m(0)] &= \mathcal{G}^{(0)}[\phi_n(\tau)\phi_m(0)] + \lambda^2 \int_0^\beta d\tau_1 \int_0^\beta d\tau_2 \mathcal{G}^{(0)}[\phi_n(\tau)Q_0(\tau_1)] \\
&\times \mathcal{G}^{(0)}[\sigma_z(\tau_1)\sigma_z(\tau_2)]\mathcal{G}^{(0)}[Q_0(\tau_2)\phi_m(0)] + \frac{\lambda^4}{2} \int_0^\beta d\tau_1 \int_0^\beta d\tau_2 \int_0^\beta d\tau_3 \int_0^\beta d\tau_4 \\
&\times \mathcal{G}^{(0)}[\phi_n(\tau)Q_0(\tau_1)]\mathcal{G}^{(0)}[\sigma_z(\tau_1)\sigma_z(\tau_2)\sigma_z(\tau_3)\sigma_z(\tau_4)]\mathcal{G}^{(0)}[Q_0(\tau_3)Q_0(\tau_4)] \\
&\times \mathcal{G}^{(0)}[Q_0(\tau_2)\phi_m(0)] + \mathcal{O}(\lambda^6). \tag{5.6}
\end{aligned}$$

It is seen that the second (fourth) order correction contains the two (four)-point spin-spin Green's function. If we consider higher orders corrections, e.g., $2n$ ($n \geq 3$, n integer)-th orders corrections, there will be additional spin-spin Green's functions $\mathcal{G}^{(0)}[\sigma_z(\tau_1)\sigma_z(\tau_2)\cdots\sigma_z(\tau_{2n-1})\sigma_z(\tau_{2n})]$.

To interpret the results using Feynman diagrams, we first define the basic diagrams in Fig. 5.1. The thin (blue) solid line (a) represents the unperturbed time-ordered Green's functions $\mathcal{G}^{(0)}[X(\tau)Y(0)]$; while the thick (blue) solid line (b) represents $\mathcal{G}[X(\tau)Y(0)]$, where X, Y are either phase or charge operators. Spin-spin time-ordered Green's functions are drawn as (orange) dashed ovals. The thin dashed oval (c) represents the two-point unperturbed time-ordered Green's function $\mathcal{G}^{(0)}[\sigma_z(\tau_1)\sigma_z(\tau_2)]$; while the thick dashed oval (d) represents $\mathcal{G}[\sigma_z(\tau_1)\sigma_z(\tau_2)]$. Besides, the diagrams (e) and (f) correspond to the four-point time-ordered Green's function $\mathcal{G}^{(0)}[\sigma_z(\tau_1)\sigma_z(\tau_2)\sigma_z(\tau_3)\sigma_z(\tau_4)]$ and the six-point time-ordered Green's function $\mathcal{G}^{(0)}[\sigma_z(\tau_1)\sigma_z(\tau_2)\sigma_z(\tau_3)\sigma_z(\tau_4)\sigma_z(\tau_5)\sigma_z(\tau_6)]$, respectively.

Using the diagrams defined above, we interpret Eq. (5.6) in terms of Feynman diagrams, shown in Fig. 5.2.

Next, we use the same procedure to evaluate the two-point spin-spin Green's

⁴The detailed calculation is presented in Appendix D.

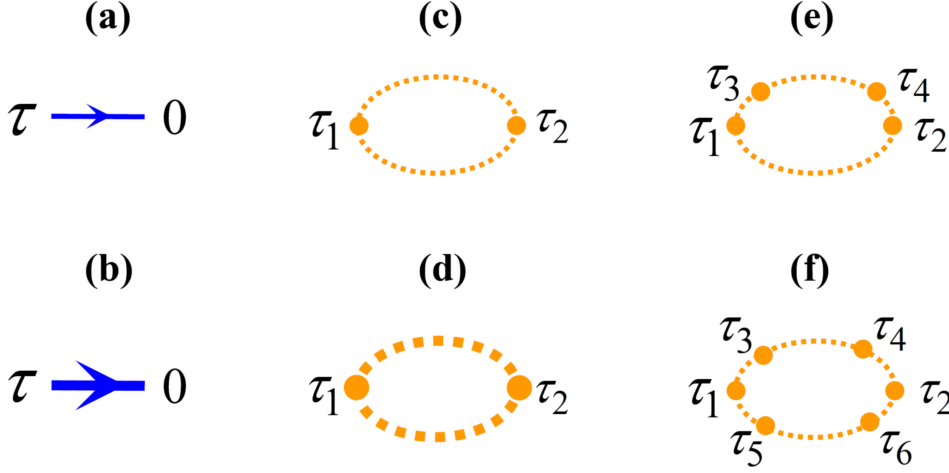


Figure 5.1: The basic Feynman diagrams of the corresponding time-ordered Green's functions in strongly nonlinear regime. The unperturbed (perturbed) phase-phase propagators are represented by a thin (a) [thick (b)] solid lines; while the unperturbed (perturbed) spin-spin propagators are represented by thin (c) [thick (d)] dashed ovals. Besides, the diagrams (e) and (f) correspond to the unperturbed four-point and six-point Green's functions. We will use these diagrams to interpret the perturbation results.

function $\mathcal{G}[\sigma_z(\tau_1), \sigma_z(\tau_2)]$. Expanding to the fourth order in λ , we obtain

$$\begin{aligned}
 \mathcal{G}[\sigma_z(\tau_1)\sigma_z(\tau_2)] &= \mathcal{G}^{(0)}[\sigma_z(\tau_1)\sigma_z(\tau_2)] + \frac{\lambda^2}{2} \int_0^\beta d\tau_3 \int_0^\beta d\tau_4 \mathcal{G}^{(0)}[Q_0(\tau_3)Q_0(\tau_4)] \\
 &\times \mathcal{G}^{(0)}[\sigma_z(\tau_1)\sigma_z(\tau_2)\sigma_z(\tau_3)\sigma_z(\tau_4)] + \frac{\lambda^4}{8} \int_0^\beta d\tau_3 \int_0^\beta d\tau_4 \int_0^\beta d\tau_5 \int_0^\beta d\tau_6 \\
 &\times \mathcal{G}^{(0)}[Q_0(\tau_3)Q_0(\tau_4)] \mathcal{G}^{(0)}[\sigma_z(\tau_1)\sigma_z(\tau_2)\sigma_z(\tau_3)\sigma_z(\tau_4)\sigma_z(\tau_5)\sigma_z(\tau_6)] \\
 &\times \mathcal{G}^{(0)}[Q_0(\tau_5)Q_0(\tau_6)] + \mathcal{O}(\lambda^6). \tag{5.7}
 \end{aligned}$$

The Feynman diagrams of the equation above are shown in Fig. 5.3.

Considering the perturbation series to all orders in λ (see Appendix D), and comparing with the expressions of $\mathcal{G}[\phi_n(\tau)\phi_m(0)]$ and $\mathcal{G}[\sigma_z(\tau_1)\sigma_z(\tau_2)]$, we get a relatively simpler result. The two-point phase-phase Green's function can be expressed only in terms of the full two-point spin-spin time-ordered Green's function as well as the two-point phase-phase (and phase-charge) unperturbed Green's

$$\tau \rightarrow 0 = \tau \rightarrow 0 + \tau \rightarrow \tau_1 \text{ (dashed orange loop)} \tau_2 \rightarrow 0 + \tau \rightarrow \tau_1 \text{ (dashed orange loop)} \tau_2 \rightarrow \tau_3 \text{ (dashed orange loop)} \tau_4 \rightarrow \tau_2 \rightarrow 0 + O(\lambda^6)$$

Figure 5.2: The Feynman diagrams of the two-point time-ordered Green's function $\mathcal{G}[\phi_n(\tau)\phi_m(0)]$. It corresponds to Eq. (5.6).

$$\tau_1 \text{ (dashed orange loop)} \tau_2 = \tau_1 \text{ (dashed orange loop)} \tau_2 + \tau_1 \text{ (dashed orange loop)} \tau_2 \text{ with } \tau_3 \rightarrow \tau_4 + \tau_1 \text{ (dashed orange loop)} \tau_2 \text{ with } \tau_3 \rightarrow \tau_4 \text{ and } \tau_5 \rightarrow \tau_6 + O(\lambda^6)$$

Figure 5.3: The Feynman diagrams for the two-point time-ordered Green's function $\mathcal{G}[\sigma_z(\tau_1)\sigma_z(\tau_2)]$. The corresponding time-ordered Green's function is shown in Eq. (5.7).

functions. Namely,

$$\begin{aligned} \mathcal{G}[\phi_n(\tau)\phi_m(0)] &= \mathcal{G}^{(0)}[\phi_n(\tau)\phi_m(0)] + \lambda^2 \int_0^\beta d\tau_1 \int_0^\beta d\tau_2 \mathcal{G}^{(0)}[\phi_n(\tau)Q_0(\tau_1)] \\ &\quad \times \mathcal{G}[\sigma_z(\tau_1)\sigma_z(\tau_2)]\mathcal{G}^{(0)}[Q_0(\tau_2)\phi_m(0)]. \end{aligned} \quad (5.8)$$

The representation in term of Feynman diagrams is shown in Fig. 5.4. It is indeed easily obtained by comparing the Feynman diagrams of Fig. 5.2 and Fig. 5.3, the orange part (including the inside) of the diagrams in Fig. 5.2 can be exactly replaced by the thick dashed oval. Note that the pre-factors⁵ of the corresponding diagrams are the same as well.

$$\tau \rightarrow 0 = \tau \rightarrow 0 + \tau \rightarrow \tau_1 \text{ (thick dashed orange oval)} \tau_2 \rightarrow 0$$

Figure 5.4: A simplified Feynman diagram of $\mathcal{G}[\phi_n(\tau)\phi_m(0)]$ expressed in term of $\mathcal{G}[\sigma_z(\tau_1)\sigma_z(\tau_2)]$. The corresponding time-ordered Green's function is shown in Eq. (5.8).

Taking the Fourier transform of Eq. (5.8), and replacing the resulting Matsubara frequency $i\omega_\nu$ by $\omega + i0^+$, we get the retarded Green function which is

⁵See details in Appendix D.

useful for further computing the phase-phase correlator. It reads

$$G_R(\phi_n, \phi_m; \omega) = G_R^{(0)}(\phi_n, \phi_m; \omega) + \lambda^2 G_R^{(0)}(\phi_n, Q_0; \omega) G_R(\sigma_z, \sigma_z; \omega) G_R^{(0)}(Q_0, \phi_m; \omega), \quad (5.9)$$

where the term $\lambda^2 G_R(\sigma_z, \sigma_z; \omega)$ can be regarded as the T matrix .

The unperturbed retarded Green's functions $G_R^{(0)}$ in the equation above are easily solved. First of all, the two-point phase-phase Green's function was already computed in chapter 3 when we studied the case of a pure transmission line. It reads $G_R^{(0)}(\phi_n, \phi_m; \omega) = i[\pi/(\hbar\omega)](Z_0/R_Q)e^{ik|n-m|}$. Then, we evaluate the other two-point phase-charge Green's functions by rewriting the phase and charge operators in terms of the creation (a_k^\dagger) and annihilation (a_{-k}) operators [see Eq. (2.47)]. The resulting two-point Green's functions in- k space are evaluated in Appendix E. Using Eqs. (E.4) and (E.5), we obtain $G_R^{(0)}(\phi_n, Q_0; \omega) = G_R^{(0)}(Q_0, \phi_n; \omega) = \lambda e/(\hbar\omega_0)e^{i\omega/\omega_0|n|}$.

Substituting the results of these unperturbed Green's functions into Eq. (5.9), we obtain

$$G_R(\phi_n, \phi_m; \omega) = i\frac{\pi}{\hbar\omega} \frac{Z_0}{R_Q} e^{i\frac{\omega}{\omega_0}|n-m|} - \left(\frac{\lambda e}{\hbar\omega_0}\right)^2 G_R(\sigma_z, \sigma_z; \omega) e^{i\frac{\omega}{\omega_0}(|n|+|m|)}. \quad (5.10)$$

Using the definition of λ , the dimensionless coupling factor ($\lambda e/\hbar\omega_0$) can be expressed in a more physical way:

$$\bar{\lambda} = \frac{\pi C_c Z_0}{2 C_\Sigma R_Q}. \quad (5.11)$$

As we took and $C_c/C_\Sigma \leq 1$, in addition to the superconductor-insulator transition restricts $Z_0/R_Q \leq 1$, the coupling strength $\bar{\lambda}$ between the transmission line and the qubit is weak.

Taking $n = m$, the local retarded Greens function needed to compute the two-point phase-phase correlator, thus, reads

$$G_R(\phi_m, \phi_m; \omega) = i\frac{\pi}{\hbar\omega} \frac{Z_0}{R_Q} - \bar{\lambda}^2 G_R(\sigma_z, \sigma_z; \omega) e^{2i\frac{\omega}{\omega_0}|m|}. \quad (5.12)$$

If there is no side-coupling, namely $\bar{\lambda} = 0$, Eq. (5.12) recovers the case of a pure transmission line [see Eq. (3.35)]. The second term is a contribution from the side-coupled qubit.

To further compute the phase-phase correlator, we make use of the relation (3.22). To do so, we obtain that the contribution of the single photon processes, i.e., $J(t) = \langle [\phi_m(t) - \phi_m(0)]\phi_m(0) \rangle_{H_{sb}}$ equals $J_0(t) + J_1(t)$. J_0 is given by

Eq. (3.23), and J_1 reads

$$J_1(t) = -\bar{\lambda}^2 \frac{\hbar}{\pi} \int_0^\infty d\omega \operatorname{Im} \left[G_R(\sigma_z, \sigma_z; \omega) e^{2i\frac{\omega}{\omega_0}|m|} \right] \times \left[\coth\left(\frac{\hbar\omega\beta}{2}\right) (\cos \omega t - 1) - i \sin \omega t \right]. \quad (5.13)$$

In the zero temperature limit, $J_1(t)$ reduces to

$$J_1(t) = -\bar{\lambda}^2 \frac{\hbar}{\pi} \int_0^\infty d\omega \operatorname{Im} \left[G_R(\sigma_z, \sigma_z; \omega) e^{2i\frac{\omega}{\omega_0}|m|} \right] (e^{-i\omega t} - 1). \quad (5.14)$$

Using Green's function perturbation theory, we have transformed the calculation of a two-point phase-phase correlator into that of a two-point spin-spin Green's function. Since the latter one has been widely studied, we can directly use part of the results.

5.2.2 Two photon processes

Now, we turn to the study of two photons processes. Compared to the case of single photon processes with the exception of freely propagating photons, it becomes now possible to have an effective photon-photon interaction through the strong coupling between the transmission line and the side-coupled qubit. This is likely to lead to new features on the current-voltage characteristic.

We will use the same method as for single photon processes to evaluate the four-point time-ordered Green's functions, which are needed to compute the four-point phase-phase correlators. Since the calculations are rather long, we will only present the calculation of $\mathcal{G}[\phi_n^2(\tau)\phi_m^2(0)]$, and write down directly the results of the other two Green's functions, $\mathcal{G}[\phi_n^3(\tau)\phi_m(0)]$ and $\mathcal{G}[\phi_n(\tau)\phi_m^3(0)]$, that are computed in the same way.

The four-point time-ordered Green's function $\mathcal{G}[\phi_n^2(\tau)\phi_m^2(0)]$ is evaluated perturbatively. As a starting point, the Feynman diagrams of the zeroth order expansion (no coupling) are drawn as two thin lines. It describes two photons freely propagating along the transmission line. As before, the coupling term is taken as the perturbation. Expanding the interaction series to all orders, we obtain that the four-point Green's function consists of two different kinds of contributions. The first one is that the perturbation term interacts with only one of the line, corresponding to two photons propagate freely; the second one is that the perturbation term interacts with both of the lines. As a result, two photons interact with each other. More precisely, the imaginary-time-ordered four-point Green's function is

written as $\mathcal{G}[\phi_n^2(\tau)\phi_m^2(0)] = 2\mathcal{G}^{(0)}[\phi_n(\tau)\phi_m(0)]\mathcal{G}[\phi_n(\tau)\phi_m(0)] + \delta\mathcal{G}^{\text{int}}[\phi_n^2(\tau)\phi_m^2(0)]$ where the latter term reading

$$\begin{aligned}
 & \lambda^4 \int_0^\beta d\tau_1 \int_0^\beta d\tau_2 \int_0^\beta d\tau_3 \int_0^\beta d\tau_4 \mathcal{G}^{(0)}[\phi_n(\tau)Q_0(\tau_1)]\mathcal{G}^{(0)}[\phi_n(\tau)Q_0(\tau_2)] \\
 & \times \mathcal{G}^{(0)}[\sigma_z(\tau_1), \sigma_z(\tau_2), \sigma_z(\tau_3), \sigma_z(\tau_4)]\mathcal{G}^{(0)}[Q_0(\tau_3)\phi_m(0)]\mathcal{G}^{(0)}[Q_0(\tau_4)\phi_m(0)] \\
 & + \frac{\lambda^6}{2} \int_0^\beta d\tau_1 \int_0^\beta d\tau_2 \int_0^\beta d\tau_3 \int_0^\beta d\tau_4 \int_0^\beta d\tau_5 \int_0^\beta d\tau_6 \mathcal{G}^{(0)}[\phi_n(\tau)Q_0(\tau_1)] \\
 & \times \mathcal{G}^{(0)}[\phi_n(\tau)Q_0(\tau_2)]\mathcal{G}^{(0)}[\sigma_z(\tau_1), \sigma_z(\tau_2), \sigma_z(\tau_3), \sigma_z(\tau_4), \sigma_z(\tau_5), \sigma_z(\tau_6)] \\
 & \times \mathcal{G}^{(0)}[Q_0(\tau_5)Q_0(\tau_6)]\mathcal{G}^{(0)}[Q_0(\tau_3)\phi_m(0)]\mathcal{G}^{(0)}[Q_0(\tau_4)\phi_m(0)] \\
 & + \mathcal{O}(\lambda^8).
 \end{aligned} \tag{5.15}$$

The representation in terms of Feynman diagrams is shown in Fig. 5.5.

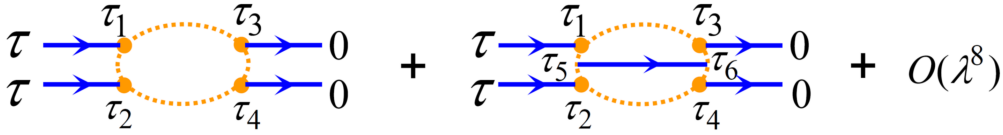


Figure 5.5: The Feynman diagrams of the four-point time-ordered Green's function $\delta\mathcal{G}^{\text{int}}[\phi_n^2(\tau)\phi_m^2(0)]$. The corresponding time-ordered Green's function is shown in Eq. (5.15).

Next, we evaluate the four-point spin-spin time-ordered Green's function $\mathcal{G}[\sigma_z(\tau_1), \sigma_z(\tau_2), \sigma_z(\tau_3), \sigma_z(\tau_4)]$. Expanding the interaction series to the second order in λ , we obtain

$$\begin{aligned}
 & \mathcal{G}[\sigma_z(\tau_1), \sigma_z(\tau_2), \sigma_z(\tau_3), \sigma_z(\tau_4)] = \mathcal{G}^{(0)}[\sigma_z(\tau_1), \sigma_z(\tau_2), \sigma_z(\tau_3), \sigma_z(\tau_4)] \\
 & + \frac{\lambda^2}{2} \int_0^\beta d\tau_5 \int_0^\beta d\tau_6 \mathcal{G}^{(0)}[\sigma_z(\tau_1), \sigma_z(\tau_2), \sigma_z(\tau_3), \sigma_z(\tau_4), \sigma_z(\tau_5), \sigma_z(\tau_6)] \\
 & \times \mathcal{G}^{(0)}[Q_0(\tau_5)Q_0(\tau_6)] + \mathcal{O}(\lambda^4).
 \end{aligned} \tag{5.16}$$

The corresponding Feynman diagrams are shown in Fig. 5.6.

Expanding λ to higher orders⁶, and comparing with $\delta\mathcal{G}^{\text{int}}[\phi_n^2(\tau)\phi_m^2(0)]$ and the four-point Green's function $\mathcal{G}[\sigma_z(\tau_1)\sigma_z(\tau_2)\sigma_z(\tau_3)\sigma_z(\tau_4)]$, or considering the

⁶The calculation is similar to the two-point case, which is presented in Appendix D.

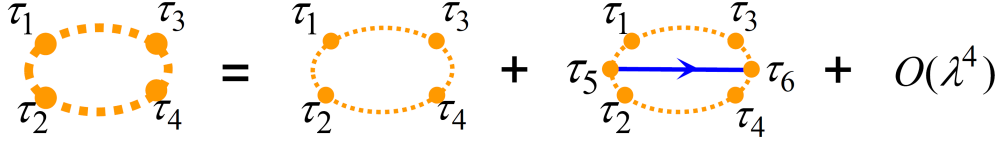


Figure 5.6: The Feynman diagrams of the four-point time-ordered Green's function $\mathcal{G}[\sigma_z(\tau_1)\sigma_z(\tau_2)\sigma_z(\tau_3)\sigma_z(\tau_4)]$. The corresponding time-ordered Green's function is shown in Eq. (5.16).

Feynman diagrams of Fig. 5.5 and Fig. 5.6, we obtain

$$\begin{aligned} \delta\mathcal{G}^{\text{int}}[\phi_n^2(\tau)\phi_m^2(0)] &= \lambda^4 \int_0^\beta d\tau_1 \int_0^\beta d\tau_2 \int_0^\beta d\tau_3 \int_0^\beta d\tau_4 \mathcal{G}^{(0)}[\phi_n(\tau)Q_0(\tau_1)] \\ &\quad \times \mathcal{G}^{(0)}[\phi_n(\tau)Q_0(\tau_2)] \mathcal{G}[\sigma_z(\tau_1), \sigma_z(\tau_2), \sigma_z(\tau_3), \sigma_z(\tau_4)] \\ &\quad \times \mathcal{G}^{(0)}[Q_0(\tau_3)\phi_m(0)] \mathcal{G}^{(0)}[Q_0(\tau_4)\phi_m(0)]. \end{aligned} \quad (5.17)$$

The representation in terms of Feynman diagrams is shown in Fig. 5.7.

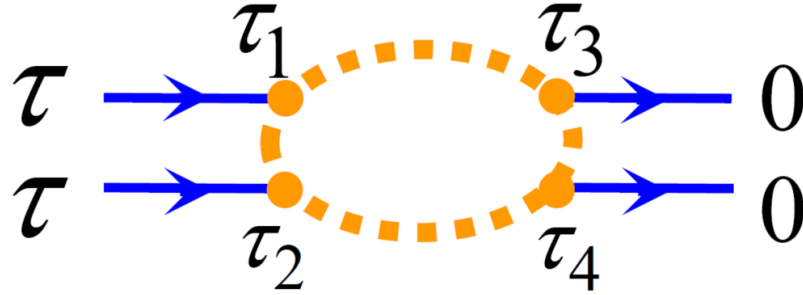


Figure 5.7: A simplified Feynman diagram of $\delta\mathcal{G}^{\text{int}}[\phi_n^2(\tau)\phi_m^2(0)]$ expressed in term of $\mathcal{G}[\sigma_z(\tau_1)\sigma_z(\tau_2)\sigma_z(\tau_3)\sigma_z(\tau_4)]$. It corresponds to Eq. (5.17).

In order to evaluate the contribution of photon-photon interactions, we first rewrite Eq. (5.17) in Matsubara frequency space, namely

$$\begin{aligned} \delta\mathcal{G}^{\text{int}}(\phi_n^2, \phi_m^2; i\omega_\nu) &= \lambda^4 \sum_{i\omega_a, i\omega_b} \mathcal{G}^{(0)}(\phi_n, Q_0; i\omega_a) \mathcal{G}^{(0)}(\phi_n, Q_0; i\omega_b) \quad (5.18) \\ &\quad \times \mathcal{G}(\sigma_z, \sigma_z, \sigma_z, \sigma_z; i\omega_a, i\omega_b, i\omega_\nu - i\omega_a - i\omega_b) \\ &\quad \times \mathcal{G}^{(0)}(Q_0, \phi_m; i\omega_\nu - i\omega_a) \mathcal{G}^{(0)}(Q_0, \phi_m; i\omega_\nu - i\omega_b). \end{aligned}$$

To evaluate the unperturbed Green's functions $\mathcal{G}^{(0)}$, we first rewrite the phase and charge operators with the creation and annihilation operators. Then, the resulting new Green's functions⁷ in k space are easily solved from their equations of motion. Substituting them into Eq. (5.18), and replacing Matsubara frequency $i\omega_\nu$ by $\omega + i0^+$, we obtain the corresponding retarded Green's function:

$$\delta G_R^{\text{int}}(\phi_n^2, \phi_m^2; \omega) = \bar{\lambda}^4 e^{i\frac{\omega}{\omega_0}(|n|+|m|)} \sum_{i\omega_a, i\omega_b} \mathcal{G}(\sigma_z, \sigma_z, \sigma_z, \sigma_z; i\omega_a, i\omega_b, \omega), \quad (5.19)$$

where the coupling strength $\bar{\lambda}$ was defined in Eq. (5.11).

Furthermore, the local retarded Green's function which is needed to compute the correlator is obtained by taking $n = m$, namely

$$\delta G_R^{\text{int}}(\phi_m^2, \phi_m^2; \omega) = \bar{\lambda}^4 e^{2i\frac{\omega}{\omega_0}|m|} \sum_{i\omega_a, i\omega_b} \mathcal{G}(\sigma_z, \sigma_z, \sigma_z, \sigma_z; i\omega_a, i\omega_b, \omega). \quad (5.20)$$

Next, the other two four-point local retarded Green's functions $G_R(\phi_n^3, \phi_m; \omega)$ and $G_R(\phi_n, \phi_m^3; \omega)$ are evaluated. In particular, we find the results similar to Eq. (5.20):

$$G_R(\phi_m^3, \phi_m; \omega) = -\bar{\lambda}^4 e^{2i\frac{\omega}{\omega_0}|m|} \sum_{i\omega_a, i\omega_b} \mathcal{G}[\sigma_z, \sigma_z, \sigma_z, \sigma_z; i\omega_a, i\omega_a + i\omega_b; \omega]. \quad (5.21)$$

The Feynman diagram for the corresponding time-ordered Green's function is shown in Fig. 5.8(a), from which one can see that it only contains the contribution of photon-photon interactions. Besides, we also calculate $G_R(\phi_m, \phi_m^3; \omega) = G_R(\phi_m^3, \phi_m; \omega)$. The Feynman diagram for the corresponding time-ordered Green's function is shown in Fig. 5.8(b).

At the end, with the help of the relation (3.22), we use the retarded Green's functions to compute the four-point phase-phase correlators. Collecting these correlators, they are written as three part, i.e., $J_0^2(t)/2 + J_0(t)J_1(t) + \delta J^{\text{int}}(t)$. While J_0 and $J_1(t)$ were already addressed in Eq. (3.23) and Eq. (5.13), respectively; the additional contribution from interaction $\delta J^{\text{int}}(t)$ takes the same form as Eq. (4.42). Namely,

$$\delta J^{\text{int}}(t) \simeq \frac{\hbar}{\pi} \int_0^\infty d\omega \left\{ \frac{1}{4} \text{Im} \left[\delta G_R^{\text{int}}(\phi_m^2, \phi_m^2; \omega) \right] - \frac{1}{3} \text{Im} \left[G_R(\phi_m^3, \phi_m; \omega) \right] \right\} (e^{-i\omega t} - 1). \quad (5.22)$$

⁷More details see Appendix E

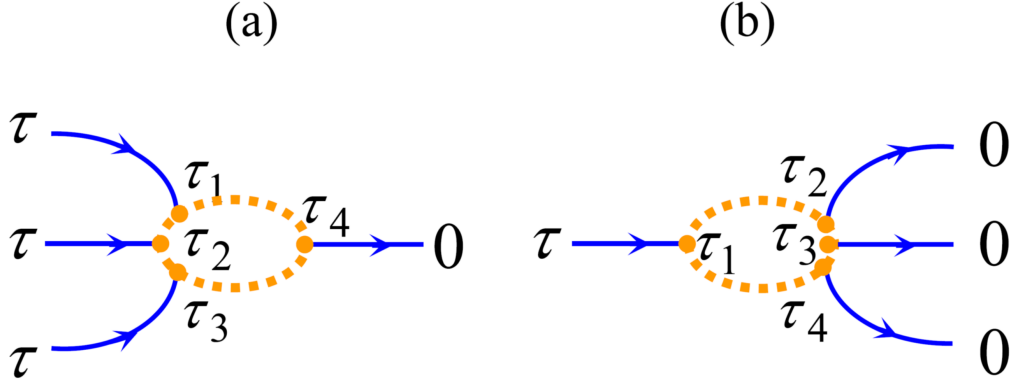


Figure 5.8: Feynman diagrams of (a) $\mathcal{G}[\phi_n(\tau)\phi_m^3(0)]$ and (b) $\mathcal{G}[\phi_n^3(\tau)\phi_m(0)]$ expressed in terms of $\mathcal{G}[\sigma_z(\tau_1)\sigma_z(\tau_2)\sigma_z(\tau_3)\sigma_z(\tau_4)]$ (the dotted oval diagrams).

To summarize, we computed the four-point time-ordered Green's functions using perturbation theory. In contrast with the single photon processes, the interactions between photons lead to additional contributions that add to those of the freely propagating photons. In particular, the Green's functions which represent the photon-photon interaction processes are expressed in terms of the four-point spin-spin Green's function $\mathcal{G}[\sigma_z, \sigma_z, \sigma_z, \sigma_z]$.

5.2.3 Multiple photon processes

To compute $2n$ -point ($n \geq 3$, integer) phase-phase correlators (multiple photon processes), perturbation theory is still valid but becomes extremely tedious. Therefore, as an alternative we use the path integral method. It is indeed a convenient way to extend the results of Green's function theory to all orders. That is we may compute the entire phase-phase correlator $\langle e^{i\phi_m(t)} e^{-i\phi_m(0)} \rangle_{H_{sb}}$.

The procedures of the path integral method were already shown in Sec. 3.4.2. In chapter 3, we considered a linear system, i.e., a pure transmission line. In contrast, we now add the nonlinearity.

In order to use the path integral method, we switch to time-ordered correlators in imaginary time space, namely $\langle T_\tau e^{i\phi_m(\tau)} e^{-i\phi_m(0)} \rangle_{H_{sb}}$.

Comparing with the linear case studied in Sec. 3.4.2, the coupling between the transmission line and the side-coupled qubit has to be considered. As a result, the action (3.74) in $q \equiv (k, \omega_n)$ space becomes

$$-s = -\frac{1}{2} \frac{1}{\beta \mathcal{L} \hbar} \sum_q \left[\begin{pmatrix} \phi_{-q} & Q_{-q} \end{pmatrix} M^{-1} \begin{pmatrix} \phi_q \\ Q_q \end{pmatrix} - 2\lambda \sigma_z Q_q \right]. \quad (5.23)$$

Note that the spin operator σ_z is only a ‘‘spectator’’, thus we do not specify its representation.

Using this action, the time-ordered phase-phase correlator can be written in the form

$$\begin{aligned} \langle T_\tau e^{i\phi_m(\tau)} e^{-i\phi_m(0)} \rangle_{H_{sb}} &= \frac{1}{Z} \int D\phi_q(\tau) DQ_q(\tau) \exp \left\{ -\frac{1}{2} \frac{1}{\beta \mathcal{L} \hbar} \right. \\ &\times \sum_q \left[\begin{pmatrix} \phi_{-q} & Q_{-q} \end{pmatrix} M^{-1} \begin{pmatrix} \phi_q \\ Q_q \end{pmatrix} - \begin{pmatrix} iA_{-q}\hbar & 0 \end{pmatrix} \begin{pmatrix} \phi_q \\ Q_q \end{pmatrix} \right. \\ &\left. \left. - \begin{pmatrix} \phi_{-q} & Q_{-q} \end{pmatrix} \begin{pmatrix} -iA_q\hbar \\ 0 \end{pmatrix} - 2\lambda \sigma_z Q_q \right] \right\}, \end{aligned} \quad (5.24)$$

where A_q [see Eq. (3.83)] is the Fourier amplitude of the operator $[\phi_m(\tau) - \phi_m(0)]$, and the partition function becomes

$$\begin{aligned} Z &= \int D\phi_q(\tau) DQ_q(\tau) \exp \left\{ -\frac{1}{2} \frac{1}{\beta \mathcal{L} \hbar} \sum_q \left[\begin{pmatrix} \phi_{-q} & Q_{-q} \end{pmatrix} M^{-1} \begin{pmatrix} \phi_q \\ Q_q \end{pmatrix} \right. \right. \\ &\left. \left. - 2\lambda \sigma_z Q_q \right] \right\}. \end{aligned} \quad (5.25)$$

Computing the phase-phase correlator amounts to a phase shift ($\delta\phi_q$) and a charge shift (δQ_q), which can be absorbed by using the new variables: $\tilde{\phi}_q = \phi_q + \delta\phi_q$ and $\tilde{Q}_q = Q_q + \delta Q_q$. Using $\tilde{\phi}_q$ and \tilde{Q}_q , the integrand of Eq. (5.24) is rewritten in two parts: the first takes the same form as the partition function (5.25), and the second one is a constant that depends of $\delta\phi_q$ and δQ_q . More precisely, it reads

$$\begin{aligned} &\frac{1}{Z} \int D\tilde{\phi}_q(\tau) D\tilde{Q}_q(\tau) \exp \left\{ -\frac{1}{2} \frac{1}{\beta \mathcal{L} \hbar} \sum_q \left[\begin{pmatrix} \tilde{\phi}_{-q} & \tilde{Q}_{-q} \end{pmatrix} M^{-1} \begin{pmatrix} \tilde{\phi}_q \\ \tilde{Q}_q \end{pmatrix} \right. \right. \\ &\left. \left. - 2\lambda \sigma_z (-\omega_n) \tilde{Q}_q \right] \right\} \\ &\times \exp \left\{ \frac{1}{2} \frac{1}{\beta \mathcal{L} \hbar} \sum_q \left[\begin{pmatrix} \delta\phi_{-q} & \delta Q_{-q} \end{pmatrix} M^{-1} \begin{pmatrix} \delta\phi_q \\ \delta Q_q \end{pmatrix} - 2\lambda \sigma_z \delta Q_q \right] \right\} \end{aligned} \quad (5.26)$$

where the constants $\delta\phi_q$ and δQ_q are exactly cancel the second and third terms (in the parenthesis) of Eq. (5.24). Comparing Eqs. (5.24) and (5.26), we find:

$$\begin{pmatrix} \delta\phi_q \\ \delta Q_q \end{pmatrix} = M \begin{pmatrix} iA_q\hbar \\ 0 \end{pmatrix} = \frac{1}{\omega_n^2 + (k\omega_0)^2} \begin{pmatrix} i\frac{(2e)^2}{C_0} A_q \\ i2e\omega_n A_q \end{pmatrix}. \quad (5.27)$$

Substituting Eqs. (5.25) and (5.26) into Eq. (5.24), and using the Gaussian integral [see Eq. (3.75)], we obtain the needed correlator

$$\langle T_\tau e^{i\phi_m(\tau)} e^{-i\phi_m(0)} \rangle_{H_{sb}} = \exp[J_0(\tau)] \langle T_\tau \exp[J'(\tau)] \rangle_{H_{sb}} \quad (5.28)$$

with

$$J_0(\tau) = \frac{1}{2} \frac{1}{\beta \mathcal{L} \hbar} \sum_q \begin{pmatrix} \delta\phi_{-q} & \delta Q_{-q} \end{pmatrix} M^{-1} \begin{pmatrix} \delta\phi_q \\ \delta Q_q \end{pmatrix}, \quad (5.29)$$

$$J'(\tau) = -\frac{\lambda}{\beta \mathcal{L} \hbar} \sum_q \sigma_z \delta Q_q. \quad (5.30)$$

Using (5.27), the equations above can be rewritten as

$$J_0(\tau) = -\frac{(2e)^2}{\hbar C_0} \frac{1}{\beta \mathcal{L}} \sum_q \frac{1 - \cos \omega_n \tau}{\omega_n^2 + (k\omega_0)^2}, \quad (5.31)$$

$$J'(\tau) = -\lambda \frac{2e}{\hbar} \frac{1}{\beta \mathcal{L}} \sum_q \frac{i\omega_n}{\omega_n^2 + (k\omega_0)^2} e^{-ikm} (e^{i\omega_n \tau} - 1) \sigma_z. \quad (5.32)$$

In absence of side-coupling, namely $\lambda = 0$, $J'(\tau)$ equals zero. Therefore, Eq. (5.28) reduces to $\exp[J_0(\tau)]$. It corresponds to the case of a pure transmission line [see Eq. (3.88)]. We already evaluated $J_0(\tau)$ and found that it is a constant dependent the normalized impedance Z_0/R_Q of the transmission line. In contrast, $J'(\tau)$ contains the spin operator σ_z , which reflects the role of the side-coupled qubit.

Next, we need to compute $J'(\tau)$ and then further calculate $\langle T_\tau \exp[J'(\tau)] \rangle_{H_{sb}}$.

Considering the transmission line to be infinite, i.e., $\mathcal{L} \rightarrow \infty$, we rewrite Eq. (5.32) as

$$J'(\tau) = \frac{2\lambda e}{\hbar \omega_0^2} \frac{1}{\beta} \sum_{\omega_n} (e^{i\omega_n \tau} - 1) \sigma_z \int_{-\infty}^{\infty} \frac{dk}{2\pi i} \frac{e^{-ikm}}{k^2 + (\omega_n/\omega_0)^2}. \quad (5.33)$$

Using the residue theorem to evaluate the second integral, we obtain

$$J'(\tau) = -i \frac{\lambda e}{\hbar \omega_0} \frac{1}{\beta} \sum_{\omega_n} \frac{\omega_n}{|\omega_n|} (e^{i\omega_n \tau} - 1) \sigma_z e^{-\frac{|\omega_n|}{\omega_0} |m|}. \quad (5.34)$$

Note that $J'(\tau)$ can be written as $O(\tau) - O(0)$ with

$$O(\tau) = -i \frac{\lambda e}{\hbar \omega_0} \frac{1}{\beta} \sum_{\omega_n} \frac{\omega_n}{|\omega_n|} e^{i\omega_n \tau} \sigma_z e^{-\frac{|\omega_n|}{\omega_0} |m|}. \quad (5.35)$$

Thus, we have

$$\langle T_\tau \exp[J'(\tau)] \rangle_{H_{sb}} = \langle T_\tau \exp[O(\tau) - O(0)] \rangle_{H_{sb}}. \quad (5.36)$$

The equation above is evaluated using the same idea of computing the phase-phase correlator in nonlinear case [see Eq. (3.48)]. We expand it in powers of

$O(\tau)$ (in terms of the spin operator σ_z). As a result, Eq. (5.36) is expressed in terms of single-point, two-point, etc., spin correlators. They correspond to the first order correction, second order correction, etc., which reflect the effect of the side-coupled qubit. As we argued at the beginning of this section, at the charge degeneracy points the contributions of the odd order corrections equal zero, thus only the even order corrections contribute. Indeed, one can verify the second order correction corresponds to $J_1(t)$ we obtained before. The fourth order correction representing photon-photon interaction corresponds to $\delta J^{\text{int}}(t)$.

With the results above, we now write the phase-phase correlator needed to calculate the current-voltage characteristic in the following form:

$$\langle e^{i\phi_m(t)} e^{-i\phi_m(0)} \rangle_{H_{\text{sb}}} \simeq \exp \left[J^{(0)}(t) \right] \left[1 + J_1(t) + \delta J^{\text{int}}(t) \right]. \quad (5.37)$$

In term of Feynman diagrams, the corresponding time-ordered Green's function of the equation above is expressed in Fig. 5.9. In particular, $J^{(0)}(t)$ [see Eq. (3.92)] corresponds to the contribution of photons freely propagating down the transmission line. Then, $J_1(t)$ which is expressed in terms of the two-point spin-spin Green's function (corresponding to the first diagram of Fig. 5.9) was shown in Eq. (5.14). This contribution originates from the coupling between a single photon and the side-coupled qubit. Finally, $\delta J^{\text{int}}(t)$ which is expressed in terms of four-point spin-spin Green's functions (corresponding to the last three diagrams of Fig. 5.9) was shown in Eq. (5.22). It is the contribution of interactions between two photons. In the following calculations, we will use the contribution of $J^{(0)}(t)$ as a background, and then add the corrections from $J_1(t)$ and $\delta J^{\text{int}}(t)$.

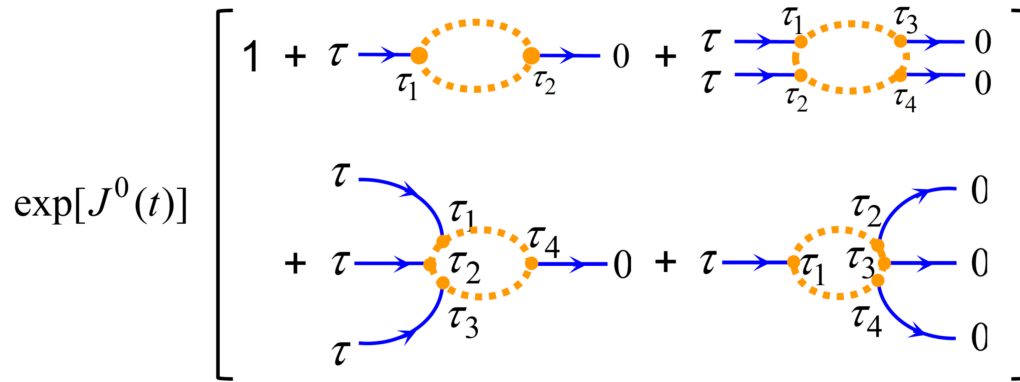


Figure 5.9: Feynman diagrams of the time-ordered Green function that corresponds to the phase-phase correlator $\langle e^{i\phi_m(t)} e^{-i\phi_m(0)} \rangle_{H_{\text{sb}}}$.

5.3 Spin-spin Green's function

In the last section, we obtained the result that the phase-phase correlators [e.g., $J_1(t)$ and $\delta J^{\text{int}}(t)$] are expressed in terms of the spin-spin Green's functions. In particular, the two-point as well as the four-point spin-spin Green's functions are needed. As we stated before spin-1/2 commutation relations are not fermionic nor bosonic, therefore we are not allowed to apply Wick's theorem and perturbation theory to do the calculations. To work around this difficulty, we use Bloch equations.

If we neglect the Kondo effect, then the Bloch approach [142] is appropriate to compute the spin-spin susceptibility χ_{zz} , and further obtain the two-point retarded Green's function $G_R(\sigma_z, \sigma_z; \omega)$.

In absence of the coupling, $\lambda = 0$, the system Hamiltonian which contains spin operators reduces to $-(E_J^s/2)\sigma_x$. The eigenstates are a superposition of the "spin-up" state $|0\rangle$ and "spin-down" state $|1\rangle$ [see Eq. (2.19)]. As a result, the evolution of $\langle\sigma_z(t)\rangle$ takes the form

$$\langle\sigma_z(t)\rangle = \cos(\omega_{\text{qb}} t), \quad (5.38)$$

i.e., the spin oscillates periodically between the eigenvalues ± 1 . Such an oscillation is a clear signature of quantum coherence.

However, when the coupling to the bath is involved, coherence effects will be destroyed. In particular, we consider the weak-coupling limit. In this way, the coupling (H_c) is sufficiently weak to treat it as a perturbation. Let us see in detail the consequences of doing so.

This problem is exactly analogous to that of the well-known nuclear magnetic resonance of a particle of spin-1/2 in a constant field E_J^s in the x direction, while the bosonic bath causes fluctuations of the field in the z direction. Considering the Born approximation (the total density matrix is decoupled into spin density matrix and bosonic density matrix, i.e., $\rho_{\text{tot}} = \rho_s(t) \otimes \rho_B$) and Markovian evolution (the evolution of the system at time t does not depend on previous times), we can then write down the Bloch equations of the system,

$$\frac{d}{dt}\langle\sigma_x(t)\rangle = -\frac{\langle\sigma_x(t)\rangle - \langle\sigma_x\rangle_{\text{equi}}}{\tau_1}, \quad (5.39)$$

$$\frac{d}{dt}\langle\sigma_y(t)\rangle = \omega_{\text{qb}}\langle\sigma_z(t)\rangle - \frac{\langle\sigma_y(t)\rangle}{\tau_2}, \quad (5.40)$$

$$\frac{d}{dt}\langle\sigma_z(t)\rangle = -\omega_{\text{qb}}\langle\sigma_y(t)\rangle. \quad (5.41)$$

Here τ_1 represents the spin relaxation time which tends to the thermal equilibrium value $\langle\sigma_x\rangle_{\text{equi}} = \tanh(\beta E_J^s/2)$; while τ_2 is the decoherence time. Note that

the decoherence time does not appear in the equation of σ_z , simply because the fluctuating environmental fields are exclusively along the z direction. If we consider the limiting cases that the time scales τ_1 and τ_2 go to infinity (meaning the bosonic bath is isolated from the system), the Bloch equations above reduces the result $d\langle\sigma_\alpha(t)\rangle/dt = i/\hbar[\sigma_\alpha(t), -E_j^s\sigma_z/2]$. This equation describes the Larmor precession of the nuclear magnetization in an external magnetic field.

When the influence of the bosonic bath is switched on, the relaxation time and the decoherence time take finite values. Perturbation theory to second order in the coupling term yields [140, 141]

$$\tau_1^{-1} = \tau_2^{-1} = (1/\hbar) \mathcal{J}(\omega_{\text{qb}}) \coth(\beta E_j^s/2), \quad (5.42)$$

where, $\mathcal{J}(\omega)$ is spectral density of the bath.

The spectral density can be obtained by computing the Fourier transform of the symmetrized correlation function of the bath operator $X = -\lambda Q_0$ coupled to σ_z :

$$\langle XX \rangle_\omega \equiv \frac{\lambda^2}{2} \langle \{Q_0(t)Q_0(0)\} \rangle_\omega = \hbar \mathcal{J}(\omega) \coth(\beta \hbar \omega/2). \quad (5.43)$$

Rewriting the charge operator in terms of creation and annihilate operators [see Eq. (2.47)], and using the diagonal form of H_T , we find

$$\langle XX \rangle_\omega = \frac{1}{\pi} \left(\frac{\lambda e}{\hbar \omega_0} \right)^2 \frac{R_Q}{Z_0} \omega \quad (5.44)$$

Collecting Eqs. (5.42), (5.43) and (5.44), the relaxation time is expressed as

$$\tau_2^{-1} = \frac{1}{\pi} \left(\frac{\lambda e}{\hbar \omega_0} \right)^2 \frac{R_Q}{Z_0} \omega_{\text{qb}}. \quad (5.45)$$

Using the definition of λ , it is expressed as

$$\tau_2^{-1} = \frac{1}{4} \frac{C_c^2}{C_0 C_\Sigma} \frac{\omega_p^2}{\omega_0}. \quad (5.46)$$

where ω_p is the plasma frequency⁸ of the Cooper pair box.

Then, taking time derivation upon equation (5.41), using equation (5.40), we derive the equation of motion of $\langle\sigma_z(t)\rangle$:

$$\frac{d\langle\sigma_z(t)\rangle}{dt^2} + \tau_2^{-1} \frac{d\langle\sigma_z(t)\rangle}{dt} + \omega_{\text{qb}}^2 = 0. \quad (5.47)$$

⁸It has the relation $\omega_p = \sqrt{8E_j^s E_{C_\Sigma}}/\hbar$, where $E_{C_\Sigma} = e^2/(2C_\Sigma)$ is the charging energy.

Using the linear response theory, and considering $\sigma_y, \sigma_z \ll \sigma_x$, we can obtain the spin-spin susceptibility χ_{zz} from Eq. (5.47). In frequency space, it takes the form

$$\chi_{zz} = -\frac{1}{\hbar} \frac{\omega_{qb}}{\omega^2 - \omega_{qb}^2 + i\frac{\omega}{\tau_2}}. \quad (5.48)$$

Actually, in the language of Green's functions, we have $G_R(\sigma_z, \sigma_z; \omega) = \chi_{zz}$, which can be verified using the linear response theory. Hence,

$$G_R(\sigma_z, \sigma_z; \omega) = -\frac{1}{\hbar} \frac{\omega_{qb}}{\omega^2 - \omega_{qb}^2 + i\frac{\omega}{\tau_2}}. \quad (5.49)$$

Using this result, we can evaluate the two-point phase-phase retarded Green's function [Eq. (5.12)] which is required for calculating the current-voltage characteristic of the probe junction. In particular, substituting Eq. (5.49) into Eq. (5.12), we obtain a similar form as in the case [shown in chapter 4] where a transmission line was coupled with a harmonic oscillator. It reads

$$G_R^{(0)}(\phi_m, \phi_m; \omega) = i\frac{\pi}{\hbar} \frac{Z_0}{\omega R_Q} \left[1 + \bar{r}(\omega) e^{2ik|m|} \right]. \quad (5.50)$$

where the reflection coefficient is given as

$$\bar{r}(\omega) = -\frac{1}{\pi} \bar{\lambda}^2 \frac{R_Q}{Z_0} \omega_{qb} \tau_2 \left[1 - i \frac{\omega^2 - \omega_{qb}^2}{\omega \tau_2^{-1}} \right]^{-1}. \quad (5.51)$$

Substituting τ_2 into the equation above, we find that the prefactor equals one. Hence, the expression reduces to

$$\bar{r}(\omega) = - \left[1 - i \frac{\omega^2 - \omega_{qb}^2}{\omega \tau_2^{-1}} \right]^{-1}. \quad (5.52)$$

Under the condition $C_c^2/(C_0 C_\Sigma) \ll 1$ and $\omega_{qb} \ll \omega_0$, the reflection coefficient has a narrow resonance at $\omega = \omega_{qb}$. The width is

$$\bar{\Gamma} = \tau_2^{-1} = \frac{1}{4} \frac{C_c^2}{C_0 C_\Sigma} \frac{\omega_p^2}{\omega_0}, \quad (5.53)$$

Comparing with the linear case [see Eq. (4.13)] in chapter 4, we find it has an exactly same width. Close to the resonance, we can approximate the reflection coefficient (5.52) by the simple form $\bar{r}(\omega) = - [1 - i(\omega - \omega_{qb})/\bar{\Gamma}]^{-1}$.

To summarize, the two-point spin-spin retarded Green's function was calculated using the Bloch equations in the weak coupling regime. Using this result, we computed the local phase-phase retarded Green's function which is needed to compute the current-voltage characteristic in the next section. At the single photon level, the resulting phase-phase retarded Green's function has a form that is very similar to the case of side-coupling a harmonic oscillator.

5.4 Current-voltage characteristic

Using the results obtained in previous sections, we now compute the current through the probe junction.

As did in chapter 4, we first use Eqs. (5.37), (5.14) and (5.49) to determine $P(E)$. At zero temperature, the current flowing through the probe junction reads:

$$I(V) \simeq e(E_J^p)^2 \left\{ \frac{1}{2} \int_{-\infty}^{\infty} dt \exp [i2eVt + J^{(0)}(t)] + \text{Im} \left[G_R(\sigma_z, \sigma_z; \omega) e^{2i\frac{\omega}{\omega_0} m} \right] \right\}. \quad (5.54)$$

Note that the first term describes the $I - V$ characteristic of the background, when the environment contains only the transmission line. This calculation can be done numerically using the integral equation [see Eq. (3.42)]. The second term describes the interaction effects between the single photon and the qubit. The resulting current-voltage characteristic is plotted in Fig. 5.10: the current of the background decreases with increasing voltage as expected; in addition, there is a clear resonance feature at $2eV = \hbar\omega_{qb}$. Here, we take the same characteristic current as in last chapter, namely, $I_0 = [\pi e(E_J^p)^2 / \hbar^2 \omega_s] (Z_0 / R_Q)$ [see Eq. (4.26)].

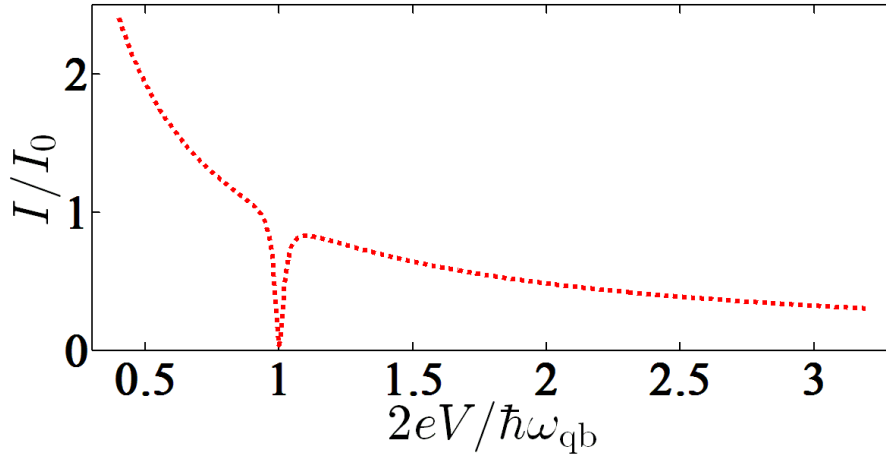


Figure 5.10: The strongly nonlinear regime: current-voltage characteristic of the probe Josephson junction when placed at $m = 0$. The parameters are $\bar{\Gamma} / \omega_{qb} = 0.02$, $E_{\text{cut-off}} / (\hbar\omega_{qb}) = 20$, and $Z_0 / R_Q = 0.01$. The side-coupled qubit causes a resonance at $2eV = \hbar\omega_{qb}$. The current vanishes at the resonance.

The resonance at $2eV = \hbar\omega_{qb}$ originates from the contribution of two-point spin-spin Green's function, i.e., $G_R(\sigma_z, \sigma_z; \omega)$. It describe a process in which a Cooper pair tunnels inelastically through the probe junction, simultaneously

emitting one photon to the environment. The photon travels along the transmission line. When the photons has a frequency close to the resonance frequency ω_{qb} , it is on resonance with the qubit. As a result, the photon is blocked completely. Thus, no current contributes in this process. From the plot, we can see clearly that the current indeed vanishes for weak impedance, e.g., $Z_0/R_Q = 0.01$. This is because multiple-photon processes are suppressed, and only single photon processes play a role.

More precisely, the current amplitude $\delta I(\delta V)$ (at single photon level) of this feature at voltages $V = \hbar\omega_{qb} + \delta V$ is formulated. It takes a similar form as Eq. (4.27). Namely

$$\frac{\delta I(\delta V)}{I_0} = \frac{-\bar{\Gamma}^2}{(2e\delta V)^2 + \bar{\Gamma}^2} \left(\cos \bar{\alpha} - \frac{2e\delta V}{\bar{\Gamma}} \sin \bar{\alpha} \right), \quad (5.55)$$

where $\bar{\alpha} = 2m\omega_{qb}/\omega_0$. By varying the placement (namely, m) of the probe junction, the shape of the resonance feature⁹ is different. Besides, from the equation above, it is clear that the width of the resonance is given by $\bar{\Gamma}/e$, where $\bar{\Gamma}$ was given in Eq. (5.53).

To summarize, the current-voltage characteristic was studied in the strongly nonlinear regime. we found that there is a resonance arising in the current-voltage characteristic at $2eV = \hbar\omega_{qb}$. This feature comes from the coupling between the single photon and the qubit. Using this result as a starting point, it will be interesting to see how the photon-photon interactions (corresponding to the four-point spin-spin Green's functions) will modify the resonance feature.

5.5 Summary

In this chapter, we studied the strongly nonlinear system which consists of a transmission line side-coupled to a charge qubit. As before, a probe junction attached to the line was used to detect the properties of the photons, which are created and engineered by the strongly nonlinear system. In particular, the environment seen by the probe junction can be described by a spin-boson model, which consists of a charge qubit (the spin) linearly coupled to the photons (the bosons) in the transmission line. Using Green's function theory and the path integral method, we calculated the environmental phase-phase correlators that are directly related to the current through the probe junction. Our results indicate that scattering of individual photons by the side-coupled qubit results in a resonance feature in the current-voltage characteristic of the probe junction at $2eV = \omega_{qb}$,

⁹It is shown in Fig. 4.5.

where ω_{qb} is the resonance frequency of the qubit. In addition, Kondo correlations actually cannot be ignored at low temperature and the charging degeneracy points of the qubit. For instance, one can check that the correction to the resonance frequency ω_{qb} due to the coupling with the environment has a logarithm divergence. Therefore, it would be interesting to see whether such Kondo correlations manifest in the multiple photon processes. To do so, one needs to compute the four-point spin-spin Green's function or even the exponential-spin correlator $\langle e^{i\sigma_z(t)} e^{-i\sigma_z(0)} \rangle$. In principle, Bloch equations could still be used.

Conclusion and perspectives

In this thesis, we mainly proposed a method to detect photon-photon interactions in a superconducting circuit. In particular, a local interaction between photons can be engineered by coupling a nonlinear system to a transmission line. The required transmission line can be conveniently formed from a chain of Josephson junctions. The nonlinearity is generated by side-coupling this chain to a Cooper pair box. We propose to probe the resulting photon-photon interactions via a voltage-biased Josephson junction (the probe junction) connected to the line. When a finite voltage V (smaller than the superconducting gap voltage) is applied, a Cooper pair tunnels inelastically through the probe junction, simultaneously releasing the energy $2eV$ (e is elementary charge) to the environment via emitting one or several photons. The emission depends on the properties of the environment. In our case, individual photons freely propagate along the transmission line and are scattered by the side-coupled Cooper pair box. When multiple photons are emitted, these photons may interact with each other. The elastic and inelastic scattering properties of photons will in turn influence the current through the probe junction. Therefore, the dc current-voltage characteristic of the Josephson junction provides a probe to study photon-photon interactions in a nonlinear environment.

We first considered a weakly nonlinear regime in chapter 4 where the side-coupled Cooper pair box was simplified as an weakly anharmonic oscillator with resonance frequency ω_s . We used Green's function perturbation theory to handle the single photon processes and two (and multiple) photons processes, respectively. For single photon processes, we found that the nonlinearity renormalizes the resonance frequency to ω'_s with a small shift. The current-voltage characteristic shows a resonant feature around $2eV = \omega'_s$. This is easily understood: when the photon took energy ω'_s , it was tuned to be on resonance with the side-coupled harmonic circuit, then the system would block the transmission of the photon due to destructive interference between the directly transmitted photon and the photon re-emitted by the side-coupling. As for two (and multiple) photon processes, in addition to freely propagating photons, photon-photon interactions play a role

as well. Our results show that the interactions due to the nonlinearity yield an additional resonance features at $2eV = 2\omega'_s$ (two photon processes). Finally, we also used the realistic parameters to estimate the amplitudes of the peaks, the current signal around $2eV = 2\omega'_s$ (reflecting the interaction between two photons) is expected to be on the order of pA, which is well within the reach of current measuring techniques.

The strongly nonlinear regime where the charging energy of the Cooper pair box dominates over the Josephson energy was studied in chapter 5. In this regime, the side-coupled Cooper pair box reduces effectively to a two-state qubit under certain conditions. The coupling between the transmission line and the qubit was described by a spin-boson Hamiltonian. It consists of a charge qubit (the spin) linearly coupled to the photons (the bosons) in the transmission line. We applied both perturbation theory and path integral method to compute the phase-phase correlator. We found that they are related exactly to $2n$ (n integer)-point spin-spin Green's functions. Furthermore, we used Bloch equations to calculate the spin-spin susceptibility in weak coupling regime, and obtained the corresponding two-point spin-spin Green's function. Our result showed that the current flowing through the probe junction yields a feature around $2eV = \hbar\omega_{qb}$, where ω_{qb} is the resonance frequency of the qubit. Such a feature appears due to the coupling between the single-photon and the qubit.

Regarding future studies, we first want to evaluate the four-point spin-spin Green's functions or even the entire exponential-spin correlator in the strongly nonlinear regime. With the results, the current-voltage characteristic of the probe at two photons level (even multiple level) can be obtained. Furthermore, the features due to the photon-photon interactions can be predicted. Moreover, Kondo correlations may play a role. It will be interesting to study how the Kondo correlations manifest in multiple-photon processes. In our project, we mainly focus on studying how the current-voltage characteristic of the probe junctions is affected by a nonlinear environment. As we argued, the probe junction emit simultaneously single or multiple photons to the environment. Very recently, the photonic side was also explored [88, 143]. Therefore, it will be interesting to study the properties of the radiation emitted by a Josephson junction into the nonlinear environment. However, the calculation is very involved as it would going beyond the first order in the Josephson energy of the probe junction. In addition, the work of chapter 5 is a good starting point for exploring the entanglement of several qubits, which is quite interesting from the viewpoint of potential application in quantum information processing.

For the experimental realizations, we expect that our predictions concerning the resonance features in the current-voltage characteristic of the probe junction can be observed. It will be interesting since it provides a sensitive probe to explore photon-photon interaction in circuit QED.

The Hamiltonian of the studied circuit

In this appendix, we show in details the derivation of the Hamiltonian used in chapter 4 and chapter 5.

As shown in Fig. A.1, the circuit consists of a transmission line¹ capacitively side-coupled to a Cooper pair box. Comparing with the circuit shown in Fig. 4.1, we now technically replaced the gate voltage V_g of the cooper pair box by a capacitor C_Ψ ².

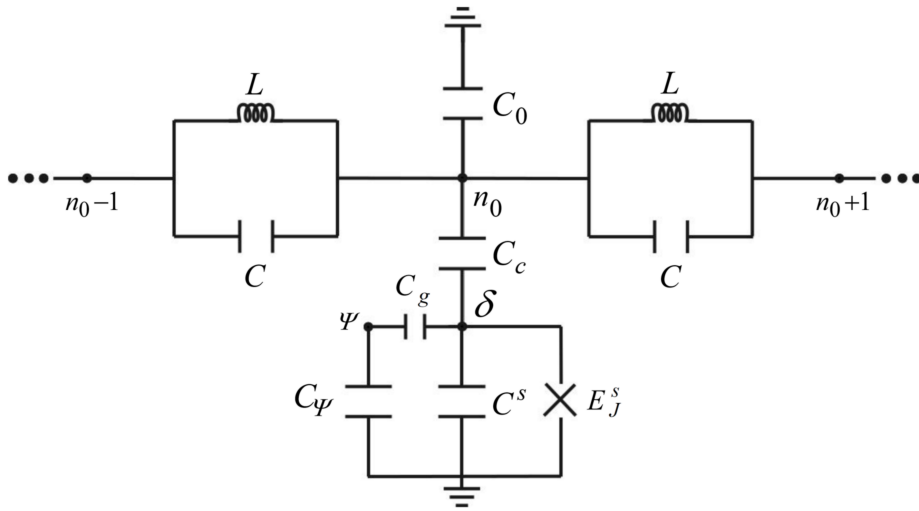


Figure A.1: Three nodes $n_0 - 1$, n_0 and $n_0 + 1$ of the studied circuit. It consists of a transmission line capacitively (capacitance C_c) coupled to a Cooper pair box at node n_0 . The transmission line is realized by a set of identical LCC_0 oscillators. The gate voltage of the Cooper pair box is replaced by a capacitor C_Ψ .

¹It is formed by a set of LCC_0 harmonic oscillators. In chapter 4 and chapter 5, we took $C \ll C_0$.

²It has the relation $C_\Psi = Q_\Psi/V_g$, where Q_Ψ is the charge on node Ψ .

To derive the system Hamiltonian, we use the standard way: the method allows us to write down the Hamiltonian of any quantum circuits consisting of capacitors, inductors and Josephson junctions, which was first proposed by Yurke and Denker [102], and then analysed in detail by Devoret [103]. The procedure is as follows: present the equations of motion of the phase, write down the Lagrangian of the circuit, check the Lagrangian is fine, and finally obtain the Hamiltonian.

First of all, we apply Kirchoff's current conversion laws to an arbitrary node n ($n \neq n_0$) along the line (see Fig. A.1): the currents flowing into the node should equal the currents flowing out of the node. Thus,

$$\frac{\phi_{n-1} - \phi_n}{L} + C(\ddot{\phi}_{n-1} - \ddot{\phi}_n) = \frac{\phi_n - \phi_{n+1}}{L} + C(\ddot{\phi}_n - \ddot{\phi}_{n+1}) + C_0 \ddot{\phi}_n. \quad (\text{A.1})$$

Similarly, for nodes n_0 , δ , and Ψ (see Fig. A.1), the additional equations are

$$\begin{aligned} \frac{\phi_{n_0-1} - \phi_{n_0}}{L} + C(\ddot{\phi}_{n_0-1} - \ddot{\phi}_{n_0}) &= \frac{\phi_{n_0} - \phi_{n_0+1}}{L} + C(\ddot{\phi}_{n_0} - \ddot{\phi}_{n_0+1}) \\ &\quad + C_0 \ddot{\phi}_{n_0} + C_c(\ddot{\phi}_{n_0} - \ddot{\phi}_\delta), \\ C_c(\ddot{\phi}_{n_0} - \ddot{\phi}_\delta) + C_g(\ddot{\phi}_\Psi - \ddot{\phi}_\delta) &= C^s \ddot{\phi}_\delta + 2eI_c^s \sin \phi_\delta, \\ C_g(\ddot{\phi}_\Psi - \ddot{\phi}_\delta) + C_\Psi \ddot{\phi}_\Psi &= 0, \end{aligned} \quad (\text{A.2})$$

where I_c^s is the critical current of the side-coupled Josephson junction with Josephson energy E_J^s . The relation between them is $E_J^s = I_c^s/2e$.

Then, the system Lagrangian can be constructed as

$$\begin{aligned} L(\dot{\phi}_n, \phi_n, \dot{\phi}_\delta, \phi_\delta, \dot{\Psi}, t) &= \left(\frac{\hbar}{2e}\right)^2 \sum_n \left[\frac{C(\dot{\phi}_{n-1} - \dot{\phi}_n)^2}{2} + \frac{C_0 \dot{\phi}_n^2}{2} + \frac{C_c(\dot{\phi}_{n_0} - \dot{\phi}_\delta)^2}{2} \right. \\ &\quad \left. + \frac{C_g(\dot{\phi}_\Psi - \dot{\phi}_\delta)^2}{2} + \frac{C^s \dot{\phi}_\delta^2}{2} + \frac{C_\Psi \dot{\phi}_\Psi^2}{2} - \frac{(\phi_{n-1} - \phi_n)^2}{2L} \right] + E_J^s \cos \phi_\delta \end{aligned} \quad (\text{A.3})$$

The charge operators (Q_n , Q_δ and Q_Ψ) conjugate to the corresponding phase operators (ϕ_n , ϕ_δ and ϕ_Ψ), i.e., $Q = (2e/\hbar)(\partial L/\partial \dot{\phi})$, are given as

$$Q_n = \frac{\hbar}{2e} [(C_0 + 2C + \delta_{n,n_0} C_c) \dot{\phi}_n - C \dot{\phi}_{n-1} - C \dot{\phi}_{n+1} - \delta_{n,n_0} C_c \dot{\phi}_\delta], \quad (\text{A.4})$$

$$Q_\delta = \frac{\hbar}{2e} [(C_c + C_g + C^s) \dot{\phi}_\delta - C_c \dot{\phi}_{n_0} - C_g \dot{\phi}_\Psi], \quad (\text{A.5})$$

$$Q_\Psi = \frac{\hbar}{2e} [(C_g + C_\Psi) \dot{\phi}_\Psi - C_g \dot{\phi}_\delta]. \quad (\text{A.6})$$

In matrix notation, Eq. (A.4) is rewritten as,

$$Q_n = \frac{\hbar}{2e} \sum_m (C_{n,m} \dot{\phi}_m - \delta_{n,n_0} C_c \dot{\phi}_\delta), \quad (\text{A.7})$$

where we define the capacitance matrix $C_{n,m}$ with elements

$$C_{n,m} = (C_0 + 2C + \delta_{n,n_0}C_c)\delta_{n,m} - C\delta_{n-1,m} - C\delta_{n+1,m}. \quad (\text{A.8})$$

Using the matrices $C_{n,m}$ and $L_{n,m}^{-1}$ (see Eq. (2.45)), the Lagrangian (A.3) is rewritten as

$$\begin{aligned} L(\dot{\phi}_n, \phi_n, \dot{\phi}_\delta, \phi_\delta, \dot{\Psi}) = & \left(\frac{\hbar}{2e}\right)^2 \left[\frac{1}{2} \sum_{n,m} (\dot{\phi}_n C_{n,m} \dot{\phi}_m - \phi_n L_{n,m}^{-1} \phi_m) + \frac{1}{2} (C_c + C_g \right. \\ & \left. + C^s) \dot{\phi}_\delta^2 + \frac{1}{2} (C_g + C_\Psi) \dot{\phi}_\Psi^2 - C_c \dot{\phi}_\delta \dot{\phi}_{n_0} - C_g \dot{\phi}_\Psi \dot{\phi}_\delta \right] + E_J^s \cos \phi_\delta. \end{aligned} \quad (\text{A.9})$$

To check whether the Lagrangian is correct, we derive the equations of motion that yielded by the Lagrangian (A.9):

$$\begin{aligned} \frac{\partial}{\partial t} \frac{\partial L}{\partial \dot{\phi}_n} - \frac{\partial L}{\partial \phi_n} &= \sum_m [C_{n,m} \ddot{\phi}_m - \delta_{n,n_0} C_c \ddot{\phi}_\delta + L_{n,m}^{-1} \phi_m] = 0, \\ \frac{\partial}{\partial t} \frac{\partial L}{\partial \dot{\phi}_\delta} - \frac{\partial L}{\partial \phi_\delta} &= \left(\frac{\hbar}{2e}\right)^2 [(C_c + C_g + C_J) \ddot{\phi}_\delta - (C_c \ddot{\phi}_{n_0} + C_g \ddot{\Psi})] + E_J \sin \phi_\delta = 0, \\ \frac{\partial}{\partial t} \frac{\partial L}{\partial \dot{\phi}_\Psi} - \frac{\partial L}{\partial \phi_\Psi} &= (C_g + C_\Psi) \ddot{\phi}_\Psi - C_g \ddot{\phi}_\delta = 0. \end{aligned} \quad (\text{A.10})$$

Comparing Eq. (A.10) with Eqs. (A.1) and (A.2), we find that they are consistent. This means the Lagrangian (A.9) well describes the studied circuit.

Next, the system Hamiltonian is obtained as

$$H = \frac{\hbar}{2e} \left[\sum_n Q_n \dot{\phi}_n + Q_\delta \dot{\phi}_\delta + Q_\Psi \dot{\Psi} \right] - L. \quad (\text{A.11})$$

Since the Hamiltonian is expressed in terms of phases ϕ (ϕ_n, ϕ_δ) and charges Q (Q_n, Q_δ), we have to replace $\dot{\phi}$ of Eq. (A.11) by Q . To do so, we first solve $\dot{\phi}_\Psi$ from Eq. (A.6)

$$\dot{\phi}_\Psi = 2eV_g. \quad (\text{A.12})$$

Then we substitute Eq. (A.12) into Eq. (A.5) to obtain

$$\frac{2e}{\hbar} (Q_\delta + C_g V_g) = (C_c + C_g + C^s) \dot{\phi}_\delta - C_c \dot{\phi}_{n_0}. \quad (\text{A.13})$$

Using Eq. (A.7), we get

$$\dot{\phi}_n = \frac{2e}{\hbar} \sum_m C_{n,m}^{-1} Q_m + C_c C_{n,n_0}^{-1} \dot{\phi}_\delta. \quad (\text{A.14})$$

Thus, for the node n_0 , the equation above reads naturally,

$$\dot{\phi}_{n_0} = \frac{2e}{\hbar} \sum_m C_{n_0,m}^{-1} Q_m + C_c C_{n_0,n_0}^{-1} \dot{\phi}_\delta. \quad (\text{A.15})$$

Combining Eqs. (A.13) and (A.15), we obtain,

$$\dot{\phi}_\delta = \frac{2e}{\hbar} \frac{Q_\delta + C_g V_g + C_c \sum_m C_{n_0,m}^{-1} Q_m}{C_c + C_g + C^s - C_c^2 C_{n_0,n_0}^{-1}}. \quad (\text{A.16})$$

Substituting Eqs. (A.9), (A.12), and (A.14) into Eq. (A.11), we get

$$\begin{aligned} H &= \sum_n Q_n \left(\sum_m C_{n,m}^{-1} Q_m + C_c C_{n,n_0}^{-1} \dot{\phi}_\delta \right) + \frac{\hbar}{2e} Q_\delta \dot{\phi}_\delta + Q_\Psi V_g \\ &\quad - \left(\frac{\hbar}{2e} \right)^2 \left[\frac{1}{2} \sum_{n,m} (\dot{\phi}_n C_{n,m} \dot{\phi}_m - \phi_n L_{n,m}^{-1} \phi_m) - \frac{C_c + C_g + C^s}{2} \dot{\phi}_\delta^2 \right. \\ &\quad \left. + C_c \delta_{n,n_0} \dot{\phi}_n \dot{\phi}_\delta \right] + \frac{\hbar}{2e} C_g V_g \dot{\phi}_\delta - \frac{C_g + C_\Psi}{2} V_g^2 - E_J^s \cos \phi_\delta. \end{aligned} \quad (\text{A.17})$$

Using the following three relations,

$$\begin{aligned} Q_\delta \dot{\phi}_\delta &= \frac{\hbar}{2e} [(C_c + C_g + C^s) \dot{\phi}_\delta^2 - C_c \delta_{n,n_0} \dot{\phi}_n \dot{\phi}_\delta] - C_g V_g \dot{\phi}_\delta, \quad (\text{A.18}) \\ Q_\Psi V_g &= (C_g + C_\Psi) V_g^2 - \frac{\hbar}{2e} C_g V_g \dot{\phi}_\delta, \\ \left(\frac{\hbar}{2e} \right)^2 \sum_{n,m} \dot{\phi}_n C_{n,m} \dot{\phi}_m &= \sum_{n,m} Q_n C_{n,m}^{-1} Q_m + 2C_c \sum_n Q_n C_{n,n_0}^{-1} \dot{\phi}_\delta + C_c^2 C_{n_0,n_0}^{-1} \dot{\phi}_\delta^2. \end{aligned}$$

one can simplify Eq. (A.17) as

$$\begin{aligned} H &= \frac{1}{2} \sum_{n,m} \left[Q_n C_{n,m}^{-1} Q_m + \left(\frac{\hbar}{2e} \right)^2 \phi_n L_{n,m}^{-1} \phi_m \right] \\ &\quad + \left(\frac{\hbar}{2e} \right)^2 \frac{C_c + C_g + C_J - C_c^2 C_{n_0,n_0}^{-1}}{2} \dot{\phi}_\delta^2 - E_J^s \cos \phi_\delta. \end{aligned} \quad (\text{A.19})$$

Finally, plugging Eq. (A.16) into Eq. (A.19), we obtain the Hamiltonian:

$$\begin{aligned} H &= \frac{1}{2} \sum_{n,m} \left[Q_n C_{n,m}^{-1} Q_m + \left(\frac{\hbar}{2e} \right)^2 \phi_n L_{n,m}^{-1} \phi_m \right] \\ &\quad + \frac{(Q_\delta + C_g V_g + C_c \sum_m C_{n_0,m}^{-1} Q_m)^2}{2(C_c + C_g + C^s - C_c^2 C_{n_0,n_0}^{-1})} - E_J^s \cos \phi_\delta. \end{aligned} \quad (\text{A.20})$$

With the conditions specified in chapter 4, i.e., $C_c \ll C_0$, $C_g + C^s$ and $C \ll C_0$, the Hamiltonian (A.20) reduces to Eq. (4.1).

Quantum theory of the transmission line

In this appendix, we present the quantum theory of the transmission line.

The transmission line described by the Hamiltonian H_T is given by Eq. (2.44). Inspired by the method used in the case of the harmonic crystal in solid state physics, one can obtain the standard diagonal form,

$$H_T^{\text{diag}} = \sum_k \hbar \omega_k \left(a_k^\dagger a_k + \frac{1}{2} \right), \quad (\text{B.1})$$

by expressing the phase and charge operators in terms of the photon creating operator a_k and photon annihilation operator a_{-k}^\dagger :

$$\phi_n = \frac{1}{\sqrt{N}} \sum_k \alpha_k e^{ikn} (a_k + a_{-k}^\dagger), \quad Q_n = \frac{e}{\sqrt{N}} \sum_k \frac{1}{i\alpha_k} e^{ikn} (a_k - a_{-k}^\dagger), \quad (\text{B.2})$$

where α_k is a coefficient that needs to be determined. The canonical commutation relation $[\phi_n, Q_m] = 2ie\delta_{n,m}$ and the identify $\sum_n e^{i(k_1-k_2)n} = N\delta_{k_1,k_2}$ implies that $[a_{k_1}, a_{k_2}^\dagger] = \delta_{k_1,k_2}$.

To find α_k and ω_k , we substitute Eq. (B.2) and the Fourier form of matrices L and C ,

$$L_{n,m}^{-1} = \frac{1}{N} \sum_k e^{ik(n-m)} \frac{2}{L} (1 - \cos k), \quad C_{n,m}^{-1} = \frac{1}{N} \sum_k e^{-ik(n-m)} \frac{1}{C_0 + 2C(1 - \cos k)}, \quad (\text{B.3})$$

into Eq. (2.44), to obtain

$$\begin{aligned} H_T = & \frac{1}{2} \frac{1}{N^2} \sum_{k_1, k_2, k_3} \sum_{n, m} \left[\frac{e^2}{i\alpha_{k_1}} e^{ik_1 n} (a_{k_1} - a_{-k_1}^\dagger) e^{-ik_2(n-m)} \frac{1}{C_0 + 2C(1 - \cos k_2)} \right. \\ & \times \frac{1}{i\alpha_{k_3}} e^{ik_3 m} (a_{k_3} - a_{-k_3}^\dagger) + \left(\frac{\hbar}{2e} \right)^2 \alpha_{k_1} e^{ik_1 n} (a_{k_1} + a_{-k_1}^\dagger) \\ & \left. \times e^{ik_2(n-m)} \frac{2}{L} (1 - \cos k_2) \alpha_{k_3} e^{ik_3 m} (a_{k_3} + a_{-k_3}^\dagger) \right]. \quad (\text{B.4}) \end{aligned}$$

To simplify the Hamiltonian (B.4), we first sum over n, m . It reduces to delta functions, i.e., $(1/N) \sum_n \exp[i(k_1 - k_2)n] = \delta_{k_1, k_2}$ and $(1/N) \sum_m \exp[i(k_2 + k_3)m] = \delta_{k_2, -k_3}$. Then Eq. (B.4) becomes

$$H_T = \frac{1}{2} \sum_k \left[\frac{e^2}{i\alpha_k i\alpha_{-k}} \frac{1}{C_0 + 2C(1 - \cos k)} (a_k - a_{-k}^\dagger)(a_{-k} - a_k^\dagger) + \left(\frac{\hbar}{2e}\right)^2 \alpha_{-k} \alpha_k \frac{2}{L} (1 - \cos k)(a_{-k} + a_k^\dagger)(a_k + a_{-k}^\dagger) \right]. \quad (\text{B.5})$$

Using the identity $\phi_n = \phi_n^\dagger$, one can certify that α_{-k} equals α_k^* . As a result, the terms in the square brackets are an even function of k , which means we can change k by $-k$ if necessary. Moreover, we also apply the commutation relation $[a_k, a_k^\dagger] = 1$. Using these relations, the Hamiltonian above is rewritten as

$$H_T = \frac{1}{2} \sum_k \left[-\frac{e^2}{|\alpha_k|^2} \frac{1}{C_0 + 2C(1 - \cos k)} + \left(\frac{\hbar}{2e}\right)^2 |\alpha_k|^2 \frac{2}{L} (1 - \cos k) \right] \times (a_k a_{-k} + a_{-k}^\dagger a_k^\dagger) + \sum_k \left[\frac{e^2}{|\alpha_k|^2} \frac{1}{C_0 + 2C(1 - \cos k)} + \left(\frac{\hbar}{2e}\right)^2 |\alpha_k|^2 \frac{2}{L} (1 - \cos k) \right] \times \left(a_k^\dagger a_k + \frac{1}{2} \right). \quad (\text{B.6})$$

Comparing with Eq. (B.6) with (2.46), we get the following two relations:

$$-\frac{e^2}{|\alpha_k|^2} \frac{1}{C_0 + 2C(1 - \cos k)} + \left(\frac{\hbar}{2e}\right)^2 |\alpha_k|^2 \frac{2}{L} (1 - \cos k) = 0, \quad (\text{B.7})$$

$$\frac{e^2}{|\alpha_k|^2} \frac{1}{C_0 + 2C(1 - \cos k)} + \left(\frac{\hbar}{2e}\right)^2 |\alpha_k|^2 \frac{2}{L} (1 - \cos k) = \hbar \omega_k. \quad (\text{B.8})$$

From these two equations, we find

$$\alpha_k^2 = \frac{e^2}{\hbar} \sqrt{\frac{L}{C}} \sqrt{\frac{1}{1 - \cos k + C_0/2C} \frac{1}{1 - \cos k}}, \quad (\text{B.9})$$

$$\omega_k = \sqrt{\frac{1}{LC}} \sqrt{\frac{1 - \cos k}{1 - \cos k + C_0/2C}}. \quad (\text{B.10})$$

Eq. (B.10) is exactly the dispersion relation (2.33) which was obtained using the classical approach.

Photon-photon interactions: weakly nonlinear regime

This appendix aims to calculate the current correction at $2eV = \hbar\omega'_s$ studied in chapter 4. In particular, this resonance feature comes from the contribution of the four-point retarded Green's function $\sim \delta G_R^{\text{int}}(\phi_m^2, \phi_m^2; \omega)$. Here, we calculate this Green's function in the vicinity of $2eV = \hbar\omega'_s$.

First of all, the four-point retarded Green's function $\delta G_R^{\text{int}}(\phi_m^2, \phi_m^2; \omega)$ takes the form $(E_j^s/\pi^2)f^2(\omega)$, where $f(\omega)$ takes the form [see Eq. (4.38)]:

$$\sum_{\pm} \int_0^{\infty} d\omega_1 \Im [G_R(\phi_m, \phi_\delta; \omega_1)] G_R(\phi_m, \phi_\delta; \omega \pm \omega_1). \quad (\text{C.1})$$

The integral is dominated by frequencies where both Green's functions are close to resonance, $\omega_1 \approx \omega \pm \omega_1 \approx \omega'_s$. This requires $\omega \approx 2\omega'_s$. We, thus, approximate $\omega = 2\omega'_s + \delta\omega$ and $\omega_1 = \omega'_s + \delta\omega_1$. The Green's functions (4.18) close to resonance take the form

$$G_R(\phi_\delta, \phi_m; \omega'_s + \delta\omega) \simeq 2 \frac{\pi}{\omega'_s} \frac{1}{R_Q C_c \omega'_s} \frac{1}{1 - i \frac{\delta\omega}{\Gamma}} e^{i \frac{\omega'_s}{\omega_0} |m|}. \quad (\text{C.2})$$

We then rewrite

$$f(\omega) \simeq \left(\frac{2\pi}{R_Q C_c (\omega'_s)^2} \right)^2 e^{i \frac{\omega'_s}{\omega_0} |m|} \int_{-\infty}^{\infty} d\delta\omega_1 \frac{\sin \frac{\omega'_s |m|}{\omega_0} + \frac{\delta\omega_1}{\Gamma} \cos \frac{\omega'_s |m|}{\omega_0}}{1 + \left(\frac{\delta\omega_1}{\Gamma} \right)^2} \frac{1}{1 - i \frac{\delta\omega - \delta\omega_1}{\Gamma}}. \quad (\text{C.3})$$

It is straightforward to evaluate the convolution integrals to obtain

$$\text{Re}[f(\omega)] \simeq \pi \left(\frac{\pi C_c}{2R_Q C_0 C_\Sigma} \right)^2 \frac{\delta\omega \cos \alpha' + 2\Gamma \sin \alpha'}{(\delta\omega)^2 + 4\Gamma^2}, \quad (\text{C.4})$$

$$\text{Im}[f(\omega)] \simeq -\pi \left(\frac{\pi C_c}{2R_Q C_0 C_\Sigma} \right)^2 \frac{2\Gamma \cos \alpha' - \delta\omega \sin \alpha'}{(\delta\omega)^2 + 4\Gamma^2}. \quad (\text{C.5})$$

Finally, to compute the current-voltage characteristic, we need

$$\begin{aligned} \text{Im} \left[\delta G_R^{\text{int}}(\phi_m^2, \phi_m^2; 2\omega'_s + \delta\omega) \right] &\simeq \frac{2E_J^s}{\pi^2} \text{Re} [f(2\omega'_s + \delta\omega)] \Im [f(2\omega'_s + \delta\omega)] \\ &\simeq -\frac{\pi^2}{8E_J^s} \left(\frac{Z_0}{R_Q} \right)^2 \frac{4\Gamma^2}{[(\delta\omega)^2 + 4\Gamma^2]^2} \left\{ 2\delta\omega\Gamma \cos(2\alpha') - \frac{(\delta\omega^2 - 4\Gamma^2)}{2} \sin(2\alpha') \right\}. \end{aligned} \quad (\text{C.6})$$

This is the result used to compute the current correction δI_2 [see Eq. (4.44)] due to photon-photon interactions (two photons processes).

Time-ordered Green's function: strongly nonlinear regime

In this appendix, we present the derivation of the two-point time-ordered Green's functions $\mathcal{G}[\phi_n(\tau)\phi_m(0)]$ in strongly nonlinear regime.

This Green's function is defined as

$$\langle T_\tau \phi_n(\tau)\phi_m(0) \rangle_{H_{\text{sb}}} = \frac{\langle T_\tau \phi_n(\tau)\phi_m(0)S(\beta) \rangle_{H^{(0)}}}{\langle S(\beta) \rangle_{H^{(0)}}}, \quad (\text{D.1})$$

where we used the perturbation theory addressed in chapter 3. The S matrix $S(\beta) = T_\tau \exp\left[-\int_0^\beta d\tau V(\tau)\right]$. Inserting the interaction term, i.e., Eq. (5.3), we get

$$S(\beta) = 1 + \sum_{n=1}^{\infty} \frac{(-1)^n \lambda^n}{n!} \int_0^\beta d\tau_1 \int_0^\beta d\tau_2 \dots \int_0^\beta d\tau_n T_\tau \sigma_z(\tau_1)\sigma_z(\tau_2)\dots\sigma_z(\tau_n) \\ \times Q_0(\tau_1)Q_0(\tau_2)\dots\cdots Q_0(\tau_n). \quad (\text{D.2})$$

Substituting Eq. (D.2) into Eq. (D.1), we find only the even orders of the perturbation series contribute. This is because each phase/charge operator is expressed in terms of a combination of creation and annihilation operators, which must appear in pairs in the bracket. As a result, the numerator of Eq. (D.1) is expressed as

$$\langle T_\tau \phi_n(\tau)\phi_m(0) \rangle_{H^{(0)}} + \sum_{n=1}^{\infty} \frac{\lambda^{2n}}{(2n)!} \int_0^\beta d\tau_1 \int_0^\beta d\tau_2 \dots \int_0^\beta d\tau_{2n} \langle T_\tau \phi_n(\tau)\phi_m(0) \\ \times \sigma_z(\tau_1)\sigma_z(\tau_2)\dots\sigma_z(\tau_{2n})Q_0(\tau_1)Q_0(\tau_2)\dots\cdots Q_0(\tau_{2n}) \rangle_{H^{(0)}}. \quad (\text{D.3})$$

As we argued in chapter 3, using representation of Feynman diagrams, the vacuum polarization diagrams, i.e., the denominator of Eq. (D.1), exactly cancel the disconnected diagrams in the expansion of Eq. (D.3). Hence we only consider the connected diagrams.

As the phase/charge operator commute with the spin operator, the bracket in Eq. (D.3) is immediately factored into two separate parts

$$\langle T_\tau \phi_n(\tau) \phi_m(0) Q_0(\tau_1) Q_0(\tau_2) \cdots Q_0(\tau_{2n}) \rangle_{H(0)} \cdot \langle T_\tau \sigma_z(\tau_1) \sigma_z(\tau_2) \cdots \sigma_z(\tau_{2n}) \rangle_{H(0)}. \quad (\text{D.4})$$

Using Wick's theorem for the first part of Eq. (D.4), we consider all the possible pairings, where each pairing has to be time-ordered. It is easy to see that all the times τ_i ($i = 1, 2, \dots, 2n$) are symmetric, so a convenient way is writing down one of the possible pairing, and then counting the number of all possible pairings. Except the operators $\phi_n(\tau)$ and $\phi_m(0)$, there are $2n$ charge operators. We choose randomly two of them, $Q_0(\tau_i)$ and $Q_0(\tau_j)$, to pair with $\phi_n(\tau)$ and $\phi_m(0)$, which yields $2n \cdot (2n - 1)$ possibilities. Here, we write down one of them,

$$\langle T_\tau \phi_n(\tau) Q_0(\tau_1) \rangle_{H(0)} \langle T_\tau Q_0(\tau_2) \phi_m(0) \rangle_{H(0)}. \quad (\text{D.5})$$

Then the remaining $(2n - 2)$ charge operators Q_0 (for $n \geq 2$) pair with each other, consisting $n - 1$ charge-charge correlator. To do so, we first choose randomly two of them (i.e., the first charge-charge correlator), it counts C_{2n-2}^2 ¹ possibilities, then the second one counts C_{2n-4}^2 times, and so on till C_2^2 . Such operation indeed lead the final possibilities expanding $(n - 1)!$ times². Now we count all the possible pairings³

$$\frac{2n \cdot (2n - 1) \cdot C_{2n-2}^2 \cdot C_{2n-4}^2 \cdots C_2^2}{(n - 1)!} = \frac{2n!}{(2^{n-1})(n - 1)!}. \quad (\text{D.6})$$

One of the pairing result is expressed as

$$\langle T_\tau Q_0(\tau_3) Q_0(\tau_4) \rangle_{H(0)} \langle T_\tau Q_0(\tau_5) Q_0(\tau_6) \rangle_{H(0)} \cdots \langle T_\tau Q_0(\tau_{2n-1}) Q_0(\tau_{2n}) \rangle_{H(0)}. \quad (\text{D.7})$$

In contrast with the charge operators, spin operators in the second part of Eq. (D.4) can not be decoupled into two-point correlator. Instead, we keep them in a bracket.

Combining Eqs. (D.3) - (D.6), and rewriting the correlation functions by

¹Here, $C_n^m = n!/[m!(n - m)!]$ is a combinatorial number in algebra.

²This is due to the pairing rule: the time ordering of each pair gives the proper time ordering to the entire result.

³Indeed, it is the prefactor of the resulting pairing.

time-ordered Green's functions, we obtain

$$\begin{aligned}
 \mathcal{G}[\phi_n(\tau)\phi_m(0)] &= \mathcal{G}^{(0)}[\phi_n(\tau)\phi_m(0)] + \lambda^2 \int_0^\beta d\tau_1 \int_0^\beta d\tau_2 \mathcal{G}^{(0)}[\phi_n(\tau)Q_0(\tau_1)] \\
 &\times \mathcal{G}^{(0)}[\sigma_z(\tau_1)\sigma_z(\tau_2)] \cdot \mathcal{G}^{(0)}[Q_0(\tau_2)\phi_m(0)] + \sum_{n=2}^{\infty} \frac{2(\lambda^{2n})}{2^n(n-1)!} \int_0^\beta d\tau_1 \int_0^\beta d\tau_2 \dots \\
 &\int_0^\beta d\tau_{2n} \mathcal{G}^{(0)}[\phi_n(\tau)Q_0(\tau_1)] \mathcal{G}^{(0)}[Q_0(\tau_2)\phi_m(0)] \mathcal{G}^{(0)}[\sigma_z(\tau_1)\sigma_z(\tau_2)\dots\sigma_z(\tau_{2n})] \\
 &\times \mathcal{G}^{(0)}[Q_0(\tau_3)Q_0(\tau_4)] \mathcal{G}^{(0)}[Q_0(\tau_5)Q_0(\tau_6)] \dots \mathcal{G}^{(0)}[Q_0(\tau_{2n-1})Q_0(\tau_{2n})] \quad (\text{D.8})
 \end{aligned}$$

Next, we calculate the two-point spin-spin time-ordered Green's function $\mathcal{G}[\sigma_z(\tau_1)\sigma_z(\tau_2)]$. We define it as

$$\langle T_\tau \sigma_z(\tau_1)\sigma_z(\tau_2) \rangle_{H_{\text{sb}}} = \frac{\langle T_\tau \sigma_z(\tau_1)\sigma_z(\tau_2)S(\beta) \rangle_{H^{(0)}}}{\langle S(\beta) \rangle_{H^{(0)}}}. \quad (\text{D.9})$$

Substituting Eq. (D.2) into Eq. (D.9), we obtain that the numerator of Eq. (D.9) reads⁴

$$\begin{aligned}
 \langle T_\tau \sigma_z(\tau_1)\sigma_z(\tau_2) \rangle_{H^{(0)}} &+ \sum_{n=2}^{\infty} \frac{\lambda^{2(n-1)}}{[2(n-1)]!} \int_0^\beta d\tau_3 \int_0^\beta d\tau_4 \dots \int_0^\beta d\tau_{2n} \langle T_\tau \sigma_z(\tau_1) \\
 &\times \sigma_z(\tau_2)\sigma_z(\tau_3)\sigma_z(\tau_4) \dots \sigma_z(\tau_{2n}) \rangle_{H^{(0)}} Q_0(\tau_3)Q_0(\tau_4) \dots Q_0(\tau_{2n}) \rangle_{H^{(0)}}. \quad (\text{D.10})
 \end{aligned}$$

The result of Eq. (D.9) comes from the connected diagram of Eq. (D.10). The spin operators and charge operators are decoupled, and then the charge operators pair with each other. One of the possible pairing result is

$$\begin{aligned}
 &\langle T_\tau Q_0(\tau_3)Q_0(\tau_4) \rangle_{H^{(0)}} \langle T_\tau Q_0(\tau_5)Q_0(\tau_6) \rangle_{H^{(0)}} \dots \langle T_\tau Q_0(\tau_{2n-1})Q_0(\tau_{2n}) \rangle_{H^{(0)}} \\
 &\times \langle T_\tau \sigma_z(\tau_1)\sigma_z(\tau_2) \rangle_{H^{(0)}} \sigma_z(\tau_3)\sigma_z(\tau_4) \dots \sigma_z(\tau_{2n}) \rangle_{H^{(0)}}. \quad (\text{D.11})
 \end{aligned}$$

In the equation above, $2n - 2$ charge operators consist of $m - 1$ pairings. The number of all the pairing way is counted as

$$\frac{(2n-2)!}{2^{n-1}(n-1)!}. \quad (\text{D.12})$$

⁴The odd orders do not contribute. The argument is the same as for two-point phase-phase Green's function.

Collecting Eqs. (D.9)- (D.12), we obtain

$$\begin{aligned} \mathcal{G}[\sigma_z(\tau_1)\sigma_z(\tau_2)] &= \mathcal{G}^{(0)}[\sigma_z(\tau_1)\sigma_z(\tau_2)] + \sum_{n=2}^{\infty} \frac{2\lambda^{2(n-1)}}{2^n(n-1)!} \int_0^\beta d\tau_3 \int_0^\beta d\tau_4 \dots \\ &\int_0^\beta d\tau_{2n} \mathcal{G}^{(0)}[\sigma_z(\tau_1)\sigma_z(\tau_2)\dots\sigma_z(\tau_{2n})] \mathcal{G}^{(0)}[Q_0(\tau_3)Q_0(\tau_4)] \mathcal{G}^{(0)}[Q_0(\tau_5)Q_0(\tau_6)] \\ &\times \dots \mathcal{G}^{(0)}[Q_0(\tau_{2n-1})Q_0(\tau_{2n})]. \end{aligned} \quad (\text{D.13})$$

Comparing Eq. (D.8) and Eq. (D.13), we find a simple relation that related the two-point phase-phase Green's function and two-point spin-spin Green's function:

$$\begin{aligned} \mathcal{G}[\phi_n(\tau)\phi_m(0)] &= \mathcal{G}^{(0)}[\phi_n(\tau)\phi_m(0)] + \lambda^2 \int_0^\beta d\tau_1 \int_0^\beta d\tau_2 \mathcal{G}^{(0)}[\phi_n(\tau)Q_0(\tau_1)] \\ &\times \mathcal{G}[\sigma_z(\tau_1)\sigma_z(\tau_2)] \mathcal{G}^{(0)}[Q_0(\tau_2)\phi_m(0)]. \end{aligned} \quad (\text{D.14})$$

The result is given in Eq. (5.8), and the corresponding Feynman diagram is shown in Fig. 5.4.

Four-point phase-phase Green's functions can be evaluated in the same way. The main results are given in Eq. (5.17) [see the corresponding Feynman diagram in Fig. 5.7].

Two-point Green's functions in k -space

In order to evaluate unperturbed Green's functions $G_R^{(0)}(\phi_n, Q_0)$, $G_R^{(0)}(Q_0, \phi_m)$, and $G_R^{(0)}(Q_0, Q_0)$ in chapter 5, we first rewrite the phase/charge operators in terms of creation (a_k^\dagger) and annihilate operator (a_k) [see Eq. (2.47)]. Therefore, we need to know the two-point Green's functions in k space.

To obtain them, we define

$$G_R^{(0)}[a_{k_1}(t)a_{k_2}^\dagger(0)] = \hbar\Theta(t)\langle[a_{k_1}(t), a_{k_2}^\dagger(0)]\rangle_{H^{(0)}}, \quad (\text{E.1})$$

where $\Theta(t)$ is the Heaviside step function. The unperturbed Hamiltonian $H^{(0)}$ was given by Eq. (5.5).

Next, let us derive the equation of motion. The time derivative of the Green's function reads

$$\partial_t G_R^{(0)}[a_{k_1}(t)a_{k_2}^\dagger(0)] = i\delta_{k_1 k_2} - i\omega_{k_1} G_R^{(0)}[a_{k_1}(t)a_{k_2}^\dagger(0)]. \quad (\text{E.2})$$

Taking Fourier transform of Eq. (E.2), we get

$$(\omega - \omega_{k_1})G_R^{(0)}(a_{k_1}, a_{k_2}^\dagger; \omega) = -\delta_{k_1, k_2}. \quad (\text{E.3})$$

Hence,

$$G_R^{(0)}(a_{k_1}, a_{k_2}^\dagger; \omega) = -\frac{\delta_{k_1, k_2}}{\omega - \omega_{k_1}}. \quad (\text{E.4})$$

In the same way, we obtain

$$G_R^{(0)}(a_{k_1}^\dagger, a_{k_2}; \omega) = \frac{\delta_{k_1, k_2}}{\omega + \omega_{k_1}}. \quad (\text{E.5})$$

Using these two basic Green's function, the required Green's functions in chapter 5 can be easily evaluated.

Bibliography

- [1] J. Volz, M. Scheucher, C. Junge, and A. Rauschenbeutel, “Nonlinear $[\pi]$ phase shift for single fibre-guided photons interacting with a single resonator-enhanced atom,” *Nature Photonics*, vol. 8, no. 12, pp. 965–970, 2014.
- [2] J. C. Garrison and R. Y. Chiao, *Quantum optics*. Oxford Univ. Press, 2008.
- [3] C. Monroe, “Quantum information processing with atoms and photons,” *Nature*, vol. 416, no. 6877, pp. 238–246, 2002.
- [4] A. Imamog, D. D. Awschalom, G. Burkard, D. P. DiVincenzo, D. Loss, M. Sherwin, A. Small, *et al.*, “Quantum information processing using quantum dot spins and cavity qed,” *Physical Review Letters*, vol. 83, no. 20, p. 4204, 1999.
- [5] D. Press, S. Götzinger, S. Reitzenstein, C. Hofmann, A. Löffler, M. Kamp, A. Forchel, and Y. Yamamoto, “Photon antibunching from a single quantum-dot-microcavity system in the strong coupling regime,” *Physical Review Letters*, vol. 98, no. 11, p. 117402, 2007.
- [6] M. Lukin, S. Yelin, and M. Fleischhauer, “Entanglement of atomic ensembles by trapping correlated photon states,” *Physical Review Letters*, vol. 84, no. 18, p. 4232, 2000.
- [7] D. Englund, A. Majumdar, M. Bajcsy, A. Faraon, P. Petroff, and J. Vučković, “Ultrafast photon-photon interaction in a strongly coupled quantum dot-cavity system,” *Physical review letters*, vol. 108, no. 9, p. 093604, 2012.
- [8] A. Kuzmich, W. Bowen, A. Boozer, A. Boca, C. Chou, L.-M. Duan, and H. Kimble, “Generation of nonclassical photon pairs for scalable quantum communication with atomic ensembles,” *Nature*, vol. 423, no. 6941, pp. 731–734, 2003.

- [9] R. M. Stevenson, R. J. Young, P. Atkinson, K. Cooper, D. A. Ritchie, and A. J. Shields, “A semiconductor source of triggered entangled photon pairs,” *Nature*, vol. 439, no. 7073, pp. 179–182, 2006.
- [10] J.-T. Shen and S. Fan, “Strongly correlated two-photon transport in a one-dimensional waveguide coupled to a two-level system,” *Physical review letters*, vol. 98, no. 15, p. 153003, 2007.
- [11] P. Rabl, “Photon blockade effect in optomechanical systems,” *Physical review letters*, vol. 107, no. 6, p. 063601, 2011.
- [12] T. Li, J. Huang, and C. Law, “Scattering of two distinguishable photons by a ξ -type three-level atom in a one-dimensional waveguide,” *Physical Review A*, vol. 91, no. 4, p. 043834, 2015.
- [13] A. Biella, L. Mazza, I. Carusotto, D. Rossini, and R. Fazio, “Photon transport in a dissipative chain of nonlinear cavities,” *Physical Review A*, vol. 91, no. 5, p. 053815, 2015.
- [14] Y.-L. L. Fang, H. U. Baranger, *et al.*, “Waveguide qed: Power spectra and correlations of two photons scattered off multiple distant qubits and a mirror,” *Physical Review A*, vol. 91, no. 5, p. 053845, 2015.
- [15] R. J. Schoelkopf and S. M. Girvin, “Wiring up quantum systems,” *Nature*, vol. 451, p. 664, 2008.
- [16] S. Haroche, “Nobel Lecture: Controlling photons in a box and exploring the quantum to classical boundary,” *Rev. Mod. Phys.*, vol. 85, pp. 1083–1102, July 2013.
- [17] D. J. Wineland, “Nobel Lecture: Superposition, entanglement, and raising Schrödinger’s cat,” *Rev. Mod. Phys.*, vol. 85, pp. 1103–1114, July 2013.
- [18] I. Carusotto and C. Ciuti, “Quantum fluids of light,” *Rev. Mod. Phys.*, vol. 85, pp. 299–366, Feb. 2013.
- [19] G. Milburn, “Quantum optical fredkin gate,” *Physical Review Letters*, vol. 62, no. 18, p. 2124, 1989.
- [20] A. Imamolu, H. Schmidt, G. Woods, and M. Deutsch, “Strongly interacting photons in a nonlinear cavity,” *Physical Review Letters*, vol. 79, no. 8, p. 1467, 1997.
- [21] T. E. Northup and R. Blatt, “Quantum information transfer using photons,” *Nat. Photon.*, vol. 8, pp. 356–363, May 2014.

- [22] N. Gisin and R. Thew, “Quantum communication,” *Nat. Photon.*, vol. 1, pp. 165–171, Mar. 2007.
- [23] D. E. Chang, A. S. Sørensen, E. A. Demler, and M. D. Lukin, “A single-photon transistor using nanoscale surface plasmons,” *Nature Physics*, vol. 3, no. 11, pp. 807–812, 2007.
- [24] P. Longo, P. Schmitteckert, and K. Busch, “Few-photon transport in low-dimensional systems: interaction-induced radiation trapping,” *Physical review letters*, vol. 104, no. 2, p. 023602, 2010.
- [25] P. M. Leung and B. C. Sanders, “Coherent control of microwave pulse storage in superconducting circuits,” *Physical review letters*, vol. 109, no. 25, p. 253603, 2012.
- [26] F. Ciccarello, D. Browne, L. C. Kwek, H. Schomerus, M. Zarcone, and S. Bose, “Quasideterministic realization of a universal quantum gate in a single scattering process,” *Physical Review A*, vol. 85, no. 5, p. 050305, 2012.
- [27] C. Eichler, D. Bozyigit, and A. Wallraff, “Characterizing quantum microwave radiation and its entanglement with superconducting qubits using linear detectors,” *Physical Review A*, vol. 86, no. 3, p. 032106, 2012.
- [28] C. Lang, C. Eichler, L. Steffen, J. Fink, M. Woolley, A. Blais, and A. Wallraff, “Correlations, indistinguishability and entanglement in hongou-mandel experiments at microwave frequencies,” *Nature Physics*, vol. 9, no. 6, pp. 345–348, 2013.
- [29] W. Chen, K. M. Beck, R. Bücker, M. Gullans, M. D. Lukin, H. Tanji-Suzuki, and V. Vuletić, “All-optical switch and transistor gated by one stored photon,” *Science*, vol. 341, no. 6147, pp. 768–770, 2013.
- [30] A. Zeilinger, *Dance of the photons: From Einstein to quantum teleportation*. Macmillan, 2010.
- [31] D. Bouwmeester, J.-W. Pan, K. Mattle, M. Eibl, H. Weinfurter, and A. Zeilinger, “Experimental quantum teleportation,” *Nature*, vol. 390, no. 6660, pp. 575–579, 1997.
- [32] X.-S. Ma, T. Herbst, T. Scheidl, D. Wang, S. Kropatschek, W. Naylor, B. Wittmann, A. Mech, J. Kofler, E. Anisimova, *et al.*, “Quantum teleportation over 143 kilometres using active feed-forward,” *Nature*, vol. 489, no. 7415, pp. 269–273, 2012.

- [33] V. Giovannetti, S. Lloyd, and L. Maccone, “Quantum-enhanced measurements: beating the standard quantum limit,” *Science*, vol. 306, no. 5700, pp. 1330–1336, 2004.
- [34] S. Harris and Y. Yamamoto, “Photon switching by quantum interference,” *Physical review letters*, vol. 81, no. 17, p. 3611, 1998.
- [35] M. Mücke, E. Figueroa, J. Bochmann, C. Hahn, K. Murr, S. Ritter, C. J. Villas-Boas, and G. Rempe, “Electromagnetically induced transparency with single atoms in a cavity,” *Nature*, vol. 465, no. 7299, pp. 755–758, 2010.
- [36] A. Abdumalikov Jr, O. Astafiev, A. M. Zagoskin, Y. A. Pashkin, Y. Nakamura, and J. Tsai, “Electromagnetically induced transparency on a single artificial atom,” *Physical review letters*, vol. 104, no. 19, p. 193601, 2010.
- [37] D. Roy, “Two-photon scattering by a driven three-level emitter in a one-dimensional waveguide and electromagnetically induced transparency,” *Physical review letters*, vol. 106, no. 5, p. 053601, 2011.
- [38] K. M. Birnbaum, A. Boca, R. Miller, A. D. Boozer, T. E. Northup, and H. J. Kimble, “Photon blockade in an optical cavity with one trapped atom,” *Nature*, vol. 436, no. 7047, pp. 87–90, 2005.
- [39] O. Firstenberg, T. Peyronel, Q.-Y. Liang, A. V. Gorshkov, M. D. Lukin, and V. Vuletić, “Attractive photons in a quantum nonlinear medium,” *Nature*, vol. 502, no. 7469, pp. 71–75, 2013.
- [40] I. Fushman, D. Englund, A. Faraon, N. Stoltz, P. Petroff, and J. Vučković, “Controlled phase shifts with a single quantum dot,” *Science*, vol. 320, no. 5877, pp. 769–772, 2008.
- [41] A. Rauschenbeutel, G. Nogues, S. Osnaghi, P. Bertet, M. Brune, J. Raimond, and S. Haroche, “Coherent operation of a tunable quantum phase gate in cavity qed,” *Physical Review Letters*, vol. 83, no. 24, p. 5166, 1999.
- [42] G. Kirchmair, B. Vlastakis, Z. Leghtas, S. E. Nigg, H. Paik, E. Ginossar, M. Mirrahimi, L. Frunzio, S. M. Girvin, and R. J. Schoelkopf, “Observation of quantum state collapse and revival due to the single-photon kerr effect,” *Nature*, vol. 495, no. 7440, pp. 205–209, 2013.
- [43] D. F. Walls and G. J. Milburn, *Quantum optics*. Springer Science & Business Media, 2007.

- [44] N. K. Langford, “Circuit qed-lecture notes,” *arXiv preprint arXiv:1310.1897*, 2013.
- [45] D. Esteve, J.-M. Raimond, and J. Dalibard, *Quantum Entanglement and Information Processing: Lecture Notes of the Les Houches Summer School 2003*. Elsevier, 2004.
- [46] H. Zheng, D. J. Gauthier, and H. U. Baranger, “Waveguide qed: Many-body bound-state effects in coherent and fock-state scattering from a two-level system,” *Physical Review A*, vol. 82, no. 6, p. 063816, 2010.
- [47] Y.-L. L. Fang and H. U. Baranger, “Waveguide qed: Power spectra and correlations of two photons scattered off multiple distant qubits and a mirror,” *Phys. Rev. A*, vol. 91, p. 053845, May 2015.
- [48] H. Zheng, D. J. Gauthier, and H. U. Baranger, “Cavity-free photon blockade induced by many-body bound states,” *Physical review letters*, vol. 107, no. 22, p. 223601, 2011.
- [49] A. Akimov, A. Mukherjee, C. Yu, D. Chang, A. Zibrov, P. Hemmer, H. Park, and M. Lukin, “Generation of single optical plasmons in metallic nanowires coupled to quantum dots,” *Nature*, vol. 450, no. 7168, pp. 402–406, 2007.
- [50] J. Claudon, J. Bleuse, N. S. Malik, M. Bazin, P. Jaffrennou, N. Gregersen, C. Sauvan, P. Lalanne, and J.-M. Gérard, “A highly efficient single-photon source based on a quantum dot in a photonic nanowire,” *Nature Photonics*, vol. 4, no. 3, pp. 174–177, 2010.
- [51] D. Bozyigit, C. Lang, L. Steffen, J. Fink, C. Eichler, M. Baur, R. Bianchetti, P. Leek, S. Filipp, M. Da Silva, *et al.*, “Antibunching of microwave-frequency photons observed in correlation measurements using linear detectors,” *Nature Physics*, vol. 7, no. 2, pp. 154–158, 2011.
- [52] A. F. Van Loo, A. Fedorov, K. Lalumière, B. C. Sanders, A. Blais, and A. Wallraff, “Photon-mediated interactions between distant artificial atoms,” *Science*, vol. 342, no. 6165, pp. 1494–1496, 2013.
- [53] K. Koshino, H. Terai, K. Inomata, T. Yamamoto, W. Qiu, Z. Wang, and Y. Nakamura, “Observation of the three-state dressed states in circuit quantum electrodynamics,” *Physical review letters*, vol. 110, no. 26, p. 263601, 2013.

- [54] I.-C. Hoi, C. Wilson, G. Johansson, J. Lindkvist, B. Peropadre, T. Palomaki, and P. Delsing, “Microwave quantum optics with an artificial atom in one-dimensional open space,” *New Journal of Physics*, vol. 15, no. 2, p. 025011, 2013.
- [55] A. J. Leggett, S. Chakravarty, A. T. Dorsey, M. P. A. Fisher, A. Garg, and W. Zwerger, “Dynamics of the dissipative two-state system,” *Rev. Mod. Phys.*, vol. 59, pp. 1–85, Jan 1987.
- [56] U. Weiss, *Quantum Dissipative Systems*. Singapore: World Scientific, 4 ed., 2012.
- [57] T. Niemczyk, F. Deppe, H. Huebl, E. P. Menzel, F. Hocke, M. J. Schwarz, J. J. Garcia-Ripoll, D. Zueco, T. Hümmer, E. Solano, A. Marx, and R. Gross, “Circuit quantum electrodynamics in the ultrastrong-coupling regime,” *Nat. Phys.*, vol. 6, pp. 772–776, July 2010.
- [58] P. Forn-Díaz, J. Lisenfeld, D. Marcos, J. J. García-Ripoll, E. Solano, C. J. P. M. Harmans, and J. E. Mooij, “Observation of the Bloch-Siegert Shift in a Qubit-Oscillator System in the Ultrastrong Coupling Regime,” *Phys. Rev. Lett.*, vol. 105, p. 237001, Nov. 2010.
- [59] R. M. Bradley and S. Doniach, “Quantum fluctuations in chains of Josephson junctions,” *Phys. Rev. B*, vol. 30, pp. 1138–1147, Aug. 1984.
- [60] N. A. Masluk, I. M. Pop, A. Kamal, Z. K. Mineev, and M. H. Devoret, “Microwave characterization of Josephson junction arrays: Implementing a low loss superinductance,” *Phys. Rev. Lett.*, vol. 109, p. 137002, Sept. 2012.
- [61] M. T. Bell, I. A. Sadovskyy, L. B. Ioffe, A. Y. Kitaev, and M. E. Gershenson, “Quantum superinductor with tunable nonlinearity,” *Phys. Rev. Lett.*, vol. 109, p. 137003, Sept. 2012.
- [62] C. Altimiras, O. Parlavacchio, P. Joyez, D. Vion, P. Roche, D. Esteve, and F. Portier, “Tunable microwave impedance matching to a high impedance source using a Josephson metamaterial,” *Appl. Phys. Lett.*, vol. 103, p. 212601, Nov. 2013.
- [63] T. Weissl, G. Rastelli, I. Matei, I. M. Pop, O. Buisson, F. W. J. Hekking, and W. Guichard, “Bloch band dynamics of a Josephson junction in an inductive environment,” *Phys. Rev. B*, vol. 91, p. 014507, Jan. 2015.

- [64] Y. Makhlin, G. Schön, and A. Schnirman, “Quantum-state engineering with Josephson-junction devices,” *Rev. Mod. Phys.*, vol. 73, p. 357, May 2001.
- [65] T. Niemczyk, F. Deppe, H. Huebl, E. Menzel, F. Hocke, M. Schwarz, J. Garcia-Ripoll, D. Zueco, T. Hümmer, E. Solano, *et al.*, “Circuit quantum electrodynamics in the ultrastrong-coupling regime,” *Nature Physics*, vol. 6, no. 10, pp. 772–776, 2010.
- [66] T. Weissl, G. Rastelli, I. Matei, I. Pop, O. Buisson, F. Hekking, and W. Guichard, “Bloch band dynamics of a Josephson junction in an inductive environment,” *Physical Review B*, vol. 91, no. 1, p. 014507, 2015.
- [67] A. M. Zagoskin, *Quantum Engineering: Theory and Design of Quantum Coherent Structures*. Cambridge University Press, 2011.
- [68] Y. Makhlin, G. Schön, and A. Shnirman, “Josephson-junction qubits,” *Fortschritte der Physik*, vol. 48, no. 9-11, pp. 1043–1054, 2000.
- [69] J. I. Cirac and P. Zoller, “Quantum computations with cold trapped ions,” *Physical review letters*, vol. 74, no. 20, p. 4091, 1995.
- [70] N. A. Gershenfeld and I. L. Chuang, “Bulk spin-resonance quantum computation,” *science*, vol. 275, no. 5298, pp. 350–356, 1997.
- [71] D. G. Cory, A. F. Fahmy, and T. F. Havel, “Ensemble quantum computing by nmr spectroscopy,” *Proceedings of the National Academy of Sciences*, vol. 94, no. 5, pp. 1634–1639, 1997.
- [72] Q. A. Turchette, C. Hood, W. Lange, H. Mabuchi, and H. J. Kimble, “Measurement of conditional phase shifts for quantum logic,” *Physical Review Letters*, vol. 75, no. 25, p. 4710, 1995.
- [73] Y. A. Pashkin, T. Yamamoto, O. Astafiev, Y. Nakamura, D. Averin, and J. Tsai, “Quantum oscillations in two coupled charge qubits,” *Nature*, vol. 421, no. 6925, pp. 823–826, 2003.
- [74] A. Berkley, H. Xu, R. Ramos, M. Gubrud, F. Strauch, P. Johnson, J. Anderson, A. Dragt, C. Lobb, and F. Wellstood, “Entangled macroscopic quantum states in two superconducting qubits,” *Science*, vol. 300, no. 5625, pp. 1548–1550, 2003.
- [75] J. Plantenberg, P. De Groot, C. Harmans, and J. Mooij, “Demonstration of controlled-not quantum gates on a pair of superconducting quantum bits,” *Nature*, vol. 447, no. 7146, pp. 836–839, 2007.

- [76] D. Steffen, Z. I. Antonioli, G. P. K. Steffen, R. J. S. Jacques, M. L. d. Santos, H. T. Godoy, and S. Bogusz Júnior, “Recently added,” *Science*, vol. 313, no. 5792, pp. 1423–1425, 2006.
- [77] T. Hime, P. Reichardt, B. Plourde, T. Robertson, C.-E. Wu, A. Ustinov, and J. Clarke, “Solid-state qubits with current-controlled coupling,” *science*, vol. 314, no. 5804, pp. 1427–1429, 2006.
- [78] L. DiCarlo, J. Chow, J. Gambetta, L. S. Bishop, B. Johnson, D. Schuster, J. Majer, A. Blais, L. Frunzio, S. Girvin, *et al.*, “Demonstration of two-qubit algorithms with a superconducting quantum processor,” *Nature*, vol. 460, no. 7252, pp. 240–244, 2009.
- [79] J. Majer, J. Chow, J. Gambetta, J. Koch, B. Johnson, J. Schreier, L. Frunzio, D. Schuster, A. Houck, A. Wallraff, *et al.*, “Coupling superconducting qubits via a cavity bus,” *Nature*, vol. 449, no. 7161, pp. 443–447, 2007.
- [80] H. Zheng and H. U. Baranger, “Persistent quantum beats and long-distance entanglement from waveguide-mediated interactions,” *Physical review letters*, vol. 110, no. 11, p. 113601, 2013.
- [81] A. LeClair, F. Lesage, S. Lukyanov, and H. Saleur, “The Maxwell-Bloch theory in quantum optics and the Kondo model,” *Phys. Lett. A*, vol. 235, pp. 203–208, Nov. 1997.
- [82] J.-T. Shen and S. Fan, “Strongly correlated two-photon transport in a one-dimensional waveguide coupled to a two-level system,” *Phys. Rev. Lett.*, vol. 98, p. 153003, Apr 2007.
- [83] H. Zheng, D. J. Gauthier, and H. U. Baranger, “Waveguide QED: Many-body bound-state effects in coherent and Fock-state scattering from a two-level system,” *Phys. Rev. A*, vol. 82, p. 063816, Dec 2010.
- [84] K. Le Hur, “Kondo resonance of a microwave photon,” *Phys. Rev. B*, vol. 85, p. 140506(R), Apr 2012.
- [85] M. Goldstein, M. H. Devoret, M. Houzet, and L. I. Glazman, “Inelastic microwave photon scattering off a quantum impurity in a Josephson-junction array,” *Phys. Rev. Lett.*, vol. 110, p. 017002, Jan 2013.
- [86] S. Rebić, J. Twamley, and G. J. Milburn, “Giant Kerr nonlinearities in circuit quantum electrodynamics,” *Phys. Rev. Lett.*, vol. 103, p. 150503, Oct 2009.

- [87] G.-L. Ingold and Y. Nazarov, “Charge tunneling rates in ultrasmall junctions,” in *Single Charge Tunneling: Coulomb Blockade Phenomena in Nanostructures* (H. Grabert and M. H. Devoret, eds.), pp. 21–107, New York: Plenum, 1992.
- [88] M. Hofheinz, F. Portier, Q. Baudouin, P. Joyez, D. Vion, P. Bertet, P. Roche, and D. Estève, “Bright side of the coulomb blockade,” *Physical review letters*, vol. 106, no. 21, p. 217005, 2011.
- [89] R. Bradley and S. Doniach, “Quantum fluctuations in chains of josephson junctions,” *Physical Review B*, vol. 30, no. 3, p. 1138, 1984.
- [90] O. Parlavecchio, C. Altimiras, J.-R. Souquet, P. Simon, I. Safi, P. Joyez, D. Vion, P. Roche, D. Estève, and F. Portier, “Fluctuation-dissipation relations of a tunnel junction driven by a quantum circuit,” *Physical review letters*, vol. 114, no. 12, p. 126801, 2015.
- [91] C. Altimiras, O. Parlavecchio, P. Joyez, D. Vion, P. Roche, D. Esteve, and F. Portier, “Dynamical coulomb blockade of shot noise,” *Physical review letters*, vol. 112, no. 23, p. 236803, 2014.
- [92] C. Altimiras, O. Parlavecchio, P. Joyez, D. Vion, P. Roche, D. Esteve, and F. Portier, “Tunable microwave impedance matching to a high impedance source using a josephson metamaterial,” *arXiv preprint arXiv:1404.1792*, 2014.
- [93] M. Tinkham, *Introduction to superconductivity*. Courier Corporation, 2012.
- [94] B. D. Josephson, “Possible new effects in superconductive tunnelling,” *Physics letters*, vol. 1, no. 7, pp. 251–253, 1962.
- [95] V. Ambegaokar and A. Baratoff, “Tunneling between superconductors,” *Physical Review Letters*, vol. 10, no. 11, p. 486, 1963.
- [96] K. Likharev and A. Zorin, “Proceedings of the international conference on low temperature physics–lt-17 (contributed papers),” 1984.
- [97] M. Büttiker, “Zero-current persistent potential drop across small-capacitance josephson junctions,” *Physical Review B*, vol. 36, no. 7, p. 3548, 1987.
- [98] V. Bouchiat, D. Vion, P. Joyez, D. Esteve, and M. Devoret, “Quantum coherence with a single cooper pair,” *Physica Scripta*, vol. 1998, no. T76, p. 165, 1998.

- [99] Y. Nakamura, Y. A. Pashkin, and J. Tsai, “Coherent control of macroscopic quantum states in a single-cooper-pair box,” *Nature*, vol. 398, no. 6730, pp. 786–788, 1999.
- [100] R. Bansal, *Handbook of engineering electromagnetics*. CRC Press, 2004.
- [101] A. J. Annunziata, D. F. Santavicca, L. Frunzio, G. Catelani, M. J. Rooks, A. Frydman, and D. E. Prober, “Tunable superconducting nanoinductors,” *Nanotechnology*, vol. 21, no. 44, p. 445202, 2010.
- [102] B. Yurke and J. S. Denker, “Quantum network theory,” *Physical Review A*, vol. 29, no. 3, p. 1419, 1984.
- [103] M. H. Devoret, “Quantum fluctuations in electrical circuits,” *Les Houches, Session LXIII*, vol. 7, no. 8, 1995.
- [104] R. Fazio and H. Van Der Zant, “Quantum phase transitions and vortex dynamics in superconducting networks,” *Physics Reports*, vol. 355, no. 4, pp. 235–334, 2001.
- [105] D. Haviland, “Superconducting circuits: Quantum phase slips,” *Nature Physics*, vol. 6, no. 8, pp. 565–566, 2010.
- [106] T. Weißl, B. Küng, É. Dumur, A. K. Feofanov, I. Matei, C. Naud, O. Buisson, F. W. Hekking, and W. Guichard, “Kerr coefficients of plasma resonances in josephson junction chains,” *arXiv preprint arXiv:1505.05845*, 2015.
- [107] C. Gorter, “A possible explanation of the increase of the electrical resistance of thin metal films at low temperatures and small field strengths,” *Physica*, vol. 17, no. 8, pp. 777–780, 1951.
- [108] R. Lambeir, A. Van Itterbeek, and G. Van Den Berg, “Measurements on the electrical resistivity of thin iron films at liquid helium temperatures,” *Physica*, vol. 16, no. 11, pp. 907–914, 1950.
- [109] N. Mostovetch and B. Vodar, “Variations, en fonction du potentiel applique, de la resistance electrique des depots metalliques tres minces aux basses temperatures,” *COMPTEs RENDUS HEBDOMADAIRES DES SEANCES DE L ACADEMIE DES SCIENCES*, vol. 230, no. 10, pp. 934–936, 1950.
- [110] T. Fulton and G. Dolan, “Observation of single-electron charging effects in small tunnel junctions,” *Physical review letters*, vol. 59, no. 1, p. 109, 1987.

- [111] T.-L. Ho, “Effect of quantum voltage fluctuations on the resistance of normal junctions,” *Physical review letters*, vol. 51, no. 22, p. 2060, 1983.
- [112] M. Devoret, D. Esteve, H. Grabert, G.-L. Ingold, H. Pothier, and C. Urbina, “Effect of the electromagnetic environment on the coulomb blockade in ultrasmall tunnel junctions,” *Physical review letters*, vol. 64, no. 15, p. 1824, 1990.
- [113] J. Barber and S. Ruggiero, “Observation of the incremental charging of a particles by single electrons,” *Physical review letters*, vol. 59, no. 7, p. 807, 1987.
- [114] K. Mullen, E. Ben-Jacob, R. Jaklevic, and Z. Schuss, “I-v characteristics of coupled ultrasmall-capacitance normal tunnel junctions,” *Physical review B*, vol. 37, no. 1, p. 98, 1988.
- [115] E. Ben-Jacob and Y. Gefen, “New quantum oscillations in current driven small junctions,” *Physics Letters A*, vol. 108, no. 5, pp. 289–292, 1985.
- [116] E. Ben-Jacob, Y. Gefen, K. Mullen, and Z. Schuss, “Coherent versus non-coherent bloch oscillations in the presence of direct and alternating fields,” *Physical Review B*, vol. 37, no. 13, p. 7400, 1988.
- [117] A. N. Cleland, J. Schmidt, and J. Clarke, “Charge fluctuations in small-capacitance junctions,” *Physical review letters*, vol. 64, no. 13, p. 1565, 1990.
- [118] P. Delsing, K. Likharev, L. Kuzmin, and T. Claeson, “Time-correlated single-electron tunneling in one-dimensional arrays of ultrasmall tunnel junctions,” *Physical review letters*, vol. 63, no. 17, p. 1861, 1989.
- [119] L. Geerligs, V. Anderegg, C. Van Der Jeugd, J. Romijn, and J. Mooij, “Influence of dissipation on the coulomb blockade in small tunnel junctions,” *EPL (Europhysics Letters)*, vol. 10, no. 1, p. 79, 1989.
- [120] L. Kuzmin, Y. V. Nazarov, D. Haviland, P. Delsing, and T. Claeson, “Coulomb blockade and incoherent tunneling of cooper pairs in ultrasmall junctions affected by strong quantum fluctuations,” *Physical review letters*, vol. 67, no. 9, p. 1161, 1991.
- [121] L. Kuzmin and D. Haviland, “Observation of the bloch oscillations in an ultrasmall josephson junction,” *Physical review letters*, vol. 67, no. 20, p. 2890, 1991.

- [122] D. Haviland, L. Kuzmin, P. Delsing, K. Likharev, and T. Claeson, “Experimental evidence for the coulomb blockade of cooper pair tunneling and bloch oscillations in single josephson junctions,” *Zeitschrift für Physik B Condensed Matter*, vol. 85, no. 3, pp. 339–347, 1991.
- [123] D. Haviland, L. Kuzmin, P. Delsing, and T. Claeson, “Observation of the coulomb blockade of cooper pair tunnelling in single josephson junctions,” *EPL (Europhysics Letters)*, vol. 16, no. 1, p. 103, 1991.
- [124] A. Caldeira and A. J. Leggett, “Quantum tunnelling in a dissipative system,” *Annals of Physics*, vol. 149, no. 2, pp. 374–456, 1983.
- [125] Private communication with Inès Safi.
- [126] S. Jezouin, M. Albert, F. D. Parmentier, A. Anthore, U. Gennser, A. Cavanna, I. Safi, and F. Pierre, “Tomonaga–Luttinger physics in electronic quantum circuits,” *Nat Commun*, vol. 4, p. 1802, Apr. 2013.
- [127] P. Joyez, “Self-Consistent Dynamics of a Josephson Junction in the Presence of an Arbitrary Environment,” *Phys. Rev. Lett.*, vol. 110, p. 217003, May 2013.
- [128] J.-R. Souquet, I. Safi, and P. Simon, “Dynamical Coulomb blockade in an interacting one-dimensional system coupled to an arbitrary environment,” *Phys. Rev. B*, vol. 88, p. 205419, Nov. 2013.
- [129] T. T. Heikkilä, P. Virtanen, G. Johansson, and F. K. Wilhelm, “Measuring non-Gaussian fluctuations through incoherent Cooper-pair current,” *Phys. Rev. Lett.*, vol. 93, p. 247005, Dec 2004.
- [130] P. Minnhagen, “Exact numerical solutions of a nozieres-de dominicis-type model problem,” *Physics Letters A*, vol. 56, no. 4, pp. 327–329, 1976.
- [131] G. D. Mahan, *Many-particle physics*. Springer Science & Business Media, 2013.
- [132] M. Gell-Mann and F. Low, “Bound states in quantum field theory,” *Physical Review*, vol. 84, no. 2, p. 350, 1951.
- [133] L. S. Brown, *Quantum field theory*. Cambridge University Press, 1994.
- [134] G. Hooft, “The conceptual basis of quantum field theory,” 2007.
- [135] R. MacKenzie, “Path integral methods and applications,” *arXiv preprint quant-ph/0004090*, 2000.

- [136] J. W. Negele and H. Orland, *Quantum many-particle systems*. Westview, 1988.
- [137] D. M. Basko and F. W. J. Hekking, “Disordered Josephson junction chains: Anderson localization of normal modes and impedance fluctuations,” *Phys. Rev. B*, vol. 88, p. 094507, Sep 2013.
- [138] E. Chow, P. Delsing, and D. B. Haviland, “Length-scale dependence of the superconductor-to-insulator quantum phase transition in one dimension,” *Physical review letters*, vol. 81, no. 1, p. 204, 1998.
- [139] D. B. Haviland, K. Andersson, and P. Ågren, “Superconducting and insulating behavior in one-dimensional Josephson junction arrays,” *Journal of Low Temperature Physics*, vol. 118, no. 5-6, pp. 733–749, 2000.
- [140] A. J. Leggett, S. Chakravarty, A. Dorsey, M. P. Fisher, A. Garg, and W. Zwerger, “Dynamics of the dissipative two-state system,” *Reviews of Modern Physics*, vol. 59, no. 1, p. 1, 1987.
- [141] U. Weiss, *Quantum dissipative systems*, vol. 10. World Scientific, 1999.
- [142] F. Bloch, “Nuclear induction,” *Physical review*, vol. 70, no. 7-8, p. 460, 1946.
- [143] J. Leppkangas, M. Fogelström, A. Grimm, M. Hofheinz, M. Marthaler, and G. Johansson, “Antibunched photons from inelastic Cooper-pair tunneling,” *Physical review letters*, vol. 115, no. 2, p. 027004, 2015.

Acknowledgement

It was really an extraordinary experience to me in the past three years. Looking back to that period, I realize that I had made a right decision in 2012. There were three options including joining the army, going to a company, or exploring the external world. Due to the intensive curiosity, I chose the last one and came to Grenoble. This was the starting point of the story.

The story can never continue without my supervisors Dr. Manuel Houzet, Prof. Julia Meyer, and Prof. Frank Hekking. It was exactly them who helped me become a member of Laboratoire de Physique et Modélisation des Milieux Condensés (LPMMC). I always feel grateful for their patient guidances as long as I recall those precious moments, e.g., explaining each step of a derivation on blackboard, writing a paper paragraph by paragraph together, as well as correcting carefully my posters, slides, and thesis. You arise me up more than I can be. One more thing I must say is that our projects were done with Prof. Harold Baranger.

During the period of writing this manuscript, I received the vital helps from Zhang Gu, Zhang Yangmuzi, Prof. Zha Guo-qiao, Dr. Angelo Di Marco, Dr. Mi Shuo, Dr. Francesco Calcavecchia, Dr. Marco Cominotti, Nicolas Gheeraert, Guillaume Lang, and Malo Tarpin.

Thank you very much for my committee members Dr. Ines Safi, Dr. Fabien Portier, Dr. Fabio Pistolesi, and Prof. Wiebke Guichard. All of them gave me many valuable suggestions concerning improving the thesis.

In life, I spent a very happy time here thank to the nice friends and colleagues. Especially, I want to say thank you to Marco, Angelo, Florian. Also, I met kind good Chinese guys here, they are Zhang Shuo, Jia Tao, Hu Rui-Rui, Dr. Ding Lei, Mao Jing-Wen, Zhao Yu, Dr. Liu Fan-Yu, Dr. Li Wu, Dr. Chen Ya-Ni, Dr. Zhu Hua-Xiang, Dr Yang Zhao-Lin and Du Peng. In addition, I built a on-line discussion group with Chang Jia-Shu, Dr. Ma Jin-Wen, and Liu Na. We discussed interesting issues every weekend.

Finally, I want to say thank you to my parents and sisters. You are forever the most important persons in my life.

In the Easter of 2014, I visited Marseille with friends. I remember that there was a doodle on the wall. I would like to use it being the ending of this thesis: *La vie est un cadeau, et le bonheur est un combat.*